UNIVERSIDADE ESTADUAL DE PONTA GROSSA
SETOR DE CIÊNCIAS EXATAS E NATURAIS
PROGRAMA DE PÓS-GRADUAÇÃO EM CIÊNCIAS/FÍSICA

ALISON ANTUNES DA SILVA

QUANTUM GRAPHS: SCATTERING, RANDOMISATION, AND DEVICES MODELLING

GRAFOS QUÂNTICOS: ESPALHAMENTO, RANDOMIZAÇÃO E MODELAGEM DE DISPOSITIVOS

PONTA GROSSA
2025

ALISON ANTUNES DA SILVA

QUANTUM GRAPHS: SCATTERING, RANDOMISATION, AND DEVICES MODELLING

GRAFOS QUÂNTICOS: ESPALHAMENTO, RANDOMIZAÇÃO E MODELAGEM DE DISPOSITIVOS

Thesis presented to the Postgraduate Program in Sciences, concentration area Physics of the Universidade Estadual de Ponta Grossa, in partial fulfilment of the requirements for the degree of Doctor in Science.

Advisor: Prof. Dr. Fabiano Manoel de Andrade.

PONTA GROSSA

2025

Silva, Alison Antunes da
S586 Quantum graphs: scattering, randomisation, and devices modelling / Alison Antunes da Silva. Ponta Grossa, 2025.
125 f.

Tese (Doutorado em Ciências - Área de Concentração: Física), Universidade Estadual de Ponta Grossa.

Orientador: Prof. Dr. Fabiano Manoel de Andrade.

1. Física quântica. 2. Grafos quânticos. 3. Espalhamento. 4. Entropia. 5. Randomização. I. Andrade, Fabiano Manoel de. II. Universidade Estadual de Ponta Grossa. Física. III.T.

CDD: 530

Ficha catalográfica elaborada por Maria Luzia Fernandes Bertholino dos Santos- CRB9/986

TERMO DE APROVAÇÃO

ALISON ANTUNES DA SILVA

QUANTUM GRAPHS: SCATTERING, RANDOMISATION, AND DEVICES MODELLING

Tese aprovada como requisito parcial para obtenção do grau de Doutor em Ciências, no Programa de Pós-Graduação em Ciências, Área de Concentração: Física Teórica da Universidade Estadual de Ponta Grossa, pela seguinte banca examinadora:

gov.br Documento assinado digitalmente
FABIANO MANOEL DE ANDRADE
Data: 22/05/2025 12:28:18-0300
Verifique em https://validar.iti.gov.br

Orientador- _____

Dr. Fabiano Manoel de Andrade – UEPG –

Titular/Presidente

gov.br Documento assinado digitalmente
ANTONIO SERGIO MAGALHAES DE CASTRO
Data: 24/05/2025 08:59:36-0300
Verifique em https://validar.iti.gov.br

_____ _____

Dr. Antônio Sérgio Magalhães de Castro – UEPG – Titular

gov.br Documento assinado digitalmente
DIOGO DE OLIVEIRA SOARES PINTO
Data: 22/05/2025 13:10:39-0300
Verifique em https://validar.iti.gov.br

_____ _____

Dr. Diogo Oliveira Soares Pinto – IFSC-USP – Titular

gov.br Documento assinado digitalmente
GIULIANO GADIOLI LA GUARDIA
Data: 22/05/2025 16:28:04-0300
Verifique em https://validar.iti.gov.br

_____ _____

Dr. Giuliano Gadioli La Guardia – UEPG – Titular

gov.br Documento assinado digitalmente
RENATO MOREIRA ANGELO
Data: 22/05/2025 14:44:12-0300
Verifique em https://validar.iti.gov.br

_____ _____

Dr. Renato Moreira Angelo – UFPR – Titular

Ponta Grossa, 19 de maio de 2025.

ACKNOWLEDGEMENTS

To my wife Bruna, thank you for your love, patience, support, and encouragement throughout every step of this journey. I am deeply grateful to have you by my side and all the moments we share.

I am very grateful to my family, parents, sisters, grandmother, and in-laws, as well as to my wife's family, for their support.

A special thanks to God for granting me strength, health, perseverance, and the blessing of my family, essential throughout this journey.

I express my gratitude to my advisor, Prof. Dr. Fabiano M. Andrade, for his continuous guidance since my undergraduate studies. For all the help, the exchange of ideas, advice, guidance on new collaborations, and for his friendship.

I am also grateful for the collaboration with Prof. Dr. Dionisio Bazeia, whose advice, shared work, and guidance on academic writing have contributed to my development.

Thanks to Dr. Francesco Caravelli, for the guidance and collaboration on the study of quantum graph application on filamentary switching.

I express my gratitude to everyone who contributed to this journey. The research group QPQI (Quantum physics and quantum information), for all the topics discussed and shared ideas. The professors who inspired my curiosity and participated in all stages of my academic development. Thanks to my friends for all the companionship, encouragement, and all the meaningful moments we have shared along the way.

Finally, I thank CAPES for supporting this work. This study was financed in part by the Coordenação de Aperfeiçoamento de Pessoal de Nível Superior – Brasil (CAPES) – Finance Code 001

RESUMO

Este trabalho tem como principal tópico o estudo de espalhamento em grafos quânticos. Ao longo dele, o método da função de Green para grafos quânticos é aplicado, a qual é obtida pela matriz adjacência do grafo e fornece as amplitudes de espalhamento nessas estruturas. Uma entropia informacional de espalhamento é proposta, relacionando a probabilidade de reflexão ou transmissão para cada um dos canais de espalhamento com um conteúdo informacional sobre a distribuição desse espalhamento por meio desses canais. Propomos a aplicação de grafos quânticos para modelar a formação de filamento entre eletrodos e estudar memristores. Também estudamos o transporte em estruturas de grafos randomizados, onde, devido ao grande número de subgrafos, propomos uma aproximação tomando amostragens de seus subgrafos para o caso de grafos com um número grande de vértices. Finalmente, um modelo de estado quântico de espalhamento, onde o espalhamento em um grafo pode agir como controle da estrutura de um segundo grafo quântico, também é proposto; nele verificamos os casos em que esse sistema pode resultar em emaranhamento desses estados.

Keywords: Grafos quânticos. Entropia. Randomização. Espalhamento.

ABSTRACT

This work has as its main topic the study of scattering in quantum graphs. Throughout it, the Green's function method for quantum graphs is applied, which is obtained by the adjacency matrix of the graph and provides the scattering amplitudes in these structures. An informational entropy of scattering is proposed, relating the probability of reflection or transmission for each of the scattering channels with an informational content about the distribution of the scattering along these channels. Next, applications of quantum graphs to model the formation of a filament between electrodes and to study memristors are proposed. The transport in randomised graph structures and the approximation by taking samples of their subgraphs are also studied. Finally, a quantum state model of scattering is also proposed, where the scattering in a graph can act as a control of the structure of a second quantum graph, and the cases in which this system can result in entanglement of the states are studied.

Keywords: Quantum graph. Entropy. Randomisation. Scattering.

LIST OF FIGURES

LIST OF TABLES

SUMMARY

1 INTRODUCTION

Until the end of the XIX century, the understanding of physics was showing that everything seemed to be governed by predictable and orderly laws, in which the motion of particles was defined in a deterministic manner. This led some scientists to believe that almost everything related to physics had already been discovered. As an example, Philipp von Jolly once advised one of his students not to go into the theoretical physics area, assuming that, because physics being in a high stage of development, it soon would become in its final form, and the remaining works consisted only of filling a few holes.[1]

However, some evidence of unexplained phenomena by physics at that time was being revealed. For instance, Boltzmann had suggested that energy levels in some systems might be discrete[2], other discoveries include the discrete spectral lines of emissions in atoms, the radioactivity, anomalies in the black body radiation, and so on. When encountering some of these problems, William Thomson, also known as Lord Kelvin, presented a lecture about two clouds that were obscuring the beauty and clearness of the theories at that moment.[3] One of these clouds was the photoelectric effect, solved by Einstein by utilising the concept of packets of energy, obtained from studies on the black body radiation problem made by Max Planck[4], that same student early advertised not to go into theoretical studies.

These studies involving discrete values of energy, named quanta, marked the start of a whole new field of study, named Quantum Mechanics. In the following years, a great number of publications appeared in this area suggesting the atomic model, the properties of molecules, and some new quantised values such as the electron charge. Louis de Broglie did an interesting suggestion on his thesis, applying to particles the wave-particle duality, early described for photons. This new approach led to the development of wave mechanics with Schrödinger presenting his equation describing the particles and making predictions of quantum systems, whose

generalisation was also provided by Paul Dirac, including special relativity. Alternatively, another way to predict those quantum systems was also provided by the matrix mechanics, and from the path integral formalism, this last was defined by Feynman from the quantum action proposed by Dirac.

Among the branches of studies of quantum physics, the scattering of particles is an interesting one. It provided in the comprehension of microscopic structures and the properties of atoms or even subatomic particles. In this context, Clifford Glenwood Shull said during his speech at the Nobel ceremony in 1994:

> If one looks back through the history of advances in physics, you find many examples of notable findings from scattering experiments. In this, you introduce some entity to a target assembly and upon studying its interaction with the target you learn much about the latter. Over the last century, physicists have used light quanta electrons, alpha particles, X-rays, gamma-rays, protons, neutrons and exotic subnuclear particles for this purpose. Much important information about the target atoms or nuclei or their assemblage has been obtained in this way. In witness of this importance one can point to the unusual concentration of scattering enthusiasts among earlier Nobel Laureate physicists. One could say that physicists just love to perform or interpret scattering experiments.

This highlights the role of scattering in the development of physics, with the understanding of the microscopic world obtained from this method.

Along with the development of quantum mechanics, a model from discrete mathematics was applied on it, the graphs. These structures, which consist of elements defined by vertices and the connection between them by edges, define a mathematical approach for many models. Between them, we can highlight some studies on the modelling of molecules[5–8], quantum random walk models[9–11], spin chain structures[12,13] or for the construction of entangled states[14–17], which led to models on measurement based quantum computation[18,19].

In the context of scattering on quantum systems, this thesis focuses on the scattering phenomena in structures known as quantum graphs, defined as one-dimensional multiconnected networks. The term quantum graph originates from the studies by Kottos and Smilansky in quantum

chaos on graphs[20–23], although several other studies were also fundamental in defining this concept, as will be discussed in later chapters.

The motivation for studying quantum graphs lies in its analytical and numerical insights into quantum scattering, through mathematical methods based on graph topology. Traditionally, these models are analysed by solving the Schrödinger equation along the edges of a graph. However, a Green's function approach, initially developed for multiple well potentials[24–26], was later extended to quantum graphs, providing a method to obtain scattering amplitudes directly from the adjacency matrix[27–29].

In this work, we adopt the Green's function method for quantum graphs as the central tool for investigating the scattering processes in quantum graphs. We propose and analyse a new quantity, the scattering entropy which characterises the distribution of the distribution of scattering probabilities to different channels. Additionally, we apply quantum graphs to model filament formation in memristive systems, study transport in randomised graphs structures, and propose a quantum graph-based scheme for generating and controlling quantum states, and identify the conditions to obtain entangled states on them.

Finally, let us explain the organisation of this thesis in the chapters that follow.

1.1 THESIS ORGANISATION

The structure of this thesis is divided into chapters. Here we introduce the subjects of each of them.

In Chapter 2 we introduce the graphs. A historical context is shown. We present matrices related to graphs, graph families, and the concept of weighted and metric graphs.

Quantum graphs are presented in Chapter 3. There we show how these models are studied either by the Schrödinger function approach or by their Green's function. In the context of scattering on them, we show the scattering and transfer matrix method. In the following, we propose an

informational entropy approach to measure the distribution of the scattering probabilities in the scattering channels. Finally, examples on obtaining the transmission probability and the scattering entropy will be presented, utilising the graph families from the previous chapter and obtaining the scattering amplitudes as a function of the number of vertices, as well as to some structures in series and random arrangement of the same quantum graph.

A model for memristive devices is proposed in Chapter 4. Methods for building filaments between electrodes are shown, and the transformation of these structures into graphs is elaborated. With the obtained graph, we apply the quantum graph method and show how to obtain electrical current through this approach.

From the obtaining of random graphs as described in the previous chapter, we also elaborate a generalisation for random quantum graphs in Chapter 5. There, for a given quantum graph, the probabilities will be associated at its edges. This allows us to define an average probability transmission of the possible structures. To improve the evaluation of this method, we also propose an approximated form.

In Chapter 6, we use the quantum graph approach and the scattering matrix of them to define their scattering states. From this method and the randomisation proposed in the previous chapter, we also propose a system in which a quantum graph is controlled by another quantum graph. From this approach, we will evaluate the implications of doing so and the correlation between these systems.

Finally, in the last Chapter 7, we show the final remarks of this work. In addition, we present some future perspectives.

2 GRAPHS

In the first half of the XVIII century, a region situated on the city of Königsberg in the former Prussia, now Kaliningrad in Russia, had seven bridges on it. These bridges were used to cross four different parts of this city, as the Pregel River cuts the city into two mainlands and has two islands on it, as illustrated in Figure 2.1(a). The presence of these bridges led to a proposed challenge: to find a path where every bridge is crossed, but without repeating any of them. This became known as the problem of seven bridges of Königsberg[30–33].

Leonhard Euler was aware about the problem in some letters exchanged with Carl Leonhard Gottlieb Ehler and Heinrich Kühn from 1735 to 1742[33], in which they asked if Euler could provide a solution for it. Even initially reluctant about the relationship of the problem with mathematics, he proposed a solution in a study about the geometry of position[30]. The proposed approach to solve this problem was initially labelling the regions with the letters A to D, and bridges with a to g. That helped him to explain how to analyse the possible paths between regions and the amount of bridges needed to cross to avoid becoming stuck in some regions.

He proposed a method to verify if it is possible to find a path as the one proposed in the problem. In order to do that, we should verify how

Figure 2.1 – (a) Königsberg city representation with its four regions with labels $A - D$ and its seven bridges with labels $a - g$; (b) Graph that represents the problem of seven bridges.

(a) (b)

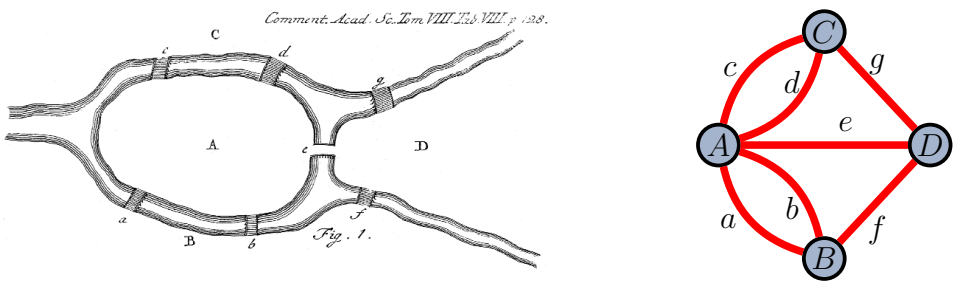

Source: (a) EULER, Leonhard. Solutio problematis in situs permanentis **Commentarii academiae scientiarum Petropolitanae**, p.128-140, 1741.[30],(b) the author.

many bridges there are in each region.

Table 2.1 – Region labels and number of bridges in the problem of seven bridges of Königsberg.

Region label	Number of bridges (n_b)
A	5
B	3
C	3
D	3

Source: the author.

For each odd number in that, there must be added one unity, and then we must divide each of these numbers by two, obtaining

Table 2.2 – Region labels and the value obtained after the procedure described by Euler in the problem of seven bridges of Königsberg.

Region label	$(n_b + 1)/2$
A	3
B	2
C	2
D	2

Source: the author.

If the sum of these numbers is equal to or less than the number of bridges between these regions with one unit added, the path proposed in the problem is possible. As the sum obtained for the problem in Königsberg is greater than eight (seven bridges plus one), Euler concluded that it is impossible to travel the city in the proposed way and also showed cases where paths like these are possible[30].

This problem is attributed to being the first one to show graph properties, and a graph is defined for this problem, as illustrated in Figure 2.1(b). The regions labeled with uppercase letters are defined as vertices and are represented by dots, whereas the connections between them, which Euler labeled with lowercase letters, are denominated as edges. This problem is so recognized in graph theory that there exist properties in them

named Eulerian paths, a path that crosses every edge of the graph without repeating them, and Eulerian cycles, similar to the Eulerian path, but the path starts and ends at the same vertex[31].

From this, applications of graph theory have been proposed in the most diverse areas, such as mathematics, physics, chemistry, computer science, information theory, linguistics, among others. An interesting case of an important application that we can mention here is Kirchhoff's law[34], in which graphs with directed edges are used to study electrical circuits. In addition, there is the Hückel theory[35], where chemical molecules are described using graphs and molecular orbitals are obtained from graph properties.

In order to study graphs, it is interesting to define notation to these models and for its properties, so that we are not dependent only on its visual illustration, and additionally have a better mathematical definition. In this way, the graphs are defined by $G(E, V)$, where $V = \{v_1, ..., v_n\}$ is a set of n vertices, and $E = \{e_1, ..., e_m\}$ is a set of m edges that connect these vertices. Edges are defined as connecting a pair of vertices and receive a notation $e_k = \{v_i, v_j\}$. They can be defined as undirected or directed edges; in the last case, the starting and final vertex of this edge must be distinguished. Additionally, there are special cases of edges, as when one connects one vertex with itself, receiving the name of loop, or for semi-infinite edges which are defined by a half-line with starting point at some vertex, this case will receive the name of "lead" in the studies of quantum graphs. Another especial case is when two vertices are connected to multiples edges at the same time, hence its graph will receive the name of multigraph[32], and these edges can be called parallel edges. In this work or main focus is on the so-called simple graphs, which are defined by graphs with simple connections, in which there are no parallel edges or loops; furthermore, they must be a connected graph, where every vertex is connected to the main structure of the graph, but in some special cases we will recover these other definitions.

From these definitions, we can obtain mathematical representations of the graphs. Next, we will explain the process of obtaining the matrices that represent graphs.

2.1 MATRIX ASSOCIATED TO GRAPHS

Usually graphs are represented by their visual model, but the same graph can be drawn in many different ways, such as by moving its vertex in the space where it is drawn. Hence, for an analysis of the characteristics of a graph and the information that it can provide, it is important to have univocal mathematical ways to represent them. A way to do that is to define the graphs through matrices that are obtained from some properties of them. Thus, we will now show some matrices associated with graphs that will be used in this work.

2.1.1 Adjacency Matrix

A matrix for defining a graph $G(V, E)$ by the connectivity of its vertices is the so-called adjacency matrix $A(G)$. The elements A_{ij} of it is defined by verifying which pair of vertices from V are connected by the edge in the set E. Thus, we say that from among all vertices in V, a pair of them is said to be adjacent, and denote it as $v_i \sim v_j$, if there is an edge $e = \{i, j\} \in E$ that connect them, and the elements of its adjacency matrix is hence defined by[36]

$$A_{ij} = \begin{cases} 1, & \text{if } v_i \sim v_j, \\ 0, & \text{otherwise.} \end{cases} \tag{2.1}$$

In this way, a matrix A, with $|V| \times |V|$ elements is obtained, where $n = |V|$ is the number of vertices in G.

Since the vertices of a graph can be labelled in multiple ways, a single graph G may correspond to several different adjacency matrices. Let A and A' be adjacency matrices of two graphs G and G', respectively. To determine whether these matrices represent the same graph structure with merely permuted vertex labels, we check if there exists a permutation

matrix P such that

$$A' = P^{-1}AP, \tag{2.2}$$

If such a matrix P exists, then G and G' are isomorphic, denoted $G \cong G'$.[32,34] On the other hand, if no such permutation matrix P can be found, then G and G' are non-isomorphic and the difference between them go beyond relabelling and reflect distinct graph structures.

2.1.2 Degree Matrix

Another characteristic of graphs that can be studied is its vertices degree. The vertex degree, with notation d_i, is defined as the number of edges that are attached to some vertex $v_i \in V$ of G. So, a $|V| \times |V|$ matrix D can be obtained by

$$D_{ij} = d_i \delta_{ij}, \tag{2.3}$$

where δ_{ij} is the Kronecker delta, $\delta_{ij} = 1$ if $i = j$, and $\delta_{ij} = 0$ if $i \neq j$.

As may be noticed, this is a diagonal matrix whose elements can also be obtained by the sum of elements in each row or column from its adjacency matrix:

$$D_{ij} = \delta_{ij} \sum_{j=1}^{|V|} A_{ij}. \tag{2.4}$$

That is possible because, by adding all the connections of a vertex, we obtain the degree of it.

2.1.3 Example

To illustrate the construction of matrices from a graph, the graph shown in Figure 2.2 will be used. This graph is defined by a set of seven edges $V = \{v_1, \ldots, v_7\}$ and a set of ten edges $E = \{e_1, \ldots, e_{10}\}$, which can be represented by $e_1 = \{v_1, v_2\}$, $e_2 = \{v_1, v_3\}$, $e_3 = \{v_2, v_3\}$.

The adjacency matrix is given by

$$A = \begin{array}{c} \begin{matrix} v_1 & v_2 & v_3 & v_4 & v_5 & v_6 & v_7 \end{matrix} \\ \begin{pmatrix} 0 & 1 & 1 & 0 & 0 & 0 & 0 \\ 1 & 0 & 1 & 1 & 1 & 0 & 0 \\ 1 & 1 & 0 & 1 & 0 & 0 & 1 \\ 0 & 1 & 1 & 0 & 1 & 0 & 0 \\ 0 & 1 & 0 & 1 & 0 & 1 & 1 \\ 0 & 0 & 0 & 0 & 1 & 0 & 0 \\ 0 & 0 & 1 & 0 & 1 & 0 & 0 \end{pmatrix} \begin{matrix} v_1 \\ v_2 \\ v_3 \\ v_4, \\ v_5 \\ v_6 \\ v_7 \end{matrix} \end{array} \tag{2.5}$$

where the red elements are the labels. And its degree matrix is obtained as a diagonal matrix, which we can define in a simplified way as

$$D = \text{diag}(2, 4, 4, 3, 4, 1, 2). \tag{2.6}$$

2.2 GRAPH SPECTRA

From the adjacency matrix of a graphs it is possible to define some properties, such as graph spectra. This property is a graph invariant, being the same for any isomorphic graph, that is, it is the same for any labelling choice.

The spectrum of a graph is obtained from the characteristic polyno-

Figure 2.2 – Example of a simple graph with vertices and edges labelled.

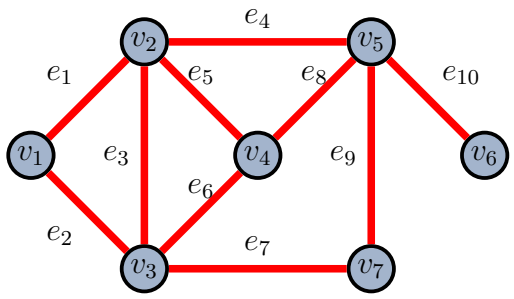

Source: the author.

mial of G[37]. Taking its adjacency matrix A, it is defined as

$$P_G(\lambda) = \det(\lambda I - A). \tag{2.7}$$

To find the Laplacian spectrum and the harmonic Laplacian spectrum, instead of the A matrix, the matrices L and $\Delta(G)$ are used, respectively. From this characteristic polynomial, the spectra are obtained as the set of eigenvalues λ of these matrices together with its multiplicities. Thus, the spectrum of G is written in the form

$$Spec(G) = \{(\lambda_1)^{m_1}, (\lambda_2)^{m_2}, ..., (\lambda_u)^{m_u}\}. \tag{2.8}$$

It is possible that two graphs G and G' can have the same spectra, they are cospectral graphs. This coespectrality does not necessarily imply that G and G' are isomorphic, as some non-isomorphic graphs can have the same spectra. However, there are some special cases where all the graphs with a given spectra are always isomorphic, in this case, they are said to be graphs determined by their spectrum.[37]

2.3 GRAPH FAMILIES

In graph theory, some commonly used structures receive names, which helps to rapidly define them. These names are utilized to define a set of graphs that follows a well-defined pattern of construction as a function of some parameter of the graph, as the number of vertices or edges, defining a family of graphs. In this section, we will define some of the most common families of graphs that will appear along the text.

2.3.1 Path Graphs

A path graph receives the notation P_n, where n is the number of vertices on it. Its construction can be made from a sequence of n vertices where each new vertex connects with the former last vertex, as illustrated in Figure 2.3, having a set of $n-1$ edges. This figure also presents a way

to label the vertices, following that, it is possible to define its adjacency matrix in a general way as

$$A\left(P_n\right) = \begin{pmatrix} 0 & 1 & 0 & \cdots & 0 & 0 \\ 1 & 0 & 1 & \cdots & 0 & 0 \\ 0 & 1 & 0 & \cdots & 0 & 0 \\ \vdots & \vdots & \vdots & \ddots & 1 & 0 \\ 0 & 0 & 0 & 1 & 0 & 1 \\ 0 & 0 & 0 & 0 & 1 & 0 \end{pmatrix}. \tag{2.9}$$

where every element is 0, except for the ones at the left and right from the main diagonal that has value 1, which can be defined by

$$A_{ij}(P_n) = \begin{cases} 1, & \text{if } j = i \pm 1, \\ 0, & \text{otherwise.} \end{cases}, \tag{2.10}$$

where $1 \leq i \leq n$ and $1 \leq j \leq n$. This can be rewritten by using Kronecker deltas,

$$A_{ij}(P_n) = \delta_{ji-1} + \delta_{ji+1}. \tag{2.11}$$

The same can be done for its degree matrix. When using this proposed labelling, only v_1 and v_n have degree 1, while the degree of the remaining vertices is 2, and its expression is

$$D_{ij}(P_n) = (2 - \delta_{i1} - \delta_{in})\delta_{ij}. \tag{2.12}$$

Figure 2.3 – Path graph P_n with 2, 3, 4 and n vertices.

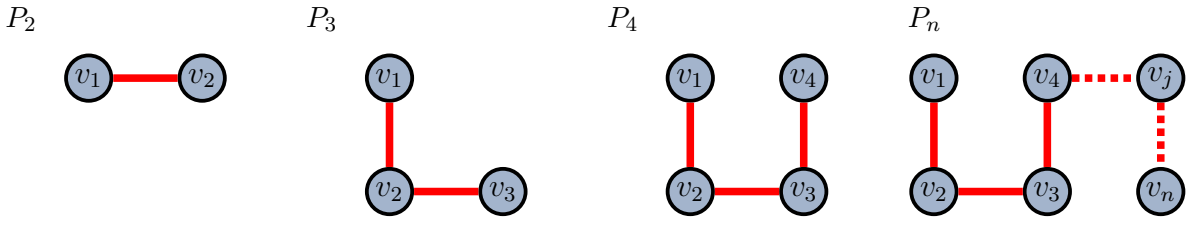

Source: the author.

2.3.2 Star Graphs

The star graphs are represented by S_n, having n vertices and $n-1$ edges on it. Here, the hub is the only vertex that is connected to all other vertices, and can be referred to as a central vertex. The other vertices are the peripheral ones and do not have any connections between them. A possible labeling is illustrated in Figure 2.4, where the central vertex is defined as v_1. From that, the following adjacency matrix is obtained

$$A(S_n) = \begin{pmatrix} 0 & 1 & 1 & \cdots & 1 \\ 1 & 0 & 0 & \cdots & 0 \\ 1 & 0 & 0 & \cdots & 0 \\ \vdots & \vdots & \vdots & \ddots & 0 \\ 1 & 0 & 0 & 0 & 0 \end{pmatrix}. \tag{2.13}$$

Here, the only non-zero elements are the ones in the column or lines with the same label as the central vertex, except for the main diagonal one. This also is obtained in the expression

$$A_{ij}(S_n) = \delta_{i1} + \delta_{j1} - 2\delta_{i1}\delta_{j1}, \tag{2.14}$$

that can be simplified to

$$A_{ij}(S_n) = (\delta_{i1} - \delta_{j1})^2. \tag{2.15}$$

The central vertex has degree $n-1$, while the remaining vertices have

Figure 2.4 – Star graph S_n with 3, 4, 5 and n vertices.

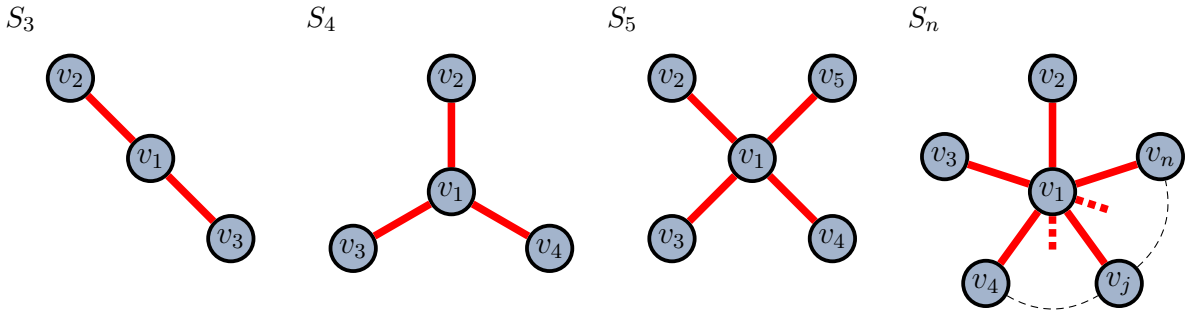

Source: the author.

degree 1. Thus, its degree matrix for star graphs can be obtained from

$$D_{ij}(S_n) = (1 + (n-2)\delta_{i1})\delta_{ij}. \tag{2.16}$$

2.3.3 Cycle Graphs

Cycle graphs C_n are defined from a sequence of n vertices where each one is connected to other two vertices, also having a number n of edges. This leads to a graph equal to a path graph P_n with an edge added, connecting the two vertices of degree 1. Its illustration is shown in Figure 2.5, where a proposed labeling way is shown. Thus, is possible to write its adjacency matrix in the following way

$$A\left(C_n\right) = \begin{pmatrix} 0 & 1 & 0 & \cdots & 0 & 1 \\ 1 & 0 & 1 & \cdots & 0 & 0 \\ 0 & 1 & 0 & \cdots & 0 & 0 \\ \vdots & \vdots & \vdots & \ddots & 1 & 0 \\ 0 & 0 & 0 & 1 & 0 & 1 \\ 1 & 0 & 0 & 0 & 1 & 0 \end{pmatrix}, \tag{2.17}$$

where the elements with the value 1 are the ones on the left and right of the main diagonal, and also the elements $A_{1,n}$ and $A_{n,1}$. From that, we also can write as function of Kronecker deltas,

$$A_{ij}(C_n) = \delta_{ij-1} + \delta_{ij+1} + \delta_{i1}\delta_{jn} + \delta_{in}\delta_{j1}. \tag{2.18}$$

Figure 2.5 – Cycle graphs C_n with 3, 4, 5 and n vertices.

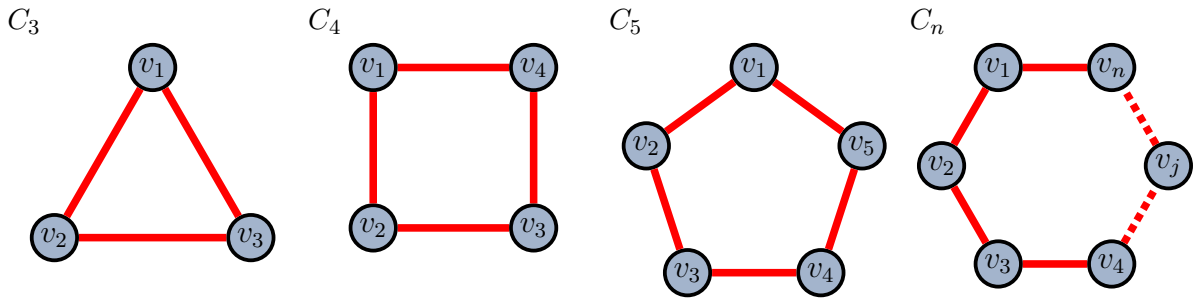

Source: the author.

As every vertex is always connected to other two vertices, its degree matrix is simply

$$D_{ij}(C_n) = 2\delta_{ij}. \tag{2.19}$$

This can also be understood as an identity matrix of dimensions $n \times n$ multiplied by two.

2.3.4 Wheel Graphs

A wheel graph is denoted by W_n and has n vertices and $2(n-1)$ edges. These graphs can be understood by a combination of construction of star graphs and cycle graphs. Similarly to star graphs, it has a central vertex, which is connected to all other vertices, but these peripheral vertices follow a construction similar to cycle graphs, where each vertex is connected to two other vertices, as illustrated in Figure 2.6.

It follows that the adjacency matrix for W_n graphs will have the form,

$$A\left(W_n\right) = \begin{pmatrix} 0 & 1 & 1 & \cdots & 1 & 1 \\ 1 & 0 & 1 & \cdots & 0 & 1 \\ 1 & 1 & 0 & \cdots & 0 & 0 \\ \vdots & \vdots & \vdots & \ddots & 1 & 0 \\ 1 & 0 & 0 & 1 & 0 & 1 \\ 1 & 1 & 0 & 0 & 1 & 0 \end{pmatrix}. \tag{2.20}$$

this is somehow similar to a combination of the adjacency matrices obtained for S_n and C_{n-1}. The first line and column is equal to the one

Figure 2.6 – Wheel graphs W_n with 4, 5, 6 and n vertices.

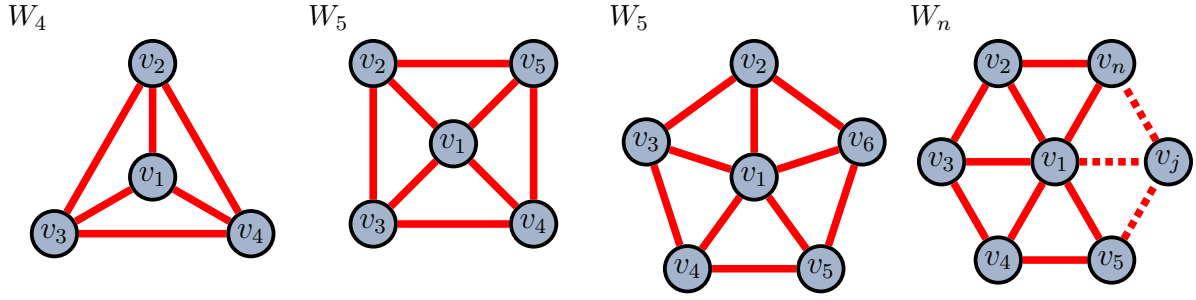

Source: the author.

obtained in star graph, due their central vertex have similar connectivity properties. The remaining parts of the matrix can be understood as equal to the adjacency matrix of a cycle vertex or $n-1$ vertices. That is, if the first line and first column are removed, obtaining the so-called principal submatrix $a_{1,1}$, it will be equal to the adjacency matrix of a C_{n-1} graph,

$$A\left(W_n\right) = \begin{pmatrix} 0 & 1 & \cdots & 1 \\ 1 & & & \\ \vdots & & C_{n-1} & \\ 1 & & & \end{pmatrix}. \tag{2.21}$$

Its elements can be obtained from the expression

$$A_{ij}\left(W_n\right) = \left(\delta_{i1} - \delta_{j1}\right)^2 + \left(1 - \delta_{i1} - \delta_{j1}\right)\left(\delta_{ij-1} + \delta_{ij+1}\right) + \delta_{i2}\delta_{jn} + \delta_{in}\delta_{j2}. \tag{2.22}$$

In the vertex degree properties in graph family, we can verify that the central vertex has a degree $(n-1)$, while the peripheral ones have the same degree 3. Thus, the elements of its degree matrix are given by

$$D_{ij}(W_n) = \left(3 + (n-4)\delta_{i1}\right)\delta_{ij}. \tag{2.23}$$

2.3.5 Complete Graphs

Complete graphs are defined as K_n and is a family of simple graphs with the highest possible number of connections between the n vertices, having $n(n-1)/2$ edges, as shown in Figure 2.7. Consequently, this graph

Figure 2.7 – Complete graphs K_n with 3, 4, 5 and n vertices.

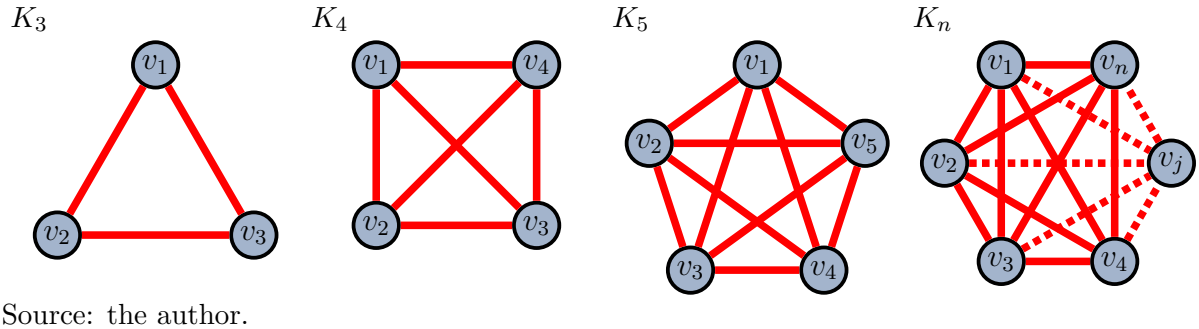

Source: the author.

is defined as fully connected, which implies that its adjacency matrix is given by

$$A\left(K_n\right) = \begin{pmatrix} 0 & 1 & 1 & \cdots & 1 & 1 \\ 1 & 0 & 1 & \cdots & 1 & 1 \\ 1 & 1 & 0 & \cdots & 1 & 1 \\ \vdots & \vdots & \vdots & \ddots & 1 & 1 \\ 1 & 1 & 1 & 1 & 0 & 1 \\ 1 & 1 & 1 & 1 & 1 & 0 \end{pmatrix}, \tag{2.24}$$

which is the same for any labelling of its vertices. As $A(K_n)$ has all of its elements equals to 1, except for the main diagonal, its elements is written as

$$A_{ij}(K_n) = 1 - \delta_{ij}. \tag{2.25}$$

For its degree matrix, we simply have that,

$$D_{ij}(K_n) = (n-1)\delta_{ij}, \tag{2.26}$$

because each vertex will always be connected to the other $n-1$ vertices.

2.4 WEIGHTED AND METRIC GRAPHS

The graphs described until now are defined by binary connections between its vertices, where either a pair of them is connected and receives a value 1, or they are not connected and receive the value 0. However, there

Figure 2.8 – Example of a metric graph where lengths $\ell_{i,j}$ are defined along each edge $e_{\{i,j\}}$ of a graph.

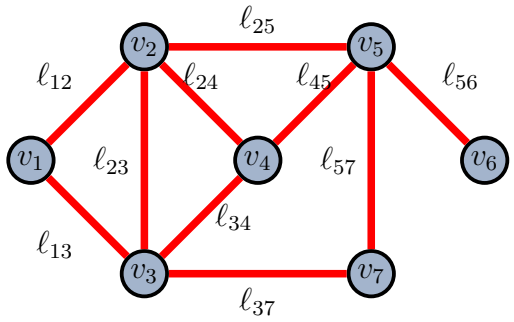

Source: the author.

are some cases where having only this relation between vertices is not sufficient. For example, when modelling networks as social networks where the frequency of contact of individuals is necessary, or in internet networks where it may be necessary to know the bandwidth between the connections.[38] In these cases, an additional value is necessary, which receives the name of weight w_e of the edge e. Thus, graphs with weight on their edges are called weighted graphs and are necessary in the analysis of networks, being used to define optimisation models.[32] Some visual representations when drawing weighted graphs can include writing the value of the edge weight next to it, or representing each edge with thickness proportional to its weight.

In some cases, such as in logistical networks where the best travel route is aimed, it is necessary to know the distance between its elements. To achieve that, it is also possible to define each edge $e_{\{i,j\}}$ of the graph that has certain lengths ℓ_{ij}. Attributing a distance between the vertices and considering these edges as one-dimensional entities also allows defining positive coordinates $x_{ij} \in [0, \ell_{ij}]$ along them. Graphs like these are called metric graphs, as the one illustrated in Figure 2.8.[36]

Some areas of physics benefit from these metric graphs, by using them to describe some structures and its metrics along the edges to define operators along it. As an example, we have the quantum graphs which are used to model the scattering in some structures, and will be the focus along the following chapters.

3 QUANTUM GRAPHS

The basis for graph theory applications to define structures of connected one-dimensional quantum wires can be retrieved from studies like the one presented by Linus Pauling in 1936, where he proposed to use rectilinear hexagonal nets to describe aromatic hydrocarbon molecules and the electron flow between adjacent atoms on them[5,6]. This led to applications in other molecules, such as in the work by John Stanley Griffith in 1952, using Schrödinger's equation for a free electron in an one-dimensional box to obtain the electron density along the naphthalene molecules.[7,8] Further studies were presented in the direction of scattering in one-dimensional multiconnected quantum systems, as the ones in connection with Anderson transition in disordered wires[39,40]. Others proposed them acting as waveguides in mesoscopic quantum systems[41,42], network models for adiabatic quantum transport[43] or in quantum Hall systems[44].

In works in quantum mechanics that are directly linked to graphs, we found the one presented by Pavel Exner and Petr Šeba in 1989, where they suggested concentrating the studies and experiments of quantum mechanics on thin wires in the so-called "quantum mechanics on graphs".[45] Further, the works of Tsampikos Kottos and Uzy Smilansky in 1997 used the term "quantum graphs" and showed that this model can be used to study quantum chaos, showing that it is possible to obtain analytical solutions in quantum graphs even when they present chaotic behaviour[20,21,46–49].

Thus, let us define these models of quantum graphs.

Definition 3.0.1 (Quantum graph)**.** *A quantum graph (QG) has a notation Γ_G, and it is defined by a triple of conditions:*[36]

i. A metric graph $G(V, E)$;

ii. A differential operator $\mathcal{H}$ (Hamiltonian) defined in each of its edges;

iii. A set of boundary conditions on its vertices.

As defined for metric graphs, each edge $e_{\{i,j\}}$ will be associated with

a positive length ℓ_{ij}. Thus, the coordinates $x_{ij} \in [0, \ell_{ij}]$ are defined along them. This allows to define an operator, such as the one-dimensional magnetic Schrödinger operator, to be applied on each edge,[27,36]

$$\mathcal{H}_{ij} = \frac{1}{2m}\left(\frac{\hbar}{i}\frac{d}{dx_{i,j}} - q\boldsymbol{\mathcal{A}}_{ij}(x_{ij})\right)^2 + qV_{ij}(x_{ij}), \tag{3.1}$$

where $\boldsymbol{\mathcal{A}}_{ij}$ is the magnetic vector potential and $V_{ij}(x_{ij})$ is the electric potential along the edge. Throughout the study here, we will consider the scattering of a free particle in a one-dimensional multiconnected system. Thus, without the action of the electric potential or the magnectic vector potential, this becomes

$$\mathcal{H}_{ij} = -\frac{\hbar^2}{2m}\frac{d^2}{dx_{ij}^2}. \tag{3.2}$$

With the operator defined along $e_{\{i,j\}}$, the functions along the graph $\psi_{ij}(x_{ij})$, as illustrated in Fig. 3.1, will be obtained from the second order differential equation

$$-\frac{d^2\psi_{ij}(x_{ij})}{dx_{ij}^2} = k^2\psi_{ij}(x_{ij}). \tag{3.3}$$

Thus, $\psi_{ij}(x_{ij})$ is a wave function with wavenumber $k = \sqrt{2\mathbf{m}\mathcal{E}/\hbar^2}$, where $\mathbf{m}$ is the mass of the particle and $\mathcal{E}$ its energy. These wavefunctions can be written in the form

$$\psi_{ij}(x) = a_{ij}e^{ikx} + b_{ij}z_{ij}e^{-ikx}, \tag{3.4}$$

Figure 3.1 – Metric graph with wavefunctions ψ_{ij} defined on each edge $e_{\{i,j\}}$.

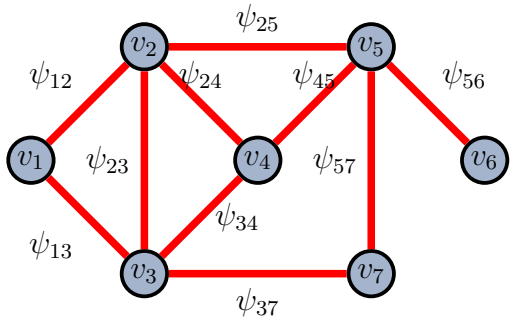

Source: the author.

where $z_{ij} = e^{ik\ell_{ij}}$ is a metric parameter for the length of the edge. A set of equations of the wavefunctions in the graph is obtained, one for each edge of the graph, defining a system of equations. To solve this system of equations, more equations are necessary, as there are two parameters (a_{ij} and b_{ij}) to be obtained from each of them. These equations are obtained from the boundary conditions.

3.1 BOUNDARY CONDITIONS

For a given vertex in the graph, we must define the boundary conditions for the wavefunctions on the edges adjacent to it. Thus, for a vertex v_i of degree d_i the set functions with ends at it

$$\Psi(v_i) = \begin{pmatrix} \psi_{i\mathcal{N}_1^i}(v_i) \\ \psi_{i\mathcal{N}_2^i}(v_i) \\ \vdots \\ \psi_{i\mathcal{N}_{d_i}^i}(v_i) \end{pmatrix}, \tag{3.5}$$

where $\mathcal{N}^i$ is the set of vertices adjacent to v_i. As the Hamiltonian is a second-order differential operator, two conditions per edge are needed, generally involving the values of the wavefunctions in $\Psi(v_i)$, as well as their derivatives.

A first example is the *Neumann* boundary conditions, sometimes also called *Neumann-Kirchhoff* or *standard conditions.*[36] This is defined so that the functions along the QG are always continuous and the current is conserved. Hence in a vertex v_i with this boundary conditions (B. C.), the following must be satisfied

$$\text{Neumann B. C.} : \begin{cases} \psi(x) \text{ is continuous at } v_i, \\ \displaystyle\sum_{j\in\mathcal{N}^i} \frac{d\psi}{dx_{ij}}(v_i) = 0. \end{cases} \tag{3.6}$$

However, in Dirichlet boundary conditions, the function is still con-

tinuous along the QG, but it vanishes on its vertices, hence

$$\text{Dirichlet B. C. } : \begin{cases} \psi(x) \text{ is continuous at } v_i, \\ \psi(v_i) = 0. \end{cases} \tag{3.7}$$

This is also known as decoupling condition, due to the fact the functions in adjacent edges do not transmit through these vertices, the results will be equivalent to detach these d_i adjacent edges, forming edges with this end at vertices of degree 1 with Dirichlet boundary condition.[50]

Both can be grouped as limiting cases of the same condition as the so-called δ boundary condition. It is analogous to conditions for the one-dimensional Schrödinger equation with a potential defined by a Dirac δ function[51]. Hence, this can be defined as

$$\delta \text{ B. C. : } \begin{cases} \psi(x) \text{ is continuous at } v_i, \\ \sum_{j \in \mathcal{N}^i} \dfrac{d\psi}{dx_{ij}}(v_i) = \alpha_{v_i} \psi(v_i), \end{cases} \tag{3.8}$$

being α_{v_i} a parameter that defines the delta function intensity at v_i. In this sense, the limit $\alpha_i = 0$ leads to the Neumann boundary condition, while the limit for $\alpha_i \to \infty$, the Dirichlet one is obtained.

These boundary conditions allow us to interpret the vertices of the QG as scattering centres, transmitting some part of the wavefunction in a given edge to the other adjacent edges, while there is also a reflected part to the same edge. From Eq. (3.8), in a given vertex with degree $d_i \geq 2$, e.g. a branch intersection of d_i scattering channels connected at this same point, the following reflection and transmission amplitudes are obtained

$$r_i = \frac{\alpha_i - (d_i - 2)\, ik}{d_i ik - \alpha_i}, \tag{3.9}$$

$$t_i = \frac{2ik}{d_i ik - \alpha_i}, \tag{3.10}$$

which are dependent on the wavenumber of the particle, the degree of the vertex, and the intensity of the delta function at it. Both of these results

can be rewritten in a single form, by considering the scattering from an edge $\{j,i\}$ to another edge $\{i,j'\}$ through the vertex v_i[21,51,52]

$$\boldsymbol{\sigma}_i^{\{j,i\},\{i,j'\}}(k) = \left(\frac{2ik}{d_i ik - \alpha_i} - \delta_{j,j'}\right), \tag{3.11}$$

from what t_i is retrieved when $j' \neq j$ and r_i for $j' = j$. Thus, for Neumann B. C., where $\alpha_i = 0$,

$$\boldsymbol{\sigma}_i^{\{j,i\},\{i,j'\}}(k) = \frac{2}{d_i} - \delta_{j,j'} \tag{3.12}$$

is obtained.

Solving for a dead end vertex, that is, for $d_i = 1$, there will be only the reflection part. Hence, the scattering amplitude at it is[28]

$$r_i = \boldsymbol{\sigma}_i^{\{j,i\},\{i,j\}}(k) = \frac{ik + \alpha_i}{ik - \alpha_i}. \tag{3.13}$$

For the limit values for $\alpha_i = 0$, the reflection amplitude with a Neumann boundary condition is $r_i = 1$, while for the Dirichlet condition, in the limit for $\alpha_i \to \infty$, it is $r_i = -1$.

3.2 GREEN'S FUNCTION FOR QUANTUM GRAPHS

When dealing with differential equations, one method to solve it is using the Green function method.[53] In the case associated to the Hamiltonian $\mathcal{H}(x_f)$ of a system, it is defined by the nonhomogeneous differential equation

$$[\mathcal{E} - \mathcal{H}(x_f)]\mathcal{G}(x_f, x_i; \mathcal{E}) = \delta(x_f - x_i), \tag{3.14}$$

where the Hamiltonian operator here could be defined by the equation (3.1), $\mathcal{E}$ is the particle energy and δ is the Dirac's delta function. For some systems such as quantum wells or square potentials, the exact form of Green's function for the system can be obtained.

The first applications of studies on quantum graphs by the Green's function method considered families of all possible paths $P_{x_i x_f}$, from a point x_i to another point x_f along the graph. At these points the particle can be

scattered according to a boundary condition there and will form another family of paths. As an example, we present the Fig. 3.2 where P_{ij} are related to the amplitudes of the wavefunction components to each direction in regions of constant potential. At some points, there will be boundary conditions associated, which implies in some reflection and transmission scattering amplitudes, in this Fig. 3.2 it occurs at the points where there are potential changes. Hence, this method dealt with the Green's functions being defined by the composition of all possible trajectories defining an action in a similar method to the path integrals proposed by Feynman, where the evaluation is also over all possible trajectories.[54,55] Further studies show a direct way to obtain the exact Green's function of a QG which is the method that we will explain and explore in this section.[27–29]

In order to study the scattering in QGs using Green's function, we should add leads on it, where the initial and final points (x_i and x_f) will be defined. The entrance vertex will be defined as v_i and the exit vertex

Figure 3.2 – Representation of one-dimensional step potentials with arrows representing the possible paths of a particle scattering on it. Below, there is its respective dressed QG, where the thickness of the edge represents the potential associated in that region, and the possible paths inside the region become the family of paths from one vertex to another P_{ij}.

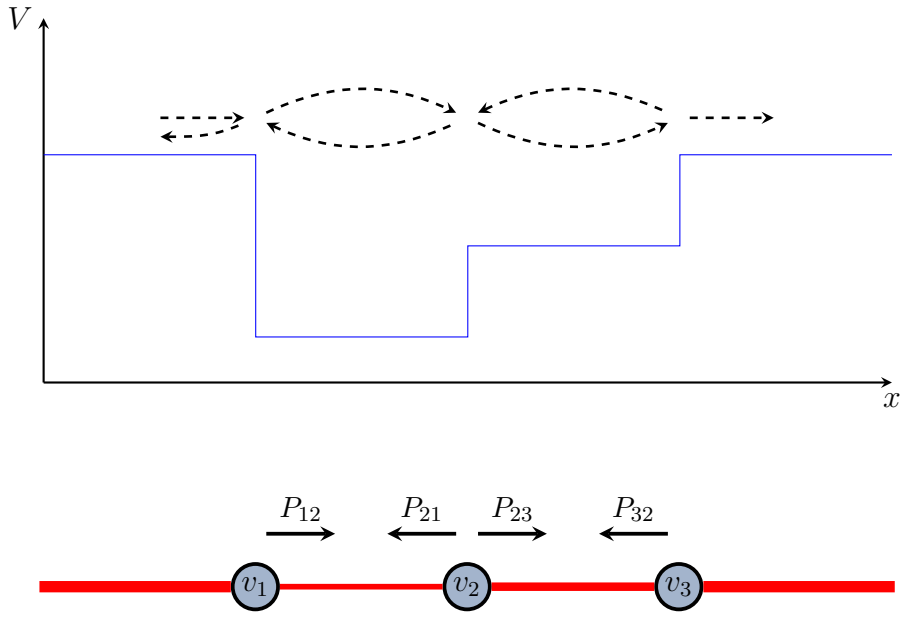

Source: the author.

will be called v_f. Hence, each of these leads increases the degree of the vertices to which they are attached ($d_{v_i} \to d_{v_i} + 1$ and $d_{v_f} \to d_{v_f} + 1$). This is exemplified in Fig. 3.3, where an initial graph G has leads attached to it at the vertices v_i and v_f.

In each edge $e_k = \{v_i, v_j\}$ of the graph, two families of paths will be defined, P_{ij} and P_{ji}, associated with the amplitudes of the wave function going from v_i to v_j and from v_j to v_i, respectively. Each of these path families will travel through a distance ℓ_{e_k} and scatter at the final vertex of this path, that is, v_j for P_{ij}. The scattering in this vertex will define the other families of paths that start in this same vertex and end on its adjacent vertices. Furthermore, if a lead is attached to this vertex, there will be transmission of the particle leaving the QGs. Thus, this approach leads to the solution of the Green's function for quantum graphs given by

Solution 1. *The Green's function for a quantum graph Γ_G^l is given by*

$$\mathcal{G}_{\Gamma_G^l}(x_f, x_i; k) = \frac{m}{i\hbar^2 k}\left[\delta_{f,i} e^{ik(|x_f - x_i|)} + \sigma_\Gamma^{(f,i)}(k)\, e^{ik(|x_f| + |x_i|)}\right], \tag{3.15}$$

where there is l leads attached to it and its scattering coefficients $\sigma_\Gamma^{(f,i)}$ are defined from one lead l_i to another lead l_f is obtained from its adjacency matrix A, the reflection $r_j = \sigma_j^{\{i,j\},\{j,i\}}$, and transmission amplitudes $t_j =$

Figure 3.3 – (a) Example of a quantum graph, (b) two leads i and f added on the vertices v_1 and v_4, (c) leads added on all vertices and a choice of i and f.

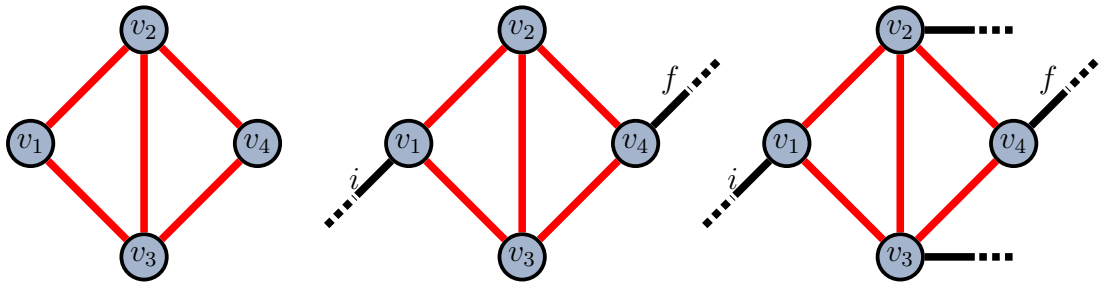

Source: the author.

$\sigma_j^{\{i,j\},\{j,l\neq i\}}$, *are in the form*[29]

$$\sigma_{\Gamma_G^l}^{(f,i)}(k) = \delta_{fi} r_i + t_i \sum_{j=1}^{|V|} A_{ij} P_{ij}. \tag{3.16}$$

With the scattering families given by the solution of a system of equations whose elements are

$$P_{ij} = z_{ij} \left[\delta_{fj} t_j + r_j P_{j,i} + t_j \sum_{l \in (V \backslash \{v_i\})} A_{jl} P_{jl} \right], \tag{3.17}$$

where $l \in (V \backslash \{v_i\})$ *defines that the summation is over all vertices* $v_l \in V$*, except* v_i *and* $z_{ij} = e^{ik\ell_{ij}}$.

This formulation for the Green's function in a QG from its adjacency matrix allows us to simplify the evaluation of the scattering in this system, as the necessary inputs are the vertices where the leads are attached, the adjacency matrix of the graph, the scattering amplitudes in each vertex, and the length associated with each edge.

The fact that the evaluation of Green's function for a QG utilises the scattering amplitudes of its vertices allows us to simplify the evaluation of QGs scattering amplitudes when the amplitudes of some internal structures of the QG are already known. In this case, a given internal structure formed by a set of vertices and edges of the original QG is rearranged to

Figure 3.4 – A quantum graph with 7 vertices and its respective simplification when the set of vertices $\{v_2, v_4, v_5\}$ and the edges between them were simplified to an effective vertex, which in this case is the quantum graph defined by K_3.

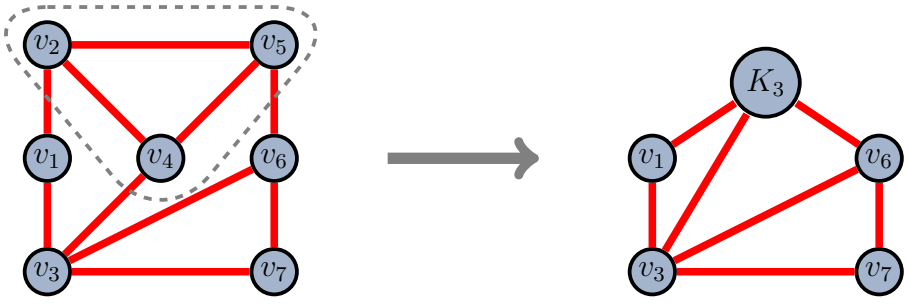

Source: the author.

an effective vertex, which should have all the same connections and the scattering amplitude of the simplified structure. Then, the scattering amplitudes in the original QG can be obtained from the Green's function evaluation of the effective QG with this new set of amplitudes on its vertices. In Figure 3.4, there is an example of a QG, where a set of vertex and edges is simplified to an effective vertex. In the following section, we will illustrate other methods used to simplify the evaluation of the scattering amplitudes.

3.3 SCATTERING MATRIX AND TRANSFER MATRIX

When dealing with wave propagation in systems, especially when studying the transmission and reflection amplitudes in these systems, the Scattering Matrix and the Transfer Matrix are important tools. As wavefunctions often appear in the quantum mechanics context, as the ones present in the scattering in QGs presented here, these matrices can appear in some definitions or be used in some analysis of these systems. Thus, in this section, we will explain their definitions, applications, and the relations between both approaches.

3.3.1 Scattering Matrix

The scattering matrix describes the relationship between the incoming and outgoing waves in a given scattering centre. For example, as illustrated in Figure 3.5, there are two waves that ends in the sample, one from

Figure 3.5 – Illustration of the incoming and outgoing waves at a scattering centre with scattering matrix S with two scattering channels.

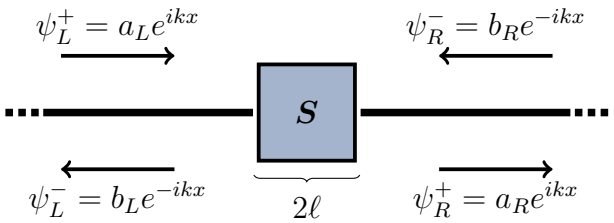

Source: the author.

the left,

$$\psi_L = \psi_L^+(x) + \psi_L^-(x) = a_L e^{ikx} + b_L e^{-ikx} \tag{3.18}$$

and another from the right

$$\psi_R = \psi_R^+(x) + \psi_R^-(x) = a_R e^{ikx} + b_R e^{-ikx} \tag{3.19}$$

where each of the + and − components are related with each direction of propagation. By defining the scattering region in the limits $-\ell < x < \ell$, the scattering matrix $\boldsymbol{S}$ of this system establishes the relationship

$$\boldsymbol{S} \begin{pmatrix} \psi_L^+(-\ell) \\ \psi_R^-(\ell) \end{pmatrix} = \begin{pmatrix} \psi_L^-(-\ell) \\ \psi_R^+(\ell) \end{pmatrix} \tag{3.20}$$

where this matrix can be rewritten as

$$\boldsymbol{S} = \begin{pmatrix} S_{1,1} & S_{1,2} \\ S_{2,1} & S_{2,2} \end{pmatrix} \tag{3.21}$$

when combined with Eq. (3.20), it gives the equations

$$\begin{cases} \psi_L^-(-\ell) = S_{1,1}\psi_L^+(-\ell) + S_{1,2}\psi_R^-(\ell) \\ \psi_R^+(\ell) = S_{2,1}\psi_L^+(-\ell) + S_{2,2}\psi_R^-(\ell) \end{cases} . \tag{3.22}$$

As one may notice, this can be related to the scattering amplitudes on the system, with $S_{1,1} = r_L$ the reflection on the left side, $S_{1,2} = t_R$ the transmission from the right to the left side, $S_{2,1} = t_L$ the transmission from the right to the left side and $S_{2,2} = r_R$ the reflection on the right. Hence,

$$\boldsymbol{S} = \begin{pmatrix} r_L & t_R \\ t_L & r_R \end{pmatrix} . \tag{3.23}$$

On the properties of this matrix, due to the conservation of current, it must be unitary,

$$\boldsymbol{S}^\dagger \boldsymbol{S} = \boldsymbol{1}, \tag{3.24}$$

where $\boldsymbol{S}^{\dagger}$ is the complex conjugate transpose matrix of $\boldsymbol{S}$

$$\boldsymbol{S}^{\dagger} = \begin{pmatrix} r_L^* & t_L^* \\ t_R^* & r_R^* \end{pmatrix}, \tag{3.25}$$

with r_j^* and t_j^* the complex conjugate from r_j and t_j, respectively. This leads to the relations

$$\begin{pmatrix} |r_L|^2 + |t_L|^2 & r_L^* t_R + t_L^* r_R \\ t_R^* r_L + r_R^* t_L & |r_R|^2 + |t_R|^2 \end{pmatrix} = \begin{pmatrix} 1 & 0 \\ 0 & 1 \end{pmatrix}, \tag{3.26}$$

which shows the unitarity of the scattering from each side of the system by $|r_j|^2 + |t_j|^2 = 1$.

A second property is related to the time reversion symmetry, as for any ψ that is a solution, ψ^* is also a solution, this leads to

$$\boldsymbol{S} \begin{pmatrix} \psi_L^{-*}(-\ell) \\ \psi_R^{+*}(\ell) \end{pmatrix} = \begin{pmatrix} \psi_L^{+*}(-\ell) \\ \psi_R^{-*}(\ell) \end{pmatrix}. \tag{3.27}$$

From the conjugate of Eq. (3.20)

$$\boldsymbol{S^*} \begin{pmatrix} \psi_L^{+^*}(-\ell) \\ \psi_R^{-*}(\ell) \end{pmatrix} = \begin{pmatrix} \psi_L^{-*}(-\ell) \\ \psi_R^{+*}(\ell) \end{pmatrix}, \tag{3.28}$$

and combining these equations, we arrive to the relation

$$\boldsymbol{S S^*} \begin{pmatrix} \psi_L^{+^*}(-\ell) \\ \psi_R^{-*}(\ell) \end{pmatrix} = \begin{pmatrix} \psi_L^{+*}(-\ell) \\ \psi_R^{-*}(\ell) \end{pmatrix}, \tag{3.29}$$

implying that $\boldsymbol{S}$ also must be symmetrical,

$$\boldsymbol{S S}^* = \mathbf{1}, \tag{3.30}$$

Thus, for a time reversal symmetry, both transmission amplitudes are equal and can be rewritten as $t_L = t_R = t$.

3.3.2 Transfer Matrix

Another interesting matrix on scattering studies is the so-called transfer matrix $\boldsymbol{M}$, in which the relationship it provides is between the wavefunctions in the left with the waves on the right side as illustrated in Figure 3.6 and equations as follows,

$$\boldsymbol{M}\begin{pmatrix}\psi_L^+(-\ell)\\ \psi_L^-(-\ell)\end{pmatrix}=\begin{pmatrix}\psi_R^+(\ell)\\ \psi_R^-(\ell)\end{pmatrix}. \tag{3.31}$$

with

$$\boldsymbol{M}=\begin{pmatrix}M_{1,1} & M_{1,2}\\ M_{2,1} & M_{2,2}\end{pmatrix}. \tag{3.32}$$

returning the relations

$$\begin{cases}\psi_R^+(\ell)=M_{1,1}\psi_L^+(-\ell)+M_{1,2}\psi_L^-(-\ell),\\ \psi_R^-(\ell)=M_{2,1}\psi_L^+(-\ell)+M_{2,2}\psi_L^-(-\ell).\end{cases} \tag{3.33}$$

The utility of this matrix becomes clear when studying scatterer disposed in a series layout. As M links the wavefunction in one scattering channel with the wavefunction in the other, this last one may be connected on other scatterer. For instance, as illustrated in Figure 3.6 (b), for three scatterers with transfer matrices M_1, M_2 and M_3, the wavefunction ψ_a and ψ_d are

Figure 3.6 – Illustration of the incoming and outgoing waves at a scattering centre with transfer matrix M with two scattering channels. (a) Only one scatterer. (b) Scatterers with transfer matrices M_1, M_2 and M_3 arranged in a series layout.

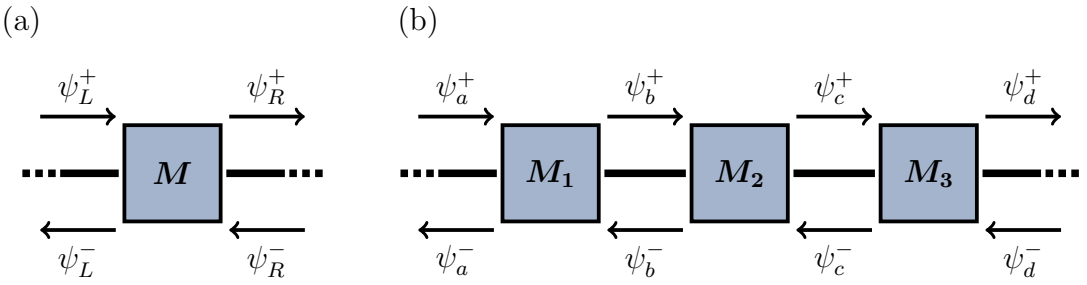

Source: the author.

linked by the product of these matrices in the form

$$\begin{pmatrix} \psi_d^+ \\ \psi_d^- \end{pmatrix} = M_3 M_2 M_1 \begin{pmatrix} \psi_a^+ \\ \psi_a^- \end{pmatrix} \tag{3.34}$$

Thus, it is helpful on evaluation of such systems by knowing the transfer matrix of each individual subsystem in series.

In order to obtain the transfer matrix from the scattering amplitudes of a given system, it is interesting to compare the system of equations in Eq. (3.33) with the one obtained in the scattering matrix case from Eq. (3.22) which can be rewritten as

$$\begin{cases} \psi_R^+(\ell) = S_{2,1}\psi_L^+(-\ell) + S_{2,2}\psi_R^-(\ell), \\ \psi_R^-(\ell) = -\frac{S_{1,1}}{S_{1,2}}\psi_L^+(-\ell) + \frac{1}{\cdot}S_{1,2}\psi_L^-(-\ell) \end{cases} \tag{3.35}$$

and by substituting the second one in the first,

$$\begin{cases} \psi_R^+(\ell) = \left(S_{2,1} - \frac{S_{2,2}S_{1,1}}{S_{1,2}}\right)\psi_L^+(-\ell) + \frac{S_{2,2}}{S_{1,2}}\psi_L^-(-\ell), \\ \psi_R^-(\ell) = -\frac{S_{1,1}}{S_{1,2}}\psi_L^+(-\ell) + \frac{1}{\cdot}S_{1,2}\psi_L^-(-\ell) \end{cases} \tag{3.36}$$

Finally, by comparing with Eq. (3.33), we find the relationship between the scattering matrix and the transfer matrix elements. Thus, the transfer matrix elements can be obtained from scattering matrix elements by

$$\boldsymbol{M} = \frac{1}{S_{1,2}} \begin{pmatrix} S_{2,1}S_{1,2} - S_{2,2}S_{1,1} & S_{2,2} \\ -S_{1,1} & 1 \end{pmatrix}, \tag{3.37}$$

or with the scattering amplitudes,

$$\boldsymbol{M} = \frac{1}{t} \begin{pmatrix} t^2 - r_R r_L & r_R \\ -r_L & 1 \end{pmatrix}. \tag{3.38}$$

Similarly, it is also possible to utilize the elements of the transfer matrix

to obtain the equivalent scattering matrix by

$$\boldsymbol{S} = \frac{1}{M_{2,2}} \begin{pmatrix} -M_{2,1} & 1 \\ M_{1,1}M_{2,2} - M_{1,2}M2,1 & M_{1,2} \end{pmatrix}. \tag{3.39}$$

This is useful to obtain the equivalent scattering amplitudes of the whole system after using the transfer matrix method to evaluate the scattering in the system. Thus, the method presented here to obtain the scattering matrix of a system consisting of subsystems in series arrangement is first to obtain the scattering matrix of each subsystem, second to transform them in their respective transfer matrix, third to multiply these transfer matrices, and fourth to transform the transfer matrix of the whole system in the scattering matrix. It is also interesting to suggest the possibility to evaluate the scattering matrix of systems in series, e.g. S_A and S_B, using the Redheffer star product $S_{A,B} = S_A \star S_B$. This directly associates the elements of the scattering matrix of each subsystem with the final scattering matrix of the system.[56,57] This application was also suggested for structures similar to QGs.[58]

3.4 SCATTERING ENTROPY OF QUANTUM GRAPHS

When dealing with probabilistic processes, a possible tool to study them is obtained from information theory, the Shannon entropy. This entropy proposed by Shannon[59] encodes the information from a given event with a set of probabilities p_j. For an event with probability $0 \leq p \leq 1$ to happen and $(1-p)$ to not happen, it will be written as

$$H(p) = -p\log_2(p) - (1-p)\log_2(1-p). \tag{3.40}$$

This entropy with the logarithm in basis 2 has unity *bit*. The maximum is at $p = 1/2$ with $H = 1$ and the minimum is at $p = 0$ or $p = 1$, acting as a measurement of the information of this event. That is, for already known results, no information is retrieved, while for equiprobable results, the information is maximal. For example, in a coin toss, the two possible

results are head, with probability p or tail, with probability $1-p$. With a fair coin, the probability of each event is the same, the informational entropy of the event is maximum, and the result of each toss has maximal surprise. However, when tossing a biased coin, one result is more probable than the other, which decreases the informational entropy, and the result becomes less surprising.

An extension is for l possible results from the same event. In this case it is defined as

$$H(p) = -\sum_{j=1}^{l} p_j \log_2(p_j), \tag{3.41}$$

with

$$\sum_{j=1}^{l} p_j = 1. \tag{3.42}$$

This is maximal for all $p_j = 1/n$ reaching $H = \log_2 n$. This entropy had been applied in the most diverse situations, such as in works on thermodynamics[60,61] or in localised energy configurations[62,63].

When dealing with QGs, the wave interference in these structures, due to their topology and its boundary conditions, returns probabilistic values in the form of transmission and reflection coefficients. In this sense, we proposed the application of the informational entropy on QGs by the following definition[64–66]

Definition 3.4.1 (Scattering entropy of quantum graph)**.** *For a chosen input channel i on a quantum graph Γ_G^l, with l scattering channels with scattering amplitudes $\sigma^{(j,i)}_{\Gamma_G^l}(k)$ which satis*

$$\sum_{j=1}^{l} \left|\sigma^{(j,i)}_{\Gamma_G^l}(k)\right|^2 = 1, \tag{3.43}$$

the scattering entropy (SE) is

$$H^{(i)}_{\Gamma_G^l}(k) = -\sum_{j=1}^{l} \left|\sigma^{(j,i)}_{\Gamma_G^l}(k)\right|^2 \log_2 \left|\sigma^{(j,i)}_{\Gamma_G^l}(k)\right|^2. \tag{3.44}$$

This entropy measures the distribution probability of the scattering for all channels. Being maximal means that the scattering process equally distributes the particle to all the channels. On the other hand, a minimal entropy (0) shows that the scattering is to only one of these channels. Extensions of this entropy, such as those proposed by Rényi and Tsallis, are also possible, and we have studied in the context of quantum graph.[66]

It can be studied in cases where the scattering coefficient has a given period K, e.g., when dealing with QGs with Neumann-Kirchhoff boundary conditions and the same edge lengths. In this case, we also propose an average scattering entropy.

Definition 3.4.2 (Average scattering entropy of quantum graphs)**.** *Let Γ_G^l be a quantum graph whose scattering probabilities have a period K, its scattering entropy will also have a period K, and its average scattering entropy (ASE) is*

$$\bar{H}^{(i)}_{\Gamma_G^l} = \frac{1}{K}\int_0^K H^{(i)}_{\sigma_{\Gamma_G^l}}(k)\,dk. \tag{3.45}$$

This is a measurement of the average equidistribution of the scattering over all channels.

3.5 RESULTS ON SCATTERING OF QUANTUM GRAPHS

Based on the definitions for QGs, the calculation of their scattering amplitudes using the Green's function method, as well as the scattering entropy and average scattering entropy, in this section, we will apply these concepts in the context of specific QG systems. The chosen QGs are defined by some construction pattern, which allows us to compare the growth of the QGs with the changes in its scattering properties. In this sense, first, we will start with some QGs families.

3.5.1 Scattering in quantum graphs families

In order to verify the behaviour of the transmission in QGs as a function of some variable, one may suggest studying it as a function of

the increase of vertices, and consequently the number of edges, in graph families. With that in mind, we focus on the family of graphs star (S_n), cycle (C_n), wheel (W_n) and complete (K_n). For scattering studies on these QGs, the studied cases have two leads i and f attached to their vertices v_1 and v_n, respectively, as illustrated in Figure 3.7 with $n = 5$. All vertices were defined with Neumann-Kirchoff boundary conditions and all the edges with same length ℓ.

The transmission amplitudes obtained on these QGs are presented up to 10 vertices, and are shown in tables in Appendix C. The results obtained for $n = 3, ..., 10$ are shown as a function of the wavenumber $\times$ edge length ($k\ell$) in Figure 3.8. Furthermore, it was possible to obtain the transmission amplitudes as a function of the vertices of the star, cycle, and complete QGs, as shown in Table 3.1.

From some early analysis of these results, it was possible to verify the following tendencies as the number of vertices in these QGs increases:

- Γ_{S_n}: its transmission peaks, localized on $k\ell$ equals to integer multiples of π, become increasingly narrow, while in the points out of these peaks there is the tendency of backscattering;
- Γ_{C_n}: the tendency is that the transmission becomes highly oscillating, but always limited inside of a certain region;
- Γ_{W_n} and Γ_{K_n}: the transmission becomes almost always suppressed, due to their transmission highly depends on its vertices degrees, which

Figure 3.7 – Examples of quantum graphs star, cycle, wheel and complete with 5 vertices and two leads i and f.

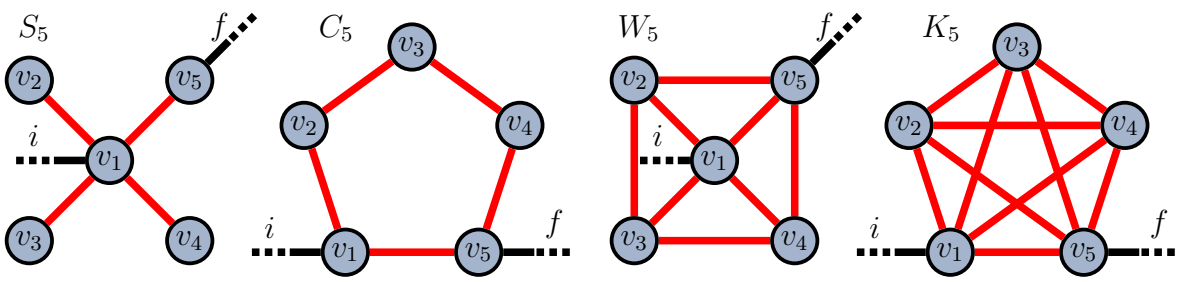

Source: the author.

increases the tendency of backscattering with n.

Next, it was possible to extend for the case of n leads, as illustrated in Figure 3.9. From this approach, the scattering amplitudes obtained as a function of the number of vertices for the quantum graphs defined by the families S_n, C_n, W_n, and K_n, are shown in Table 3.2. Due to the symmetry in the quantum graphs $\Gamma^n_{S_n}$, $\Gamma^n_{W_n}$ and $\Gamma^n_{K_n}$, their transmission amplitudes are the same for any vertices, differing only in their reflection. However, in cycle quantum graphs, the transmission amplitude of $\Gamma^n_{C_n}$ depends on the distance between the entrance vertex v_i and any possible exit vertex v_f where the chosen pair of leads i and $f \neq i$ are connected to. Also, the equation for Γ_{C_n} depends on whether n is a odd or even number. Hence, as quantum graphs with n leads have n scattering amplitudes, its anal-

Figure 3.8 – The transmission coefficient of the quantum graphs Γ^2_G with two scattering channels, defined by the quantum graph families star (S_n), cycle (C_n), wheel (W_n) and complete (K_n) as a function of wavenumber × edge length ($k\ell$).

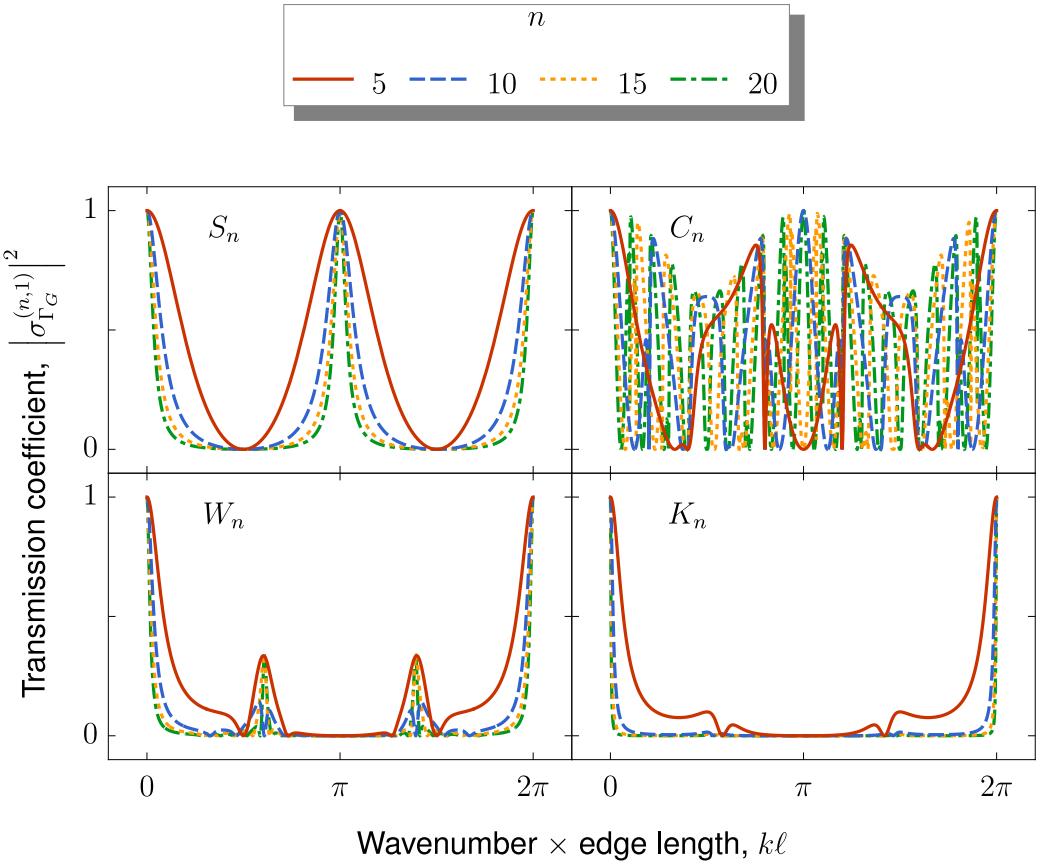

Source: the author.

Table 3.1 – Transmission amplitudes, with $z = e^{ik\ell}$, of the quantum graphs (Γ_G) with two scattering channels connected to the vertices v_i and v_n as function of their vertices number n.

G	Transmission amplitude $\sigma_{\Gamma_G}^{(f\neq i,i)}$
S_n	$\dfrac{2z(1+z^2)}{n-(n-4)z^2}$
C_n	$\dfrac{4z\left(z^n-1\right)\left(z^n+z^2\right)}{9z^2-z^4-z^{2n}-8z^{n+2}+z^{2n+2}}$
K_n	$\dfrac{4z\left(1+z\right)\left(2z+\left(n-1\right)\left(1+z^2\right)\right)}{\left(n+2z+\left(n-2\right)z^2\right)\left(n^2-n+\left(2+3n-n^2\right)z+\left(8-5n+n^2\right)z^2-\left(2-3n+n^2\right)z^3\right)}$

Source: the author.

ysis can also be simplified by the scattering entropy (SE) as illustrated in Figure 3.10, that combines all scattering amplitudes in an information measurement of the quantum graph.

The results for scattering entropy of families of quantum graphs with n scattering channels show some new interesting behaviours:

- $\Gamma_{S_n}^n$: the scattering probabilities are constant in function of $k\ell$, having the same scattering probabilities of the central vertex;
- $\Gamma_{C_n}^n$: increasing the values of n the entropy tends to the same curve. There is still a difference between some curves at $k\ell = \pi + 2j\pi$, with integer j, where the value of its entropy is the equal to the velues

Figure 3.9 – Examples of quantum graphs defined by S_n, C_n, W_n and K_n with n leads and $n = 5$ vertices.

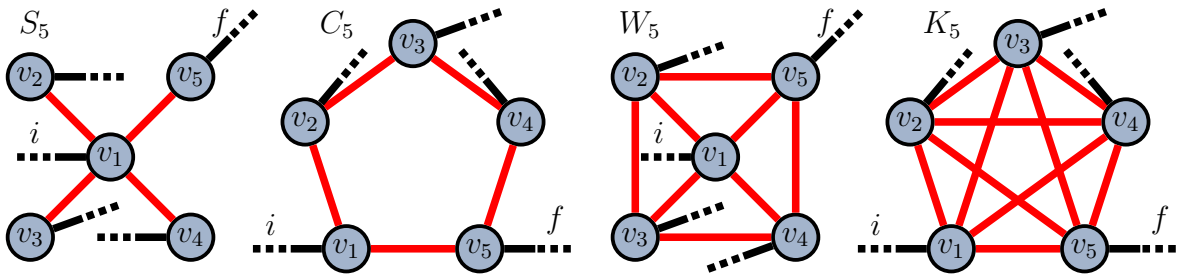

Source: the author.

Table 3.2 – Transmission amplitudes, of the quantum graphs (Γ_G^n) with n scattering channels as function of their vertices number n. With $z = e^{ik\ell}$, $\beta = \sqrt{9 - 10z^2 + z^4}$ and $\mu_\pm = 3 + z^2 \pm \beta$

G	Transmission amplitude $\sigma_{\Gamma_G^n}^{(f\neq i,i)}$
S_n	$\frac{2z}{n}$
$C_{\text{odd } n}$	$\frac{2^{2f-3} z^{(f-2)} (1+z) (\mu_+\mu_-)^{-f} \left[(4z-\mu_+) \sqrt{\mu_+^{2f+1}\mu_-^{n+4}} - (4z-\mu_-) \sqrt{\mu_+^{n+4}\mu_-^{2f+1}} \right]}{(3-z) \left[\sqrt{\mu_+\mu_-^n} (\mu_- + 4z) - \sqrt{\mu_+^n\mu_-} (\mu_+ + 4z) \right]}$
$C_{\text{even } n}$	$\frac{2^{4f-1} z^{(f-1)} \beta \mu_+\mu_- \left(\sqrt{\mu_+^{n+2-2f}} + \sqrt{\mu_-^{n+2-2f}} \right)}{(9-z^2) \mu_+\mu_- \left(\sqrt{\mu_+^n} - \sqrt{\mu_-^n} \right)}$
W_n	$\frac{2z(1+z)}{2n + (n-2)(z^2 - z^3)}$
K_n	$\frac{4z(1+z)}{n^2 - n(n-4)z + (n-2)^2 (z^2 - z^3)}$

Source: the author.

obtained on $\Gamma_{S_n}^n$ for odd n and 0 for even n;

- $\Gamma_{W_n}^n$: it is noticed a region with entropy near to 0 around $k\ell = \pi + 2j\pi$, that becomes wider with the increasing of n. It is also noticed some peaks at the ends of this region where the maximal scattering entropy for n channels is found;

- $\Gamma_{K_n}^n$: when increasing the number of vertices in a complete QG with standard boundary conditions, the tendency is to increase the backscattering. In this case, this implies in a behaviour of the scattering entropy near to zero for almost all values of $k\ell$.

Additionally, from these results on families of quantum graphs with two or n scattering channels, we can proceed and verify the average scattering entropy $\bar{H}$ as a function of the increasing vertices in both cases. The results obtained are shown in Figure 3.11, where it is possible to verify their behaviour. For S_n, in all three cases, the average scattering entropy (ASE) shows its behaviour proportional to the changes in the degree of the

central vertex. An interesting result in this QG is for the case n', where the normalised ASE is equal to 1 for $n = 4$, which is a case of equiprobable scattering on all its channels. The ASE for W_n and K_n shows a similar behaviour, which can be understood due to the higher dependence of their scattering amplitudes on their vertices degree, specifically in the K_n case where as all its vertex degrees increase with n, its ASE decreases faster. In C_n the tendency is for a saturation of the ASE as n increases, which can be expected when comparing it to the results in Figure 3.8, where the transmissions become more oscillating over the same region, and from Figure 3.10 where it was seen that the scattering entropy stabilises in some regions of $k\ell$ for higher n.

Figure 3.10 – Scattering entropy H of the quantum graphs Γ_G^n with n scattering channels, defined by the quantum graph families star (S_n), cycle (C_n), wheel (W_n) and complete (K_n) as a function of wavenumber × edge length ($k\ell$).

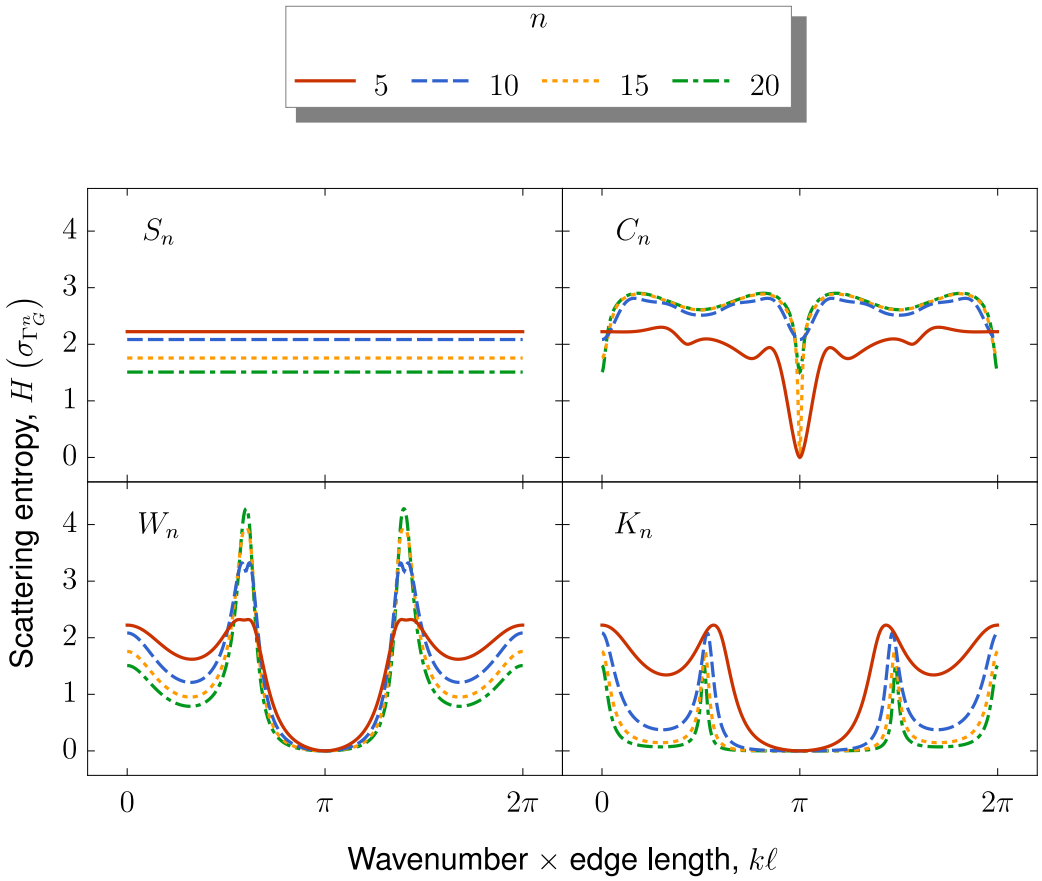

Source: the author.

3.5.2 Quantum graphs in series and parallel layouts

The scattering amplitudes of QGs can be evaluated through some simplification, such as considering an internal structure of the QG becoming an effective vertex. To do that, the scattering amplitudes of the internal structure must be known and will define the coefficients of this new vertex. Therefore, in this section, we will evaluate the scattering amplitudes of some QG which will be used to define some arrangements of other QGs. In this sense, the vertices v_j in these QGs should be defined with some scattering coefficients r_j and t_j, which can be further replaced by the coefficients of some already known QG.

Figure 3.11 – Average scattering entropy $\bar{H}$ of the quantum graphs Γ_G^c for the cases with $c = 2$ and $c = n$ scattering channels as a function of the number of vertices (n). In the n' case the scattering entropy is the same from n but divided by its maximum possible value $\log_2(n)$. The quantum graphs are defined by the families star (S_n), cycle (C_n), wheel (W_n) and complete (K_n).

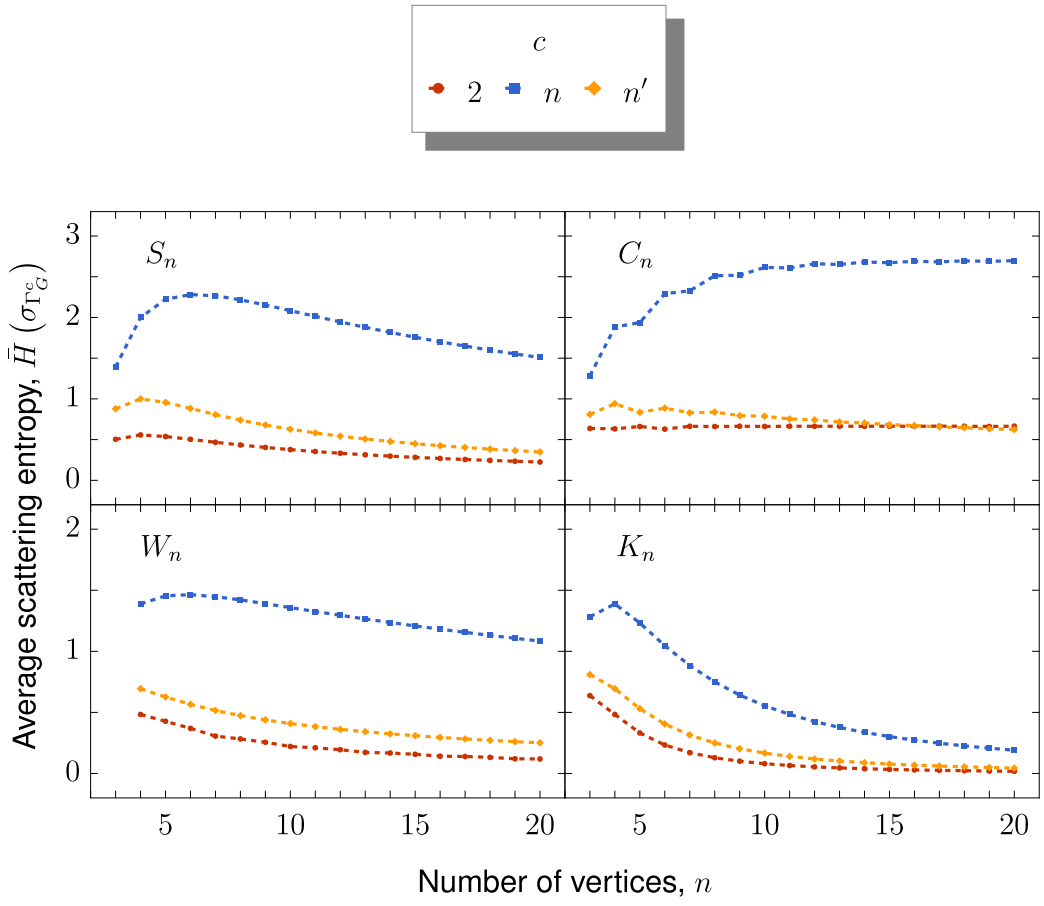

Source: the author.

In the first case, let us define a sequence of connected QGs as a series layout. The effective scattering amplitudes in this arrangement will be obtained here from a path quantum graph $\Gamma^2_{P_n}$. Initially we can define the path QG with 2 vertices, v_1 and v_2, and two leads, i and f, attached to these respective vertices, as illustrated in Figure 3.12 (a). The scattering amplitudes are

$$R_{\varsigma(v_1,v_2)} = r_1 + \frac{t_1^2 r_2 z^2}{1 - r_1 r_2 z^2}, \tag{3.46}$$

and

$$T_{\varsigma(v_1,v_2)} = \frac{t_1 t_2 z}{1 - r_1 r_2 z^2}, \tag{3.47}$$

where $z = e^{ik\ell}$ and ς is used to identify the series layout arrangement between v_1 and v_2. By doing the replacements $\{r_1, t_1\} \to \{R_{\varsigma(v_1,v_2)}, T_{\varsigma(v_1,v_2)}\}$ and $\{r_2, t_2\} \to \{r_3, t_3\}$, it will be obtained the reflection and transmission amplitudes of the case of $\Gamma^2_{P_3}$, or the series arrangement of the vertices v_1, v_2, and v_3 in the form

$$R_{\varsigma(v_1,v_2,v_3)} = R_{\varsigma(v_1,v_2)} + \frac{T^2_{\varsigma(v_1,v_2)} r_3 z^2}{1 - R_{\varsigma(v_1,v_2)} r_3 z^2}, \tag{3.48}$$

and

$$T_{\varsigma(v_1,v_2,v_3)} = \frac{T_{\varsigma(v_1,v_2)} t_3 z}{1 - R_{\varsigma(v_1,v_2)} r_3 z^2}. \tag{3.49}$$

Thus, these obtained scattering amplitudes can be extended for a chain of n vertices as in Figure 3.12 (b), forming a recursive equation system for

Figure 3.12 – (a) A path QG with two vertices, Γ_{P_2}, or a QG consisted on two vertices v_1 and v_2 in a series arrangement, $\Gamma_{\varsigma(v_1,v_2)}$. (b) A path QG with n vertices, Γ_{P_n}, or a graph consisted on n vertices $v_1, \ldots, v_n$ in a series arrangement, $\Gamma_{\varsigma(v_1,\ldots,v_n)}$.

(a) (b)

Source: the author.

$n \geq 3$ given by

$$R_{\varsigma(v_1,\ldots,v_n)} = R_{\varsigma(v_1,\ldots,v_{n-1})} + \frac{T^2_{\varsigma(v_1,\ldots,v_{n-1})} r_n z^2}{1 - R_{\varsigma(v_1,\ldots,v_{n-1})} r_n z^2}, \tag{3.50}$$

$$T_{\varsigma(v_1,\ldots,v_n)} = \frac{T_{\varsigma(v_1,\ldots,v_{n-1})} t_n z}{1 - R_{\varsigma(v_1,\ldots,v_{n-1})} r_n z^2}. \tag{3.51}$$

These equations can be used as an alternative recursive method for the transfer matrix method[67], utilising directly its coefficients without the transformations between the scattering matrix and the transfer matrix.

We can take the special case where the same quantum graph Γ_G, with scattering coefficients r_G and t_G is arranged in a series layout containing n copies of it, as illustrated in Figure 3.12 (b), for which we can define the notation $\varsigma_n(\Gamma_G)$. In this case, the reflection and transmission of the series arrangement is

$$R_{\varsigma_n(\Gamma_G)} = \frac{2\left(\Lambda_+^n - \Lambda_-^n\right) r_G}{\left(2 - \Lambda_-\right)\Lambda_+^n - \left(2 - \Lambda_+\right)\Lambda_-^n}, \tag{3.52}$$

and

$$T_{\varsigma_n(\Gamma_G)} = \frac{2^n \left(\Lambda_+ - \Lambda_-\right) t_G^n z^{n-1}}{\left(2 - \Lambda_-\right)\Lambda_+^n - \left(2 - \Lambda_+\right)\Lambda_-^n}, \tag{3.53}$$

with

$$\Lambda_\pm = 1 + \left(t_G^2 - r_G^2\right) z^2 \pm \left[1 - 2\left(r_G^2 + t_G^2\right) z^2 + \left(r_G^2 - t_G^2\right)^2 z^4\right]^{\frac{1}{2}}. \tag{3.54}$$

A second layout, starting with also two vertices v_1 and v_2 was proposed, but now they are arranged in parallel layout, $\varrho(v_1, v_2)$, as illustrated in Figure 3.13 (a). In this configuration, the central vertices are only adjacent to v_i and v_f, which are the ones connected to the leads. Let us define both vertices v_i and v_f with the amplitudes r and t, while the other vertices v_j have the amplitudes r_j and t_j and in their adjacent edges it is defined $z_j = e^{ik\ell_j}$. So, we find the scattering amplitudes for this arrangement in

the form

$$R_{\varrho(v_1,v_2)} = r + \frac{t^2}{\Lambda_{\varrho(v_1,v_2)}}\Big\{C_{1,2} + C_{2,1} + 2\left[tt_1t_2 - (2r-t)\,r_1r_2\right]z_1^2z_2^2 - 2\,(r+t)\,(r-t)^2\left(r_1^2-t_1^2\right)\left(r_2^2-t_2^2\right)z_1^4z_2^4\Big\}, \tag{3.55}$$

$$T_{\varrho(v_1,v_2)} = \frac{t^2}{\Lambda_{\varrho(v_1,v_2)}}\Big\{t_1z_1^2 + t_2z_2^2 - 2\,(r-t)\,(r_1t_2 + r_2t_1)\,z_1^2z_2^2 + (r-t)^2\left[\left(r_1^2-t_1^2\right)t_2z_1^2 + t_1\left(r_2^2-t_2^2\right)z_2^2\right]z_1^2z_2^2\Big\}, \tag{3.56}$$

where in order to simplify these equations, the following parameters were used

$$\Lambda_{\varrho(v_1,v_2)} = \left[1 - r\left(r_1z_1^2 + r_2z_2^2\right) + \left(r^2-t^2\right)(r_1r_2 + t_1t_2)\,z_1^2z_2^2\right]^2 - \left[r\left(t_1z_1^2 + t_2z_2^2\right) - \left(r^2-t^2\right)(r_1t_2 + t_1r_2)\,z_1^2z_2^2\right]^2, \tag{3.57}$$

and

$$C_{m,n} = \left[1 + r\,(r-t)\left(r_n^2-t_n^2\right)z_n^4\right]r_mz_m^2 + \left[\left(2r^2 - rt - t^2\right)r_nz_n^2 - r\right]\left(r_m^2-t_m^2\right)z_m^4. \tag{3.58}$$

This allows us to study any case of two parallel systems and also let the boundary conditions on the vertices at the ends and the edge lengths open.

Extending this study to obtain a general model of n copies of a quan-

Figure 3.13 – (a) A parallel arrangement of two vertices v_1 and v_2, $\Gamma_{\varrho(v_1,v_2)}$. (b) A parallel arrangement of n vertices $v_1,\ldots,v_n$, defined as $\Gamma_{\varrho(v_1,\ldots,v_n)}$.

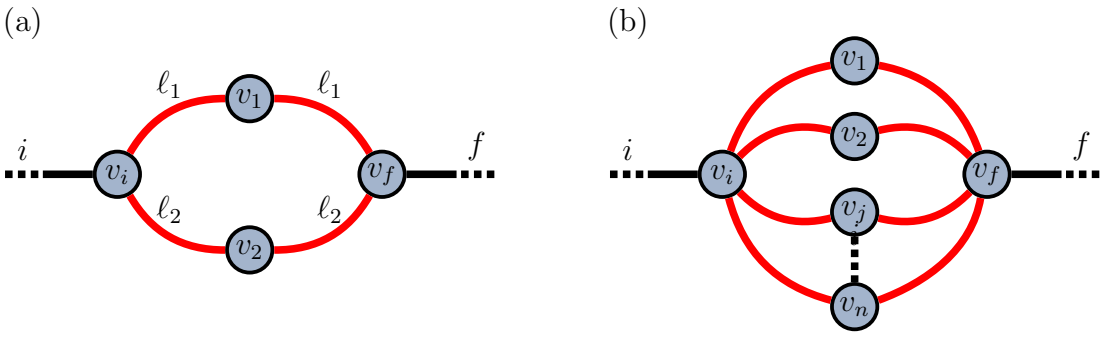

Source: the author.

tum graph Γ_G arranged in parallel, as illustrated in 3.13 (b), we used an approach where all vertices have the same scattering amplitudes r_G and t_G, all edges with the same length and the vertices connected to the leads have Neumann-Kirchoff boundary conditions on it. With these restrictions, it was possible to obtain scattering amplitudes in the form

$$R_{\varrho_n(\Gamma_G)} = \frac{2\left(n^2+1\right) r_G z^2 - \left(n^2-1\right)\left[1+\left(r_G^2-t_G^2\right) z^4\right]}{\left[n+1-(n-1)\, r_G z^2\right]^2 - (n-1)^2\, t_G^2 z^4}, \tag{3.59}$$

and

$$T_{\varrho_n(\Gamma_G)} = \frac{4 n t_G z^2}{\left[n+1-(n-1)\, r_G z^2\right]^2 - (n-1)^2\, t_G^2 z^4}. \tag{3.60}$$

In particular, one case of interest that can be obtained from this approach consists of two parallel edges, each one with a given length ℓ_1 and ℓ_2, as shown in Figure 3.14 (a). This model was used in some propositions for quantum devices[68,69], as changing the edge length parameters allows a certain control of the outcomes. To obtain this particular case, one can impose the standard boundary conditions, obtaining the scattering coefficients $r = -1/3$, $t = 2/3$, $r_j = 0$, and $t_j = e^{-ik\ell_j}$ and applying it in

Figure 3.14 – (a) Illustration of $\Gamma_{\varrho(\ell_1,\ell_2)}$ the quantum graph defined by two vertices are connected by two edges with lengths ℓ_1 and ℓ_2. (b) The QG $\Gamma_{\varrho_3(\varrho_2(\ell))}$, where three copies of the graph in (a) are arranged in parallel. (c) The QG $\Gamma_{\varsigma_3(\varrho_2(\ell))}$, where three copies of the graph in (a) are arranged in series.

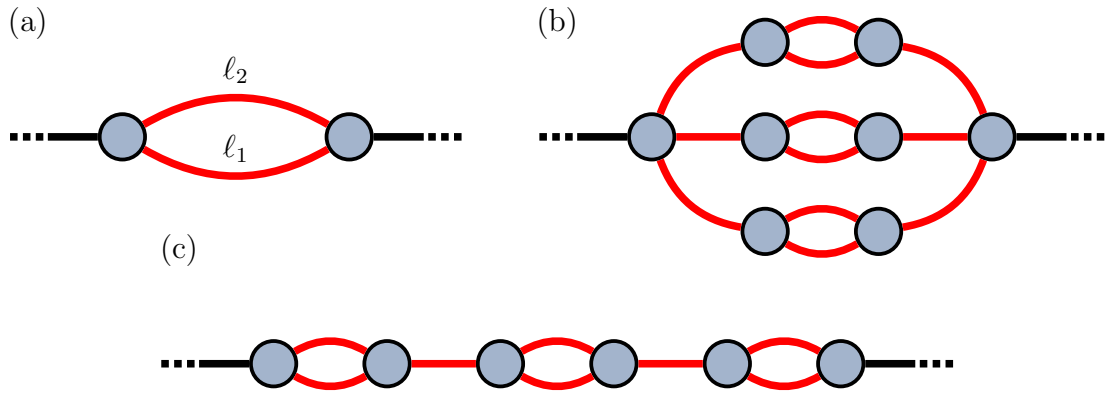

Source: the author.

equations (3.55) and (3.56), the obtained scattering amplitudes are

$$R_{\varrho(\ell_1,\ell_2)} = -\frac{3 + (z_1 - z_2)^2 - 3\,(2 - z_1 z_2)\, z_1 z_2}{(3 - z_1 z_2)^2 - (z_1 + z_2)^2}, \tag{3.61}$$

and

$$T_{\varrho(\ell_1,\ell_2)} = \frac{4\left[\left(1 - z_2^2\right) z_1 + \left(1 - z_1^2\right) z_2\right]}{(3 - z_1 z_2)^2 - (z_1 + z_2)^2}. \tag{3.62}$$

Additionally, in the limit where both edges have the same length, we thus obtain the scattering amplitudes

$$R_{\varrho_2(\ell)} = -\frac{3(1 - z^2)}{9 - z^2}, \tag{3.63}$$

$$T_{\varrho_2(\ell)} = \frac{8z}{9 - z^2}. \tag{3.64}$$

Similarly, for three edges in parallel,

$$R_{\varrho_3(\ell)} = -\frac{2(1 - z^2)}{4 - z^2}, \tag{3.65}$$

$$T_{\varrho_3(\ell)} = \frac{3z}{4 - z^2}. \tag{3.66}$$

We then propose a scheme for n copies of $\Gamma_{\varrho_2(\ell)}$ disposed in series and parallel layouts. The results of its scattering transmissions are shown in Figure 3.15, where it is possible to compare how their scattering profiles evolve by adding more copies of the same QG.

For a parallel layout, the behaviour of adding more graphs is to generally suppress the final signal, forming suppression bands whose width depends on the main structure with the influence of the degree increasing in the boundaries of the parallel system. In addition, some transmission peaks around $k\ell = \pi$ are observed, increasing the transmission coefficient compared to the transmission of structures alone ($n = 1$).

For the series layout, the suppression band formation is even more expressive, with the transmission coefficient quickly reaching 0 in the region around $k\ell = \pi$. For other values outside this gap, there is an envelope of the function that oscillates faster with the addition of more structures in series

and has maximal values 1 and the minimum values change accordingly to the structures in this layout. Something similar was found in a work that measures signal transmission in some topological quantum devices.[70]

We can analyse these scattering patterns especially in the context of the average scattering entropy (ASE). For the parallel layout, as the number of vertices increases, the tranmission quickly goes to zero and there remain some peaks, which results in the ASE having a tendency to go to zero. In the series arrangement, the ASE will have a tendency to saturate to some values that depend on the structures in these layouts, as we had studied some specific cases in this layout.[65,66]

These structures are interesting because some works have proposed cycle quantum graphs in series arrangements for quantum devices, meta-

Figure 3.15 – Transmission amplitude of n copies of $\Gamma_{\varrho_2(\ell)}$ arranged in (a) parallel, (b) series layout, and the same is done for $\Gamma_{\varrho_3(\ell)}$ in (c) parallel, (d) series layout.

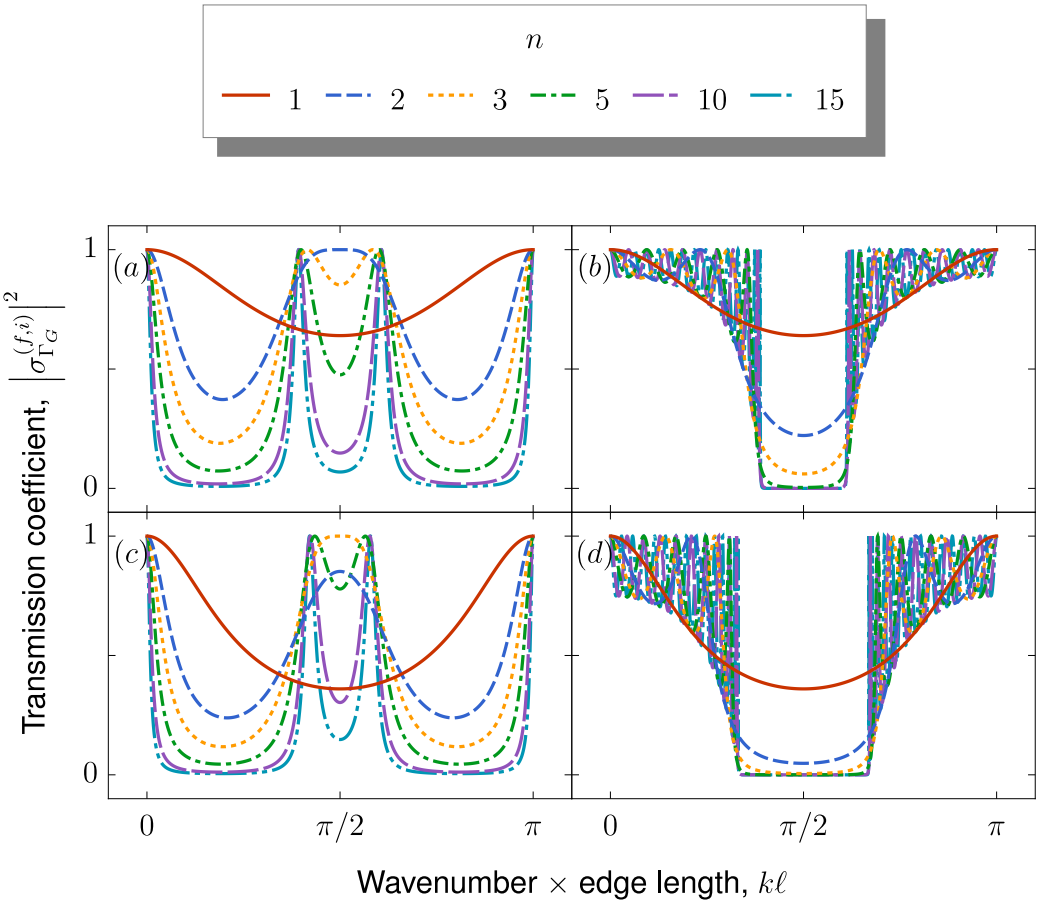

Source: the author.

networks and metamaterials using quantum graphs.[68,69,71,72] Moving forward, in the next chapter, we will also propose applications of quantum graphs acting to model the filament formation in some devices.

4 QUANTUM GRAPHS IN FILAMENTS SWITCHING MODELS

The model of quantum graphs can be used in some applications and in models of mesoscopic physics and nanotechnology. Leon Chua proposed an interesting nanodevice when he verified that nonlinear devices establish some links between voltage (V), current (I), charge (q) and magnetic flux (ϕ), such as capacitor ($dq = CdV$), inductor ($d\phi = LdI$) and resistor ($dV = RdI$), with straightforward connections of $d\phi = Vdt$ and $dq = Idt$. However, he noticed that the only relationship that had no definition at that moment was a link between the magnetic flux and charge, for what it proposes a device called memristor $d\phi = Mdq$, relating it to a resistor with memory due to its properties by combining these two quantities.[73] One of the implications of this model is the possibility of a pinched hysteresis curve in a current versus voltage curve in a current-controlled or a voltage-controlled system.[74,75] In order to model a memristor using a QG approach, let us first show how it is possible to obtain some electrical measurements on it.

4.1 LANDAUER-BÜTTIKER FORMALISM

The study of scattering in quantum systems can be applied in a context proposed by Landauer and Büttiker[76–83]. They showed a way to understand the electronic conduction at the nanoscale showing a relation between the conductance g of the scatterer and the transmission probability on it $T_{i,j}$, between any pair of scattering channels i and j, as being

$$g = g_0 \sum_{i,j} T_{i,j}, \tag{4.1}$$

where $g_0 = \frac{2q_e^2}{h}$ is the conductance quantum, with q_e the electron charge and h the Planck constant. In the case of only two scattering channels with transmission T, this becomes

$$g = g_0 T. \tag{4.2}$$

They also derived an equation relating the current I with the transmission probability T. For a system with two scattering channels i and j, it follows

$$I = g_0 \int_{-\infty}^{\infty} (f_i(\mathcal{E}) - f_j(\mathcal{E}))T(\mathcal{E})d\mathcal{E}, \tag{4.3}$$

where $\mathcal{E} = (\hbar^2 k^2/2m) + u$ is the particle energy. The distributions $f_i(\mathcal{E})$ and $f_j(\mathcal{E})$ are obtained from the particle distribution on each channel. For an electron it follows the Fermi-Dirac statistics, being the distribution in each scattering channel given by

$$f(\mathcal{E}) = \frac{1}{e^{(\mathcal{E}-\mu)/\kappa\mathbf{T}} + 1}, \tag{4.4}$$

where μ is a chemical potential, κ is the Boltzmann constant and $\mathbf{T}$ the temperature. This means that in each lead l can be assumed to have a specific μ_l or $\mathbf{T}_l$ and the difference between any of these values on different leads contributes to the current. Here, μ will be assumed depending on the voltage applied on each lead.

Thus, the electrical current in a given conductor with transmission probability T can be written as function of the difference of potential in the leads as

$$I = g_0 \int_{-\infty}^{\infty} \left(\frac{1}{e^{(\mathcal{E}-\mu_i)/\kappa\mathbf{T}} + 1} - \frac{1}{e^{(\mathcal{E}-\mu_f)/\kappa\mathbf{T}} + 1} \right) T(\mathcal{E})d\mathcal{E}. \tag{4.5}$$

This relation between the electrical current and the transmission probability allows to apply it on QGs. In order to do that, let us define a target model that can be approached by a QG.

4.2 CLASSICAL MODEL OF FILAMENT GROWTH AND EFFECTIVE QUANTUM GRAPH

In some works[84–88], the formation of a filament, which consists of the non-equilibrium process of chemically forming a filament in a narrow region, was considered, this is illustrated in Fig. 4.1 as an example of a fil-

ament formed by silver atoms. These models showed how the conductance changes with the growth of the filament.

In order to model filament growth, we first consider the simplest case of a directed random walk from the cathode to the anode. In this sense, let us start in a discrete grid of positions, as illustrated in Fig. 4.2 where the particle starts in the cathode (left), then for each iteration it always receives an increment of one position to the right together with a random increment between three possible ones: up, middle, or down. This particle travels until it reaches the anode (right), which starts the filament growth process. The next particles will also do a random walk, until they reach the other electrode or when they touch the filament that is being formed and became a part of it. This process ends when the filament connects both electrodes. Finally, a graph is constructed with its vertices placed in the same position as the particles in the obtained filament.

This model can be extended for three dimensions, for example $W \times L \times D$, with the electrodes defined by two parallel planes of dimensions $W \times L$, with a distance D between them. In this case, the random trajectory of the particle, if done in the same way as in the previous case, will occupy one from nine possible random positions in each iteration.

Next, we incorporate the voltage in the filament formation, which will allow us to make better predictions on these filament constructions, as

Figure 4.1 – Example of a filament formation of silver atoms between two electrodes.

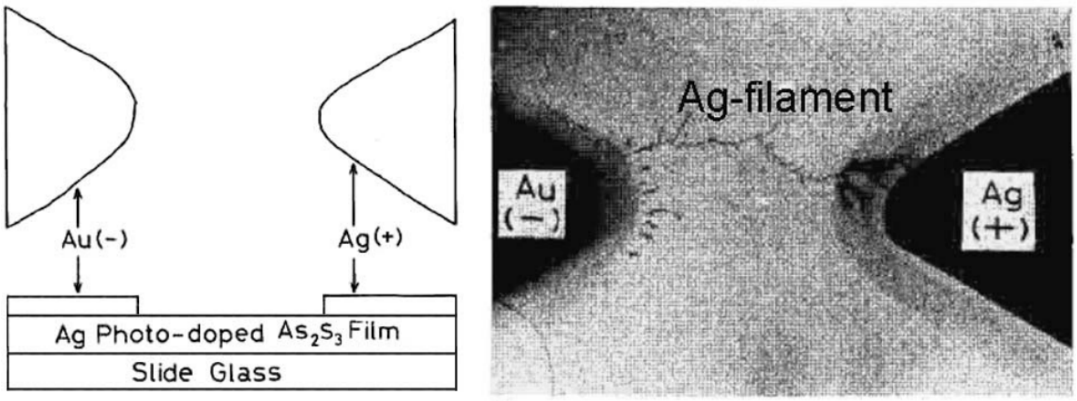

Source: AONO, M.; HASEGAWA, T. The atomic switch. **Proc. IEEE, IEEE**, v. 98, n. 12, p. 2228–2236, 2010.[84]

the particles considered here interact with the electric field. To do that, a given electric potential $V_+ = V_0(t)/2$ and $V_- = -V_0(t)/2$ are associated with each electrode. This allows us to evaluate the electric potential in the region between the anode and cathode from Laplace's equation

$$\nabla^2 V_t(\vec{r}) \;=\; 0, \tag{4.6}$$

and the boundary conditions being defined by the potential in the anode and cathode. As here the region is defined by discrete positions, it is evaluated by a discrete Laplace operator, obtained from a finite difference between the potential on each position. From that, the electric field is evaluated between the region from the gradient of the electric potential

$$\vec{E}_t(\vec{r}) \;=\; -\nabla V_t(\vec{r}). \tag{4.7}$$

Here, the time label only defines a particular time t in which the electric field is evaluated in the simulation, so that we are still solving electrostatic equations.

With the electric field obtained between the electrodes, we should describe the process of formation of the filaments. As the difference in po-

Figure 4.2 – Example of the process of filament formation through a random walk. The red and blue squares are parts of the cathode and anode. The orange squares shows the random positions through the random walk of the particle from an electrode to another, with a dashed arrow to guide the eye. The green squares shows the filament being formed, until it is complete, being represented by a respective graph.

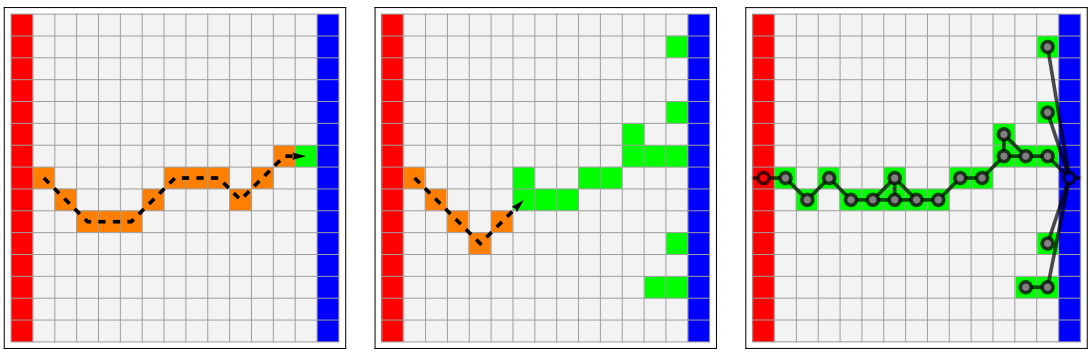

Source: the author.

tential between the cathode and the anode is V_t, a certain density per unit of time and unit of voltage ρ_0 is associated with the emission of particles from the cathode for $V > 0$ or from the anode for $V < 0$. The Eq. of motion for each ion j with mass m_p and charge e_c is given as follows

$$\frac{d^2\vec{r}_i}{dt^2} = -\frac{e_c}{m_p}\vec{E}(\vec{r}) + W(t). \tag{4.8}$$

where $W(t)$ is a Wiener noise associated with the random formation of the filament. During the motion of the particle, the simulation should verify when the particle is close enough to the other electrode, or to the filament being formed, to become attached to them.

Through the process of building the filament, this structure will have the same electric potential as the electrode in which the filament is being formed. Hence, it is important to always evaluate the electric potential of Eq. 4.6 along the steps of simulation, with the spaces occupied by the filament having the same electric potential as the electrode to which it is connected and thus becoming part of the boundary conditions of the system.

Additionally, it is possible to associate each particle attached to this structure as a vertex and the bound with the nearest particles as edges, obtained a graph associated with the filament structure. This allows us to obtain the transmission probability through the filament from the QG approach, and consequently obtain the current from Eq. 4.5. In order to simplify the evaluations, each electrode is also defined as a given vertex, which being the entrance or exit vertex according to the signal of the difference of potential in the system.

The model defined until now describes the construction of the filament, but it is also interesting to define a decay of the filament. This can happen due to two possible processes: the particle randomly detaches from the filament or when the voltage flips its sign, the constructed graph decays. These situations are modelled by a probability p_d per unit of time such that the atoms are removed. At the same time, when the voltage is

flipped, the filament growth can be restarted in the other electrode.

4.3 RESULTS

The effective conductivity of this system can be calculated from the Landauer formula from $g = I/V$. However, in experimental realisations, it is hardly possible to isolate the filament. Hence, the effective conductivity of the device will be obtained by the one of the filament plus a parallel conductive device, which can be a dielectric or a resistor. In this way, the effective current is given by

$$I(V) = g_0 \int_{-\infty}^{\infty} (f_L(\mathcal{E}) - f_R(\mathcal{E})) \left(\frac{h}{2e^2} g_r(V) + T(\mathcal{E}) \right) d\mathcal{E}. \tag{4.9}$$

Here, g_r will be considered in two possible cases, as a constant resistor and as a voltage-dependent quantity, modelling either a liner or a non-linear current behaviour. Additionally, due to the scale of the model, here we will also consider a tunnelling effect, with $g_r(V) \sim g_{0,r} e^{V/V_c}$, for which we consider the quantities $V_c = 0{,}15$ Volts, and $\frac{h}{2e^2} g_{0,r} \sim 10^3 \Omega^{-1}$, quantities compatible with some experiments found in the literature.[89,90]

For the simulations of the model elaborated here, we now should consider some parameters. The voltage was defined as a periodic function with amplitude 0,35V and frequency $\omega = 0{,}5$Hz. The strength of the stochastic force, for Eq. (4.8), has been chosen to be $\langle W(t)^2 \rangle_t = \sqrt{0{,}005}$. From that, some evaluations of filament formation were done together with its current. As an example, we get the Fig. 4.3, which shows the values of the voltage applied, the filament formed, its transmission probability and the current over time and the I versus V diagram, for either a trivial or a Frenkel-Poole insulator. This result is also available in a video[91], where it is possible to illustrate how random filaments are formed on each cycle of filament formation, as a random value of variation on the initial position of each ion is applied. Also, the filaments are attractive to the other free ions, and when a new particle becomes part of them, there will be changes on its transmission and consequently small jumps in the current curve,

and changes also occur when there is a disconnection of some part of this structure.

To obtain a general behaviour of the $I - V$ cycles, some parameters were defined for comparison, namely three values of the dressing parameters u at the edges of the QG: $u = 0{,}00$, $u = 0{,}01$ and $u = 0{,}05$, and four values of the distance D between the electrodes: $D = 5$, $D = 10$, $D = 15$, and $D = 20$. For each combination of parameters u and D, a Monte Carlo analysis was performed by evaluating the 100 cycles of filament formation, each corresponding to a period of voltage. The average value of $I - V$ hysteresis is shown in Fig. 4.4, where it is possible to verify how the memristive profile changes with different values for u and D. By increasing

Figure 4.3 – Example of a simulation for a filament formation. The left panel shows the voltage as function of the time, with different colours to guide in the visualization of the different cycles. The centre image shows an example of filament formed illustrated by its respective graph. In the right panel, the transmission probability as function of $\mathcal{E}/V_0$ is show. The profiles of the current versus time and the current versus voltage are plotted at the bottom, with the two considered cases, for a trivial insulator in the left, while for a Frenkel-Poole insulator is in the right.

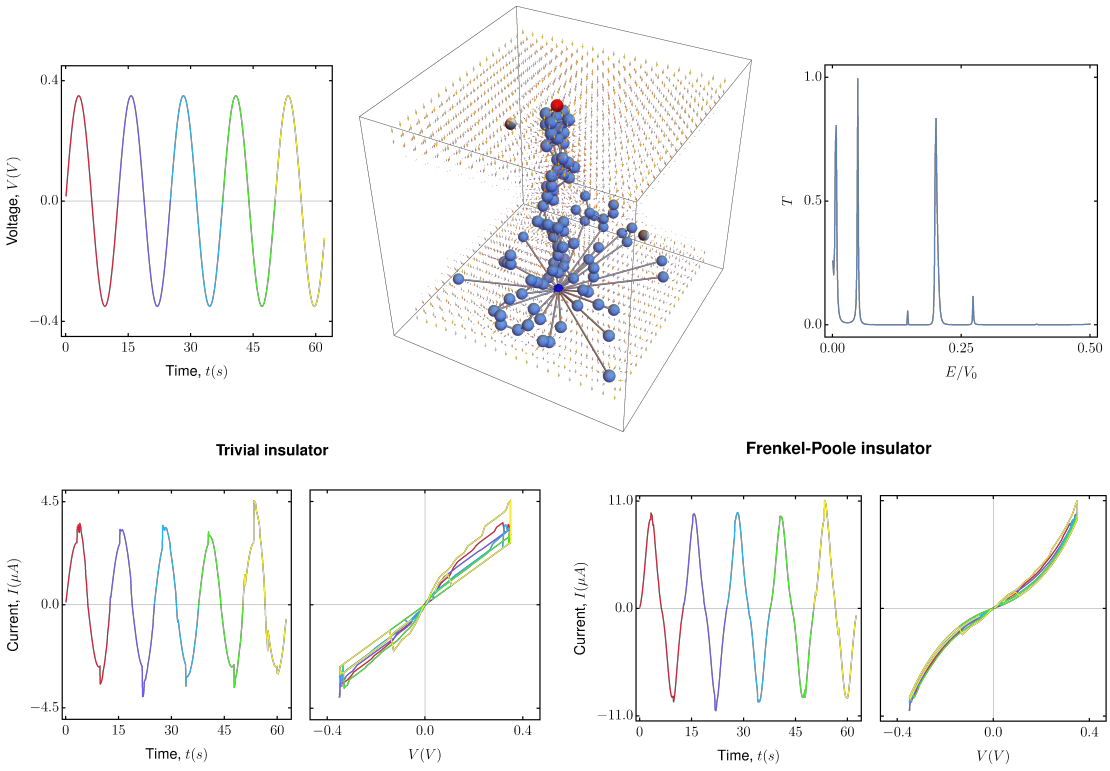

Source: the author.

D, the formation of the filament takes more time, leading to the resistivity change to occur later. The variable u is the potential along the edges of the filament, so increasing it makes the QG less transmissive, due to tunnelling and implying that the filament becomes more restive. This characteristic was also observed in the measurements of niobium oxides[92], further confirming the results obtained from hysteresis in this model.

A programme was written in Wolfram Mathematica to perform these simulations, and it is provided in Wolfram Community.[93] This led to the

Figure 4.4 – Current-Voltage characteristic within the context of the model developed in this work averaged over 100 Monte Carlo samples, and as a function of the dressing parameter u, with $u = 0{,}00$, $u = 0{,}01$ and $u = 0{,}05$, and the distance between electrodes $D = 5$, $D = 10$, $D = 15$ and $D = 20$.

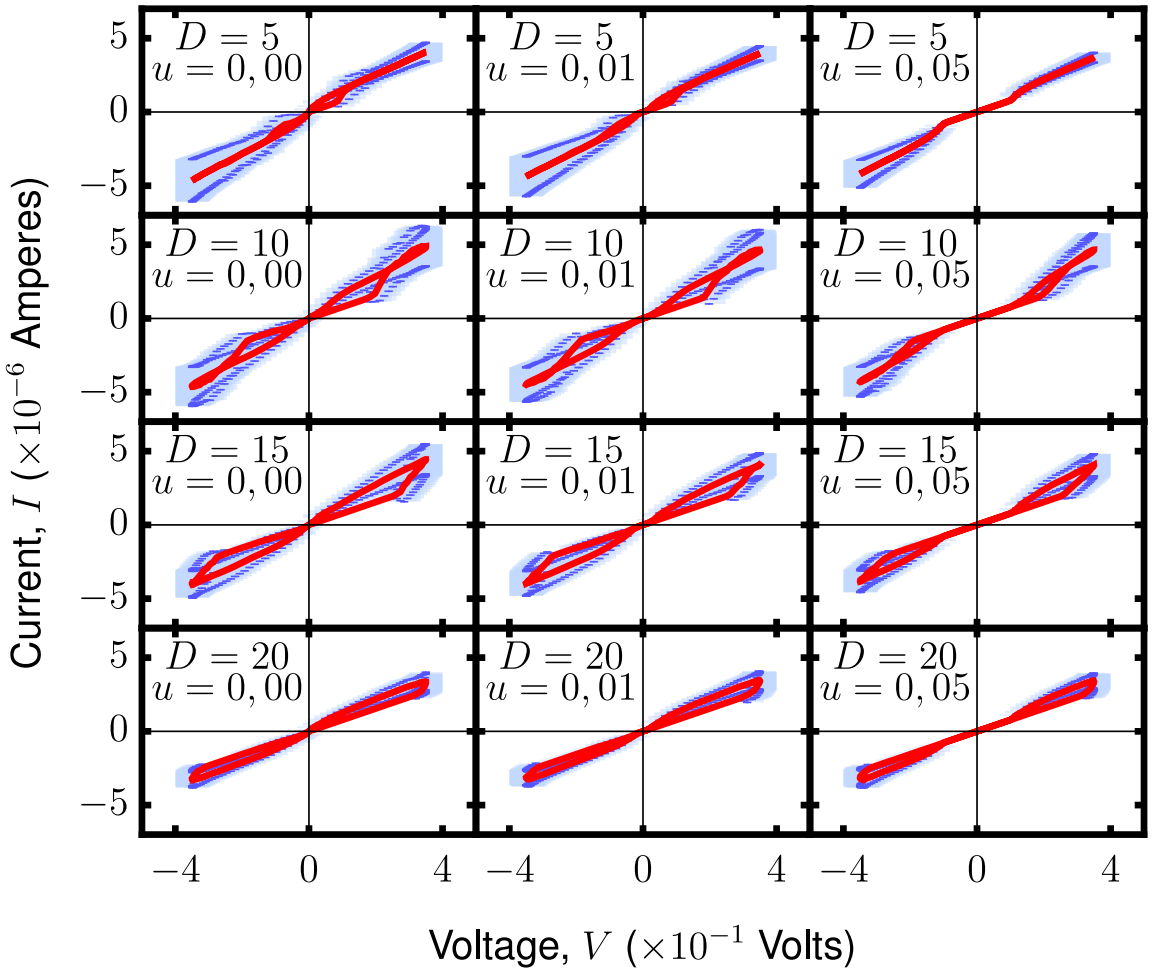

Source: the author.

discussion of such approach in a work on Phisical Review B[94] were these details were also discussed.

This model provides a specific case of a random generated graph and its respective QG analysis. Here, the QGs obtained from random graphs and its respective current obtained shows that even being random, the statistical analysis provides some properties analysis, such as the average hysteresis here. Going forward, in the next section we will try to generalise the QG obtained by random connections and verify its statistical properties.

5 RANDOMISED QUANTUM GRAPHS

Until now, the graphs were constructed through some well-defined pattern for its edges, but there are scenarios - as in the last chapter - where there is a certain randomness on them, and new approaches to define graphs and to estimate their properties are welcome. In this scenario, studies on random graphs emerge. As an example, consider a city where each of its residents is said to be the vertices of our model, and in the beginning of the day they are all disconnected from each other. When they wake up, they begin to make connections with the closest persons to them, and over the day, when interacting with other people, links are created between them. These connections are the edges of this network formed by the individuals in that city. Some people who interact more with other people, such as the sellers, create more connections as customers pass through their stores, becoming hubs in this large graph. On the other hand, some people do not talk or interact that much with others and will define vertices with a small number of connections. At the end of the day we have a graph that contains information about human interactions in this city.

Among the initial propositions of systems with random links between elements, Anatol Rapoport presented studies on mathematical biology[95,96]. His study was inspired by random connections between neurons and focused on doing statistical research on the distribution of cycles in these

Figure 5.1 – Erdős-Rényi random graphs with 8 vertices and (a) 7, (b) 14, (c) 21 and (d) 28 random edges.

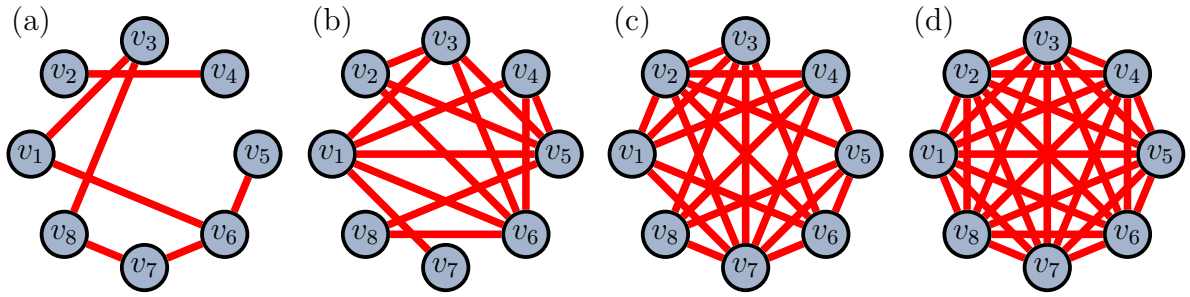

Source: the author.

networks. Some time later he also did another work with Ray Solomonoff, proposing more applications to studies of neural networks, epidemics, and mathematical genetics, highlighting other properties such as the degree distribution[97]. Later, in some ways to formally describe random graphs like these, looking to verify the possible properties that appear through this approach, two studies proposed methods to construct them.

One of these studies is the random graph model proposed by Paul Erdős and Alfréd Rényi in a paper published in 1959.[98] First, a number n of vertices and m of edges are defined. Then, pairs of vertices are randomly chosen, without repetitions, to be connected, and this process is carried out until the target value m is reached. Following this method, an Erdős-Rényi random graph is obtained, denoted by $G(n, m)$. Examples are illustrated in Fig. 5.1 with 8 vertices and $m = 5, 15, 20$ and 25 random edges. It is already possible to verify the probability of obtaining a particular graph from all the possible ones from the quantity

$$P(G(n,m)) = \frac{1}{\binom{\binom{n}{2}}{m}}, \tag{5.1}$$

as there are n vertices, which can form $\binom{n}{2}$ different pairs to be connected, and the number of connections is fixed by m.

In the same year, Edgar Nelson Gilbert proposed the other random network model[99], with just a few months of difference between their submissions. Here, a set of n vertices is also defined, but instead of fixing a number m of edges, a randomisation parameter p, where $0 \leq p \leq 1$ is used. A Gilbert random graph, $G(n, p)$, for each one of the $\binom{n}{2}$ possible edges, has a probability p of occurring; e. g. a random real number generator of values between 0 and 1 can be used to define if a pair of vertices is connected, the edge between these vertices will be constructed only if the drawn number is bigger than p. An example is shown in Fig. 5.2 where four random graphs with eight vertices and random edges were generated from four given values of p. Thus, the probability of obtaining a specific

graph with m edges from all the possible ones is given by

$$P\left(G(n,p)\right) = p^m(1-p)^{\binom{n}{2}-m}, \tag{5.2}$$

as the random event might occur m times and fail $\binom{n}{2} - m$ times. What leads to a relation between both models when we estimate the probability of obtaining a graph with exactly m edges from a random variable p is

$$P\left(G(n,p)\middle|\left|E_{G(n,p)}\right| = m\right) = \binom{\binom{n}{2}}{m} p^m(1-p)^{\binom{n}{2}-m}, \tag{5.3}$$

That is, the probability to obtain an Erdős-Rényi random graph from Gilbert's approach.

These studies have brought to light some interesting properties, such as the formation of giant components on graphs or the degrees distribution over the random graph. Thus, this model provides an approach where the properties of a random system can be studied.

5.1 SPANNING SUBGRAPHS

The subgraphs $F(V_F, E_F)$, are defined from the structure of a given original graph $G(V_G, E_G)$, with a set of vertices V_F and edges E_F being a subset of V_G and E_G, respectively. That is, $V_F \subseteq V_G$ and $E_F \subseteq E_G$. Here we will focus on the spanning subgraphs, where the set of vertices is the same as the original graph, allowing us to simplify $V_G = V$ and $V_F = V$. Thus,

Figure 5.2 – Gilbert random graphs with 8 vertices and (a) $p = 25\%$, (b) $p = 50\%$, (c) $p = 75\%$ and (d) $p = 100\%$.

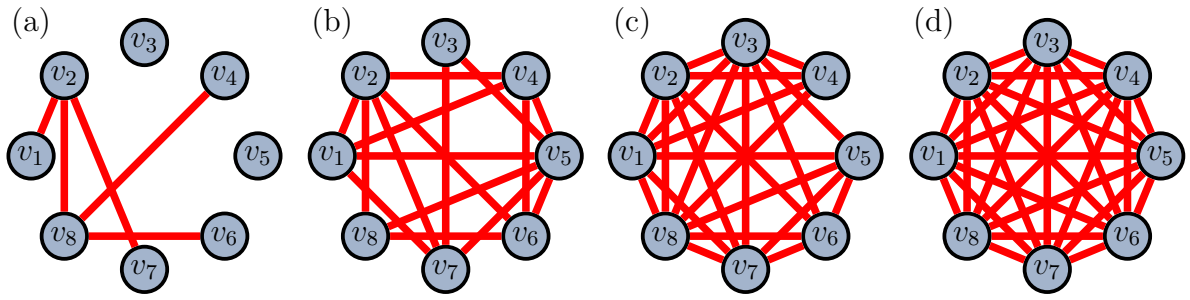

Source: the author.

$F(V, E_F)$ is a spanning subgraph of $G(V, E_G)$ if $V_F = V$ and $E_F \subseteq E_G$.[34] In Fig. 5.3 an example of spanning subgraphs is illustrated for a complete graph with three vertices (K_3).

When a target graph G is defined, there will be a set $\mathbb{S}$ of all the possible spanning subgraphs F from it. The number of elements in $\mathbb{S}$, can be verified by the summation of all the possible combinations from zero to $|E_G|$ of the number of edges in the spanning subgraphs $|E_F|$, that is,

$$|\mathbb{S}| = \sum_{|E_F|=0}^{|E_G|} \binom{|E_G|}{|E_F|}, \tag{5.4}$$

which can be simplified to

$$|\mathbb{S}| = 2^{|E_G|}. \tag{5.5}$$

Thus, the probability to random choose a spanning subgraph $F \in \mathbb{S}$ is

$$P(F) = 2^{-|E_G|}. \tag{5.6}$$

By another approach that utilizes the randomisation parameter p on its edges to obtain the spanning subgraphs, the probability to obtain an specific subgraph F with the restriction that F has exactly $|E_F| = m$ edges

Figure 5.3 – All the 8 spanning subgraphs from the complete graph K_3. (a) All the edges are included; (b-d) One edge was removed; (e-g) Two edges removed; (h) All edges removed, remaining only its vertices.

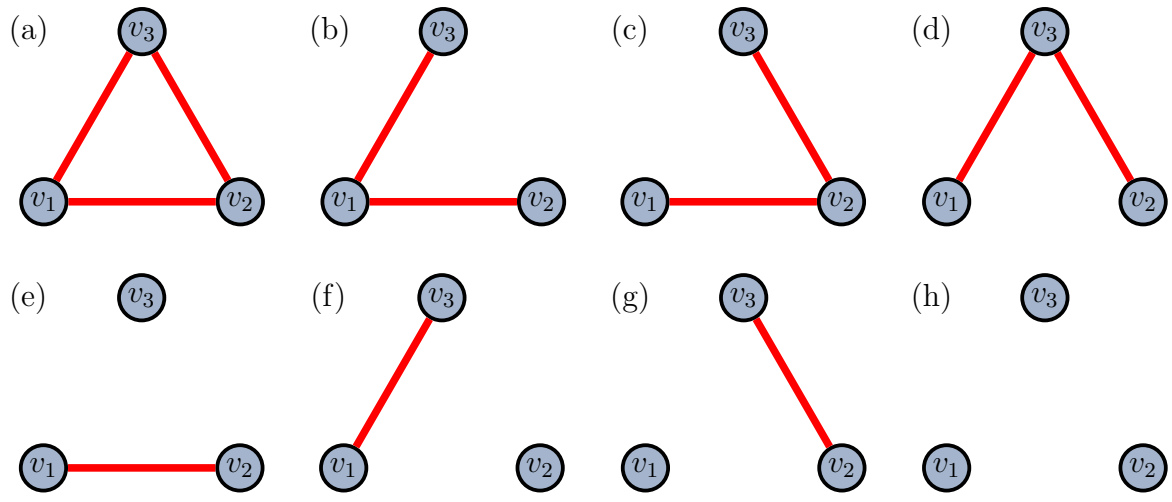

Source: the author.

is

$$P\left(F||E_F|=m\right)=p^{|E_F|}(1-p)^{|E_G\setminus E_F|}. \tag{5.7}$$

Through this model of graph randomisation using the spanning subgraphs it is possible to randomise other graphs than the K_n graphs, as where done in the initial approaches of random graphs. Thus, for a given target graph, it is possible to define a randomisation parameter p at each of its edges and understand the behaviour of its properties as a function of p.

5.2 SCATTERING TRANSMISSION ON RANDOMISED QUANTUM GRAPHS

Based on the approach to randomise discrete graphs, some works showed connections between classical random networks and formulated quantum random networks, some cases include spin arranged in graphs, quantum random walks, and so on.[100,101] Here, we defined a randomised quantum graph (RQG), with a focus on understanding the behaviour of scattering through random quantum structures. In order to randomise a given quantum graph Γ_G^c, which can be called the target quantum graph, we use the spanning subgraphs randomisation model. That is, from the set of edges $E_{\Gamma_G^c}$ we should obtain all possible subsets from it, each subset defines the set of edges $E_{\Gamma_F^c}$ that forms a subgraph Γ_F^c from Γ_G^c. This randomisation process Γ_G^c will preserve some characteristics such as the lengths in each edge, but affects the connectivity of the graphs, as some edges still remain and others are removed in this process, this leads to different degrees of vertices in each subgraph, and consequently there is a change on their scattering amplitudes.

Then, from a given quantum graph Γ_G^c, there is a set $\mathbb{S}$ of spanning quantum subgraphs Γ_F^c from it. The scattering amplitudes, represented by $\sigma_{\Gamma_F^c}^{(f,i)}(k)$, can be evaluated for each $\Gamma_F^c \in \mathbb{S}$. Taking the same pair of input and output channels (i and f) and evaluating the scattering amplitudes of all spanning quantum subgraphs of Γ_G^c, allow us to define a global scattering coefficient for RQG. This is obtained by a weighted sum of the scattering probability for each Γ_F^c multiplied by the probability that each of them

exists, obtained by the randomisation parameter p, leading to the following definition:

Definition 5.2.1 (Exact transmission coefficient of a RQG)**.** *Let Γ_G^c be a quantum graph with c scattering channels. The exact transmission coefficient associated with the randomised quantum graph $R(\Gamma_G^c)$ is defined by*

$$T^{(f,i)}_{R(\Gamma_G^c)}(k,p) = \sum_{\Gamma_F^c \ spans \ \Gamma_G^c} p^{|E_{\Gamma_F^c}|}(1-p)^{|E_{\Gamma_G^c}\setminus E_{\Gamma_F^c}|}\left|\sigma^{(f,i)}_{\Gamma_F^c}(k)\right|^2, \tag{5.8}$$

in which p is the randomisation parameter associated with the probability of the existence of an edge of the original quantum graph.

As the number of possible subgraphs obtained for a given target quantum graph Γ_G^c is $2^{|E_{\Gamma_G^c}|}$, this exponential growth may become difficult to evaluate the RQG scattering coefficients as the number of edges increases. In order to overcome these computational issues, we proposed a Monte Carlo method. To define that, let us first define the ensemble $\mathbb{S}_{|E_F|}$ containing all subgraphs with exactly $|E_F|$ edges and a sample $\mathcal{S}_{|E_F|}$ of $\left|\mathcal{S}_{|E_F|}\right|$ random elements from $\mathbb{S}_{|E_F|}$. By evaluating the scattering amplitudes for all subgraphs on $\mathcal{S}_{|E_F|}$, it allows to define an average scattering amplitude as

$$\left|\overline{\sigma}^{(f,i)}_{|E_F|}(k)\right|^2 = \frac{1}{\left|\mathcal{S}_{|E_F|}\right|}\sum_{\Gamma_F^c\in\mathcal{S}_{|E_F|}}\left|\sigma^{(f,i)}_{\Gamma_F^c}(k)\right|^2. \tag{5.9}$$

Thus, by considering all the $|E_G|+1$ different sets of possibles sets $\mathbb{S}_{|E_F|}$, it allows to rewrite the Eq.(5.8) as

$$T^{(f,i)}_{R(\Gamma_G^c)}(k,p) = \sum_{|E_F|=0}^{|E_G|}\left|\mathbb{S}_{|E_F|}\right|p^{|E_{\Gamma_F^c}|}(1-p)^{|E_{\Gamma_G^c}\setminus E_{\Gamma_F^c}|}\frac{1}{\left|\mathbb{S}_{|E_F|}\right|}\left|\sigma^{(f,i)}_{\Gamma_F^c}(k)\right|^2. \tag{5.10}$$

Finally, taking random samples $\mathcal{S}_{|E_F|} \subseteq_R \mathbb{S}_{|E_F|}$, it was possible to propose an approximate transmission coefficient as follows.

Proposition 2 (Approximated transmission coefficient for RQG)**.** *Let Γ_G^c be a quantum graph with $|E_G|$ edges and c scattering channels. $\mathbb{S}_{|E_F|}$ is the set of all subgraphs Γ_F^c with $|E_{\Gamma_F^c}|$ edges from the quantum graph Γ_G^c. Take*

samples $\mathcal{S}_{|E_F|} \subset_R \mathbb{S}_{|E_F|}$*, of size* $|\mathcal{S}_{|E_F|}|$ *and calculate the average scattering coefficient from Eq.* (5.9)*. The approximated transmission coefficient of the randomised quantum graph* $R(\Gamma^c_G)$ *is*

$$\mathcal{T}^{(f,i)}_{R(\Gamma^c_G)}(k,p) = \sum_{|E_F|=0}^{|E_G|} \binom{|E_G|}{|E_F|} p^{|E_F|}(1-p)^{|E_G \setminus E_F|} \left|\overline{\sigma}^{(f,i)}_{|E_F|}(k)\right|^2 . \tag{5.11}$$

While the size of the ensemble $\mathcal{S}_{|E_F|}$ *increases up to* $|\mathbb{S}_{|E_F|}|$*,* $\mathcal{T}^{(f,i)}_{R(\Gamma^c_G)}(k,p)$ *converges even closer to* $T^{(f,i)}_{R(\Gamma^c_G)}(k,p)$*.*

Proof. The Proposition 2 can be proved as follows: Substituting Eq. (5.9) in Eq. (5.11) the approximated transmission probability can be rewritten as

$$\mathcal{T}^{(f,i)}_{R(\Gamma^c_G)}(k,p) = \sum_{|E_{\Gamma^c_F}|=0}^{|E_{\Gamma^c_G}|} \frac{\binom{|E_{\Gamma^c_G}|}{|E_{\Gamma^c_F}|}}{|S_{|E_{\Gamma^c_F}|}|} p^{|E_{\Gamma^c_F}|}(1-p)^{|E_{\Gamma^c_G} \setminus E_{\Gamma^c_F}|} \sum_{\Gamma^c_F \in S_{|E_{\Gamma^c_F}|}} \left|\sigma^{(f,i)}_{\Gamma^c_F}(k)\right|^2 . \tag{5.12}$$

Being $\mathbb{S}_{|E_{\Gamma^c_F}|}$ the set of all subgraphs Γ^c_F with number of edges $|E_{\Gamma^c_F}|$, when

$$|S_{|E_{\Gamma^c_F}|}| \to |\mathbb{S}_{|E_{\Gamma^c_F}|}| = \binom{|E_{\Gamma^c_G}|}{|E_{\Gamma^c_F}|}, \tag{5.13}$$

we have

$$\mathcal{T}^{(f,i)}_{R(\Gamma^c_G)}(k,p) = \sum_{|E_{\Gamma^c_F}|=0}^{|E_{\Gamma^c_G}|} p^{|E_{\Gamma^c_F}|}(1-p)^{|E_{\Gamma^c_G} \setminus E_{\Gamma^c_F}|} \sum_{\Gamma^c_F \in \mathbb{S}_{|E_{\Gamma^c_F}|}} \left|\sigma^{(f,i)}_{\Gamma^c_F}(k)\right|^2 . \tag{5.14}$$

The first sum over the number of edges in the quantum subgraphs Γ^c_F, and the second one over all the possible quantum subgraphs with a given number of edges $E_{\Gamma^c_F}$, is equivalent to the sum over all the spanning subgraphs

of Γ_G^c. Then, in the limit given by (5.13) we have

$$\begin{aligned}\mathcal{T}^{(f,i)}_{R(\Gamma_G^c)}(k,p) &= \sum_{\Gamma_F^c \text{ spans } \Gamma_G^c} p^{|E_{\Gamma_F^c}|}(1-p)^{|E_{\Gamma_G^c}\setminus E_{\Gamma_F^c}|}\left|\sigma^{(f,i)}_{\Gamma_F^c}(k)\right|^2 \\ &= T^{(f,i)}_{R(\Gamma_G^c)}(k,p). \end{aligned} \tag{5.15}$$

From these definitions and propositions made along this section, the randomisation of some specific quantum graphs was done and the evaluations on the scattering transmission of the quantum subgraphs were done. The definition of these target quantum graphs and the results obtained from their randomisation will be presented in the following section.

5.3 RESULTS FOR SCATTERING TRANSMISSION ON RANDOMISED QUANTUM GRAPHS

In the context of random graphs, the final graph obtained is the complete graph with n vertices (K_n), as it is the most connected simple

Figure 5.4 – Examples of the complete graph minus one edge K_n^e with $n = 4, 6, 7$ and 8 vertices. $v_i = v_1$ in all quantum graphs while $v_f = v_{(n+2)/2}$ for even n and $v_f = v_{(n+3)/2}$ for odd n. One lead is attached to v_i and another to v_f.

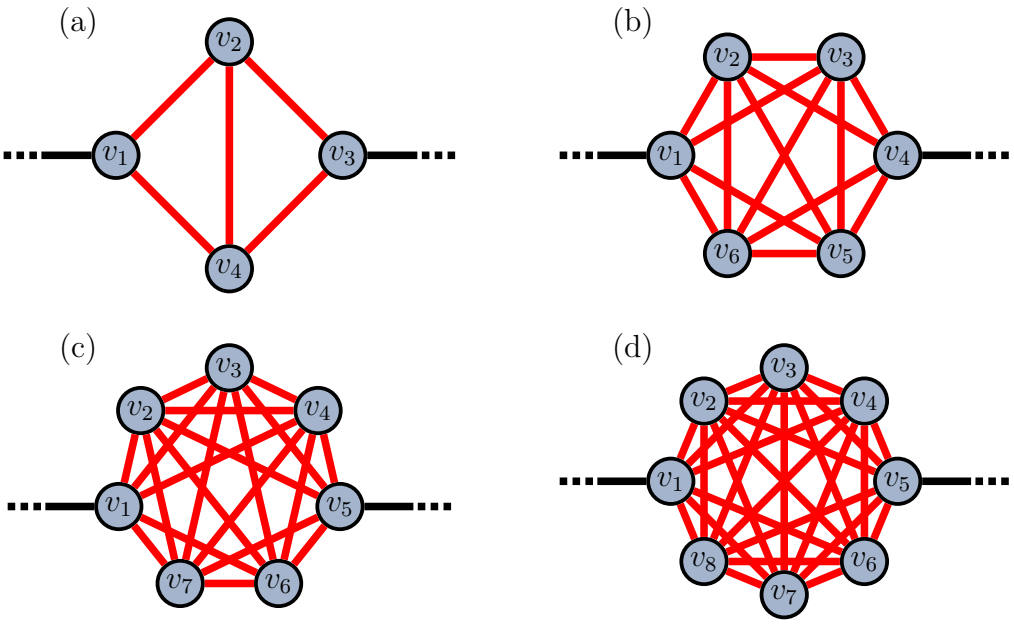

Source: the author.

graph. However, in order to explore the definition presented here, which focusses on the randomisation of the possible edges of the target quantum graph, we will define a graph that can be understood as the complete graph minus one edge (K_n^e).

In summary, the target quantum graph K_n^e that will be used throughout this section is illustrated in Fig. 5.4 for $n = 4, 6, 7$ and 8. It contains n vertices, 2 leads attached to v_i and v_f and has all the possible edges between any pair of vertices on it, with the exception of $e = \{v_i, v_f\}$. They were defined to exemplify that our method can be applied to randomise any quantum graph, and all the vertices of the target quantum graph have the same degree $(n-1)$. In the quantum graphs studied here, all edges have the same length ℓ and all vertices have the Neumann boundary condition.

The first case studied is the randomisation of the quantum graph $\Gamma^2_{K_4^e}$, illustrated in Fig. 5.4 (a). As it has 5 edges, there will be 32 quantum subgraphs, from which we found 14 groups of isomorphic QGs, which will have the same scattering transmission coefficient. This allowed us to obtain the exact transmission for the RQG $R(\Gamma^2_{K_4^e})$ by evaluating the scattering transmission for each of these 14 non-isomorphic quantum subgraphs and utilise the Eq. (5.8) without further difficulties. The results obtained are displayed on Table 5.1 showing the details of it, such as the drawing of these subgraphs, its probability, and the scattering coefficient.

From the data for the subgraphs of $\Gamma^2_{K_4^e}$, we were able to construct the plots in Figure 5.5, where the transmission coefficient for each number of edges in the spanning subgraphs of this QG was plotted in a thin blue curve, while the average transmission coefficient was evaluated with Eq. (5.9) is displayed in a thick red curve. As these transmissions are periodic, we concentrated on the period for $k\ell$ from 0 to 2π. With these results, it was verified that for the number of edges less than 2, there is no transmission, an expected behaviour, as the path from the input vertex to the exit vertex needs at least 2 edges. When there are 2 edges, the quantum graph has maximal or minimal transmission, with the predominance of the

last one being verified by the average transmission. For 3 or 4 edges, some transmission patterns start to appear due to the connectivity changes in the quantum graphs. Finally, in the last case, with $|E_F| = 5$, there is only one possible quantum graph that is the defined target quantum graph.

Therefore, from Definition 5.2.1 which gives the scattering transmission for a randomised quantum graph, the obtained data for $R(\Gamma^2_{K_4^e})$ presented in Table 5.1 can be used in the following way. First, for each line, the elements in the last three columns are multiplied. Then, the results obtained for each line are added together. This results on

Figure 5.5 – Transmission coefficients of quantum subgraphs ensembles for $\Gamma^2_{K_4^e}$ with 0 to 5 edges. The top left numbers represents the number of edges of the sugraphs in the ensemble; The thin blue curves are the individual transmission coefficients of each subgraphs. The thick red curve shows the average transmission of the ensemble.

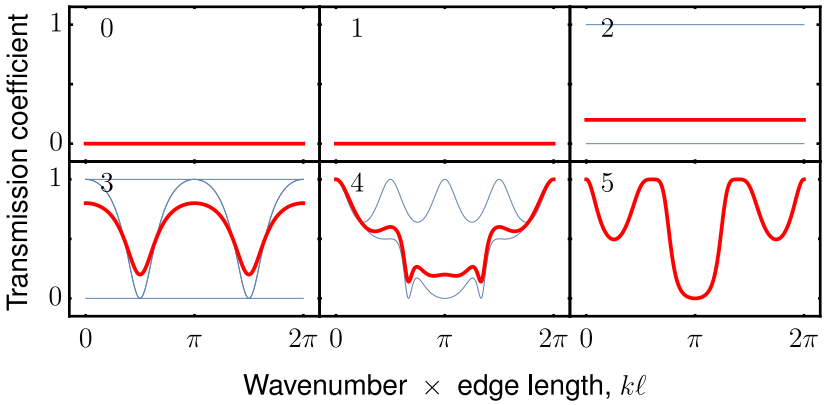

Source: the author.

Table 5.1 – Data for quantum subgraphs of $\Gamma^2_{K_4^e}$. Subgraph: illustrations for the groups of isomorphic quantum subgraphs, without the labels, which are the same from figure 5.4 and can contain permutation on its vertices labels between v_1 and v_3 or between v_2 and v_4; The transmission amplitudes were defined with $z = e^{ik\ell}$.

Subgraph	Number of edges	Number of isomorphisms	Probability	Transmission Amplitude $\sigma^{(f,i)}_{\Gamma^2_F}(k)$
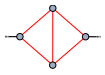	5	1	p^5	$\frac{16(1+z)z^2}{27+9z+6z^2-6z^3-z^4-3z^5}$
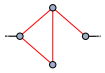	4	4	$p^4(1-p)$	$\frac{4\left(1+2z+2z^2+z^3\right)z^2}{9+9z+8z^2-z^4-z^5}$
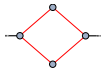	4	1	$p^4(1-p)$	$\frac{8z^2}{9-z^4}$
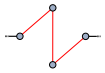	3	2	$p^3(1-p)^2$	z^3
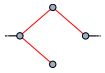	3	4	$p^3(1-p)^2$	$\frac{2\left(1+z^2\right)z^2}{3+z^2}$
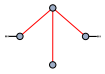	3	2	$p^3(1-p)^2$	$\frac{2\left(1+z^2\right)z^2}{3+z^2}$
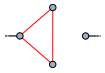	3	2	$p^3(1-p)^2$	0
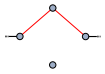	2	2	$p^2(1-p)^3$	z^2
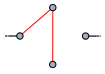	2	4	$p^2(1-p)^3$	0
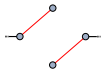	2	2	$p^2(1-p)^3$	0
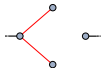	2	2	$p^2(1-p)^3$	0
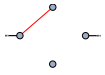	1	4	$p(1-p)^4$	0
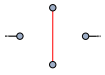	1	1	$p(1-p)^4$	0
	0	1	$(1-p)^5$	0

Source: the author.

$$
\begin{aligned}
T_{R(\Gamma^2_{\diamond})}(k,p) = {} & p^5 \left|\sigma^{(f,i)}_{\Gamma^2_{\diamond}}(k)\right|^2 + p^4(1-p)\left(4\left|\sigma^{(f,i)}_{\Gamma^2_{\diamond}}(k)\right|^2 + \left|\sigma^{(f,i)}_{\Gamma^2_{\diamond}}(k)\right|^2\right) \\
& + p^3(1-p)^2\left(2\left|\sigma^{(f,i)}_{\Gamma^2_{\diamond}}(k)\right|^2 + 4\left|\sigma^{(f,i)}_{\Gamma^2_{\diamond}}(k)\right|^2\right) \\
& + p^3(1-p)^2\left(2\left|\sigma^{(f,i)}_{\Gamma^2_{\diamond}}(k)\right|^2 + 2\left|\sigma^{(f,i)}_{\Gamma^2_{\diamond}}(k)\right|^2\right) \\
& + p^2(1-p)^3\left(2\left|\sigma^{(f,i)}_{\Gamma^2_{\diamond}}(k)\right|^2 + 4\left|\sigma^{(f,i)}_{\Gamma^2_{\diamond}}(k)\right|^2\right) \\
& + p^2(1-p)^3\left(2\left|\sigma^{(f,i)}_{\Gamma^2_{\diamond}}(k)\right|^2 + 2\left|\sigma^{(f,i)}_{\Gamma^2_{\diamond}}(k)\right|^2\right) \\
& + p(1-p)^4\left(4\left|\sigma^{(f,i)}_{\Gamma^2_{\diamond}}(k)\right|^2 + \left|\sigma^{(f,i)}_{\Gamma^2_{\diamond}}(k)\right|^2\right) \\
& + (1-p)^5\left|\sigma^{(f,i)}_{\Gamma^2_{\diamond}}(k)\right|^2 .
\end{aligned}
$$

From that, the transmission probability for $R(\Gamma^2_{K_4^e})$ can be analysed as a function of $k\ell$ and p is illustrated in Fig. 5.6.

Another case is for the complete graph minus one edge but now with six vertices ($\Gamma_{K_6^e}$), as illustrated in Fig. 5.4(b). The increment of two

Figure 5.6 – The exact transmission coefficient for the RQG $R(\Gamma^2_{K_4^e})$ as function of $k\ell$ (wavenumber × edge length) and p (randomisation parameter).

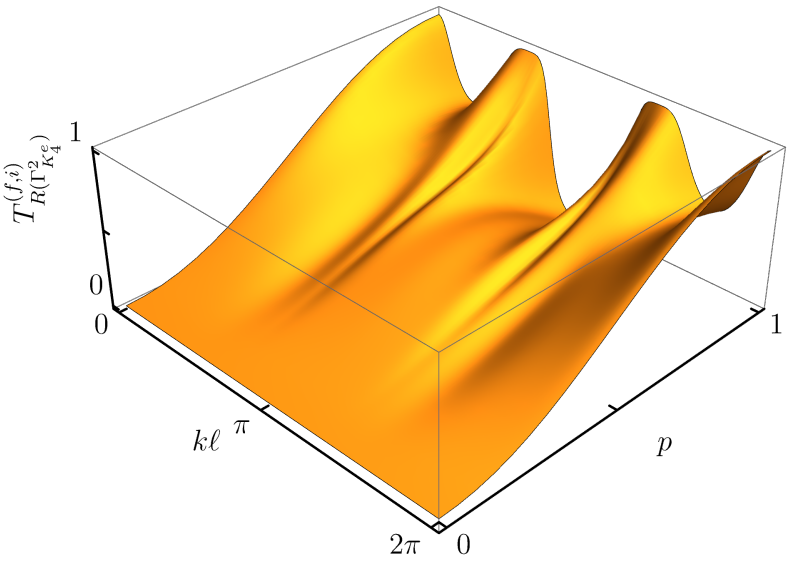

Source: the author.

vertices implies in the graph now having 14 vertices, and consequently it has $2^{14} = 16384$ subgraphs. This can be considered as a transition case, where this number of quantum graphs is not a problem in the computation of its scattering transmission, as in the case of the biggest ensemble - for the subgraphs with 7 vertices - contains $\binom{14}{7} = 3432$ subgraphs, but also it has values that are a good case to do statistics taking samples on these ensembles.

The results obtained are illustrated in Figure 5.7, where the scattering amplitudes in each subgraph are displayed in thin blue curve plots, the exact average transmission coefficient is shown in a thick red curve,

Figure 5.7 – Transmission coefficients, the exact and approximated average transmission for the ensembles of quantum subgraphs Γ_F^2 from $\Gamma_{K_6^e}^2$ with $|E_{\Gamma_F^2}| = 0, 1, \ldots, 14$. The top left numbers shows the number of edges of the subgraphs; The blue curves in the background are the transmission coefficients of the subgraphs in the ensemble, the thick red curves are the exact average transmission of the ensemble, while the thin black curves are the approximated average transmission by taking up to 250 Monte Carlo samples of subgraphs from the ensemble.

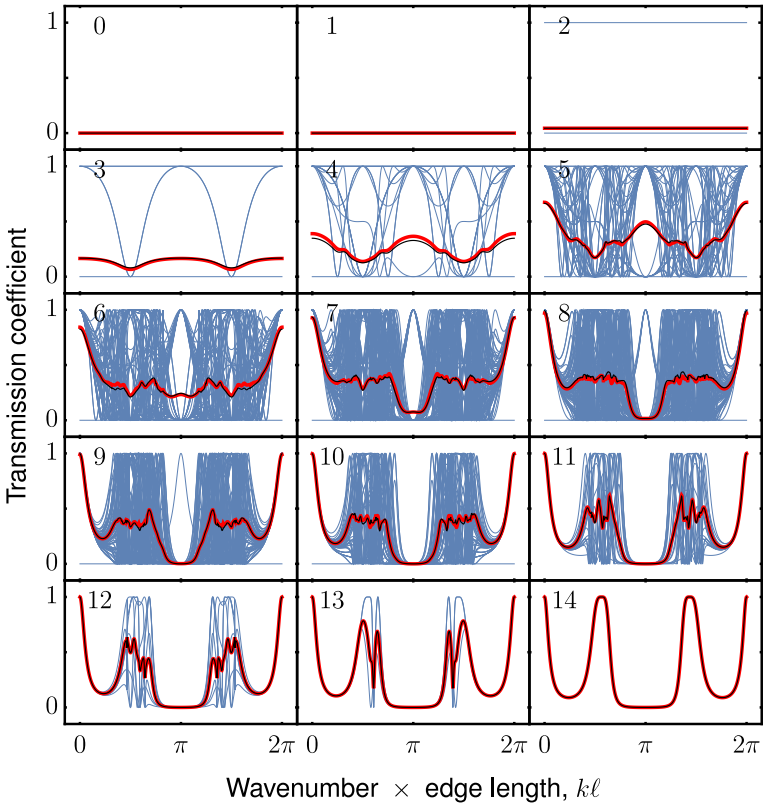

Source: the author.

while the approximated transmission coefficient, obtained by taking up to 250 Monte Carlo samples, is presented in a thin black curve. Some new behaviour was noticed when compared to the results for $R(\Gamma_{K_4^e})$, as in the case of the suppression region around $k\ell = \pi$, it was verified that this region still remains without further changes until the removal of 4 edges (10 to 14 vertices present), or even up to 7 where the transmission is very low on average. This can be interpreted as the resilience of the structure to some imperfections, such as the removal of edges. If the quantum graph aimed was used as a filter to suppress signals with this range of wavenumbers, even with some edge removal it would still be able to be used in this task.

With these average values of the transmission coefficients, the Eq. (5.11) from Definition 2 was used to obtain the result shown in Fig. 5.8. The data obtained were compared with the exact case for the same graph. The results were almost indistinguishable, with a maximum difference of 2.3%. This shows a strong agreement between both methods and confirms the validity of this approximation method.

Furthermore, instead of evaluating the transmission coefficients for

Figure 5.8 – Approximated transmission coefficient for the RQG $R(\Gamma^2_{K_6^e})$.

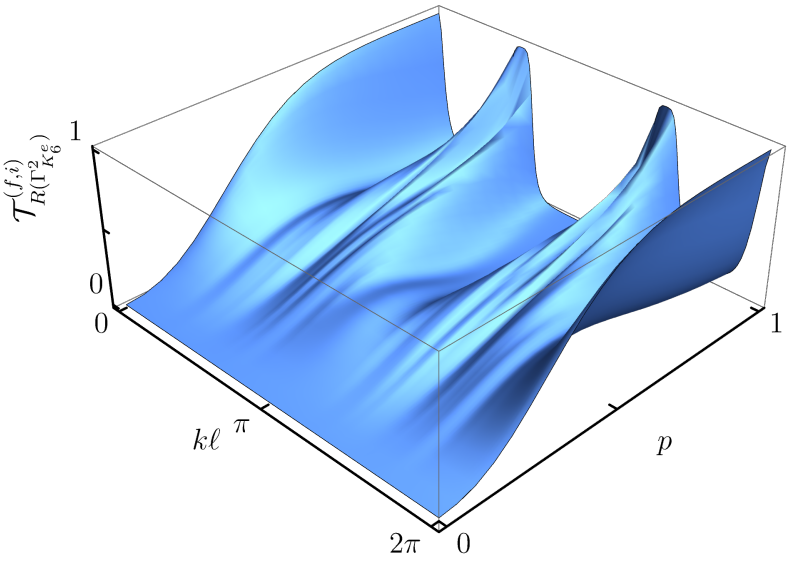

Source: the author.

all values of $k\ell$, such as those in Figure 5.7, it is possible to focus on specific values. In Figure 5.9 the transmission probability was evaluated at $k\ell = \pi/8$ and $k\ell = \pi$ as a function of the number of edges of the graph. From these results we notice for $k\ell = \pi/8$ that initially there is no transmission, their values spread, increasing the average value, reaching their maximum at 6 edges and then it decreases without reaching 0. On the other hand, at $k\ell = \pi$, the subgraphs with 2 to 9 edges, the possible transmission values are dichotomous, 0 or 1, and its average value shows the proportion of between these values, showing that the ensemble of subgraphs with 5 edges is the one that contains more subgraphs with maximal transmission.

These average values can also be weighted by $p^{|E_F|}(1-p)^{|E_G \setminus E_F|}$, as

Figure 5.9 – The scattering transmission for the quantum subgraphs of $\Gamma^2_{K_6^e}$ and its average value at $k\ell = \pi/8$ and $k\ell = \pi$, as a function of the number of edges. The blue dots are the values obtained for each element in the ensemble of spanning subraphs from $\Gamma^2_{K_6^e}$; The black dots with a dashed line are the average transmission value in the samples.

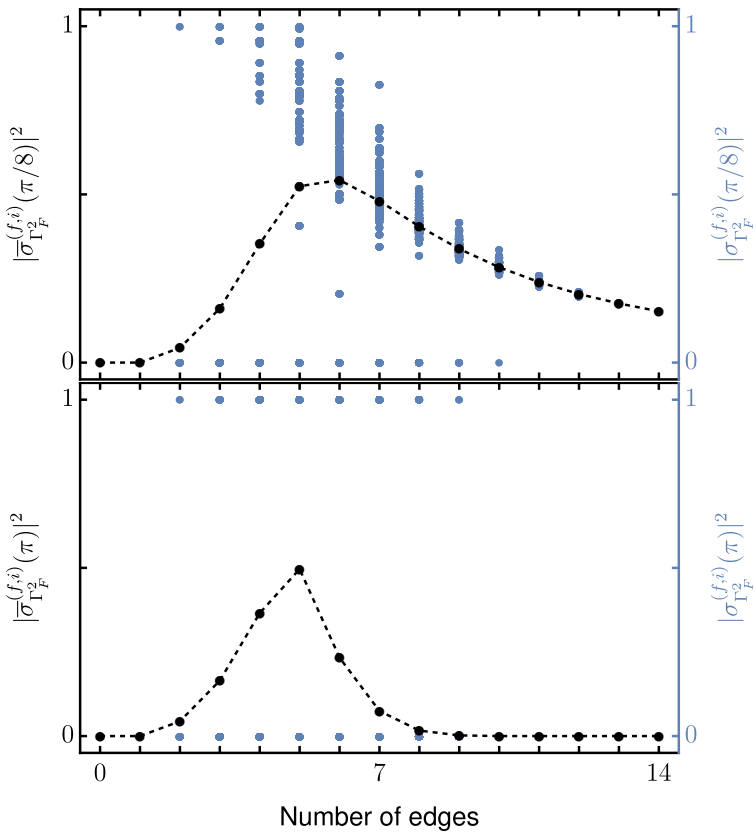

Source: the author.

in Proposition 2. This allows us to analyse the global behaviour as a function of the randomisation parameter p for the calculations of the RQG scattering coefficient. The results are illustrated in Fig. 5.10 for the RQGs $R(\Gamma^2_{K_n^e})$, with $n = 6, 7$ and 8. The maximum value of the transmission was noticed to decrease and is also shifted to the left as the number of vertices increases. Hence, Table 5.2 was constructed, which contains the values n of the vertices in the target graph, the value p_m which is the point in p where the average transmission is maximum and its respective transmission value. This shows that RQGs can have higher transmission probabilities when compared with deterministic quantum graphs (for $p = 1$), an interesting feature that can be used as a variable for optimisation in quantum graphs, to find the best values of p in which the transmission is maximised from a

Figure 5.10 – The approximated transmission for $R(\Gamma^2_{K_n^e})$ with $n = 6, 7$ and 8 for $k\ell = \pi/8$ and $k\ell = \pi$, as a function of the randomisation parameter p.

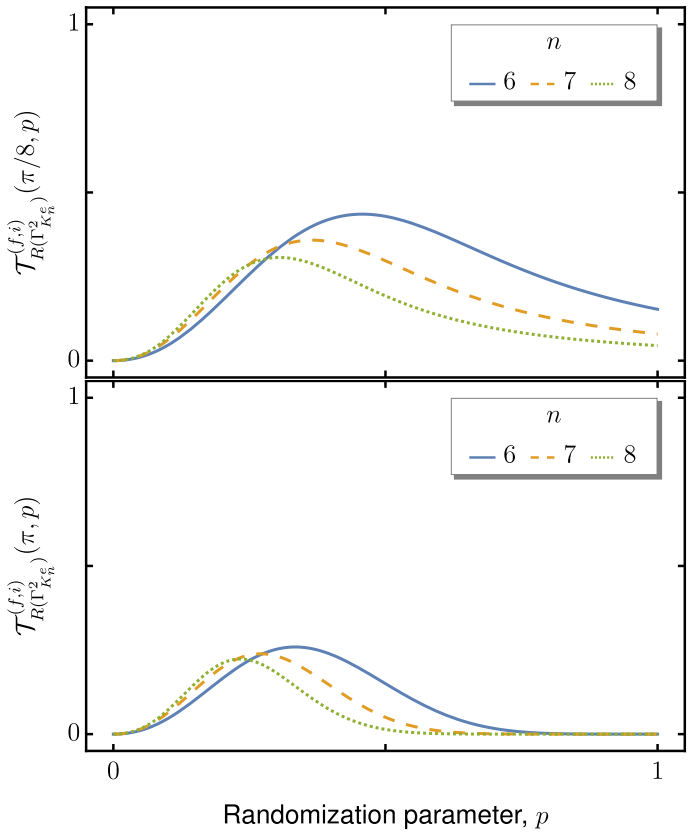

Source: the author.

given set of random edges.

Table 5.2 – Values of the randomisation parameter at the maximum of the approximated transmission probability for the RQGs of Figure 5.10. n is the number of edges; p_m: value of p in which maximal value of $\mathcal{T}$ is achieved.

n	p_m	$\mathcal{T}^{(f,i)}_{R(\Gamma^2_{K^e_n})}(\pi/8, p_m)$	n	p_m	$\mathcal{T}^{(f,i)}_{R(\Gamma^2_{K^e_n})}(\pi, p_m)$
6	0,458	0,436	6	0,334	0,259
7	0,365	0,358	7	0,271	0,239
8	0,305	0,307	8	0,233	0,223

Source: the author.

Throughout this chapter, a randomisation method was employed in which a given quantum graph had some probabilities p associated with the existence of each of its edges. On the randomisation parameter, someone can suggest utilising some quantum system as a source of random values. As a quantum graph is a quantum system from which probabilities are associated with its scattering output, in the following chapter a way to randomise a given graph by utilising the outputs of other quantum graphs will be defined, and the implications of doing so will be investigated.

6 QUANTUM STATES FROM SCATTERING IN QUANTUM GRAPHS

The processing of information obtained by quantum systems is a topic of enormous interest nowadays, as topics such as quantum cryptography and quantum computation have shown their importance in solving hard classical problems.[102] Systems in quantum information studies use qubits[103] or even qudits to define two-level or d-level systems, respectively, such as electron spin, photon polarisation, atom energy levels, and so on. In this chapter, we propose using the scattering of a particle on a QG to define these discrete quantum states.

For a given QG Γ_G^2, or simply Γ_G as we will work with only two scattering channels throughout this chapter, with leads labeled as l_0 and l_1, its scattering matrix is

$$S_{\Gamma_G} = \begin{pmatrix} r_G^{(l_0)} & t_G \\ t_G & r_G^{(l_1)} \end{pmatrix}, \tag{6.1}$$

where t_G is the transmission amplitude of the QG while $r_G^{(l_j)}$ is the reflection amplitude in a given lead l_j. For a particle in a given lead l_j, it is defined to be in a state $|l_j\rangle$, or simply $|j\rangle$, for two scattering channels, l_0 and l_1, their respective states can be written in the matrix form

$$|0\rangle = \begin{pmatrix} 1 \\ 0 \end{pmatrix}, \quad |1\rangle = \begin{pmatrix} 0 \\ 1 \end{pmatrix}. \tag{6.2}$$

Hence, its scattering matrix can be rewritten as

$$S_{\Gamma_G} = r_G^{(-)} |0\rangle\langle 0| + t_G \left(|0\rangle\langle 1| + |1\rangle\langle 0|\right) + r_G^{(+)} |1\rangle\langle 1|, \tag{6.3}$$

or for QGs with equal reflection amplitudes from both sides, with $r_G^{(+)} = r_G^{(-)} = r_G$,

$$S_{\Gamma_G} = r_G \left(|0\rangle\langle 0| + |1\rangle\langle 1|\right) + t_G \left(|0\rangle\langle 1| + |1\rangle\langle 0|\right). \tag{6.4}$$

Thus, for a particle scattering through the QG Γ_G with initial state

$|0\rangle$, the final state $|\Gamma_G\rangle$ is

$$|\Gamma_G\rangle = S_{\Gamma_G} |0\rangle , \tag{6.5}$$

from Eq. (6.4), becomes

$$|\Gamma_G\rangle = r_G |0\rangle + t_G |1\rangle , \tag{6.6}$$

a state of superposition between the two possible output channels, with amplitude obtained by the scattering process. This model is illustrated in Figure 6.1, where the particle coming from lead l_0 with the input state $|0\rangle$ scatters through the QG Γ_G and after the scattering on it, the output state is $r_G |0\rangle + t_G |1\rangle$.

6.1 CONTROLLED CHANGES BETWEEN TWO QGS

Let us introduce two QGs, Alice's QG (Γ_A) and Bob's QG (Γ_B). The system composed by them will have its Hilbert space composed by the spaces of these subsystems, $\mathcal{H} = \mathcal{H}_A \otimes \mathcal{H}_B$.

Now consider the following situation. When the particle in Alice's system is reflected, measured in the state $|0\rangle_A$, there are no changes in Bob's QG, being defined by $|\Gamma_B\rangle_B$. However, when the state $|1\rangle_A$ is measured in Alice's QG, some change is done on Bob's QG, modifying it from

Figure 6.1 – The scattering in quantum graphs. (a) Before the scattering on Γ_G the particle is on the lead l_0, with initial state $|0\rangle$. (b) After the scattering on Γ_G the output state is defined by the scattering amplitudes r_G to reflect to the same lead l_0, being in the state $|0\rangle$; and t_G to transmit through the QG to the lead l_1, being in the state $|1\rangle$. For simplicity, a general quantum graph Γ_G is represented by a single vertex, which is defined having the same scattering amplitudes.

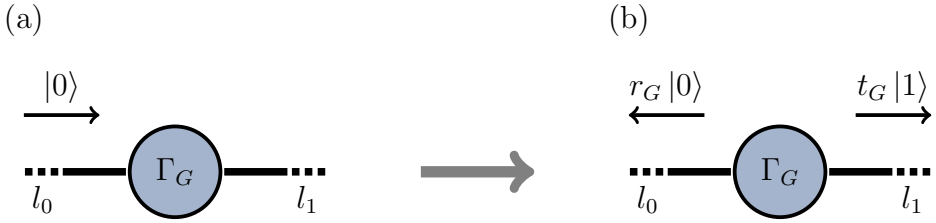

Source: the author.

Γ_B to $\Gamma_{B'}$, and consequently having the state $|\Gamma_{B'}\rangle_B$. In this case, Alice's QG acts as the controller system, while Bob's QG is the one being controlled. The possible modifications can include any changes that modify the scattering amplitudes on Bob's quantum graphs, such as edge length changes, potential applied to its edges, changes on the boundary conditions of the vertices, changes on its connectivity, and so on.

The operator that makes these controlled changes in the QG is given by

$$CS^A_{B,B'} = |0_A\rangle\langle 0_A| \otimes S_{\Gamma_B} + |1_A\rangle\langle 1_A| \otimes S_{\Gamma_{B'}}, \tag{6.7}$$

that is, a controlled gate that performs the modification $\Gamma_B \to \Gamma_{B'}$ according to the measured state of $|\Gamma_A\rangle$. Thus, the state of QG interaction, illustrated in Fig. 6.2, can be written as $|\Psi_{AB}\rangle = CS^A_{B,B'}\,|0_A\rangle \otimes |0_B\rangle = r_A\,|0_A\rangle\otimes|\Gamma_B\rangle + t_A\,|1_A\rangle\otimes|\Gamma_{B'}\rangle$. When $|\Gamma_{B'}\rangle = |\Gamma_B\rangle$, the state is easily separable as $|\Psi_{AB}\rangle = |\Gamma_A\rangle\otimes|\Gamma_B\rangle$. Using the shorthand notation $|i_A\rangle\otimes|j_B\rangle = |i,j\rangle$, we can write the scattering state as

$$|\Psi_{AB}\rangle = r_A r_B\,|0,0\rangle + r_A t_B\,|0,1\rangle + t_A r_{B'}\,|1,0\rangle + t_A t_{B'}\,|1,1\rangle\,. \tag{6.8}$$

Figure 6.2 – Illustration of the system of two quantum graphs, Γ_A connected to the scattering channels $l_{0,A}$ and $l_{1,A}$, and Γ_B connected to the scattering channels $l_{0,B}$ and $l_{1,B}$. When there is an interaction between both systems at $\mathcal{D}$ - related with the transmission in Γ_A - it results in a controlled operation applied on Γ_B turning it into $\Gamma_{B'}$. In blue the states associated with the interaction at $\mathcal{D}$ of the particle in the lead $l_{1,A}$ are represented; In red the states associated with the particle back scattered in Γ_A, reflecting to the lead $l_{0,A}$ are shown.

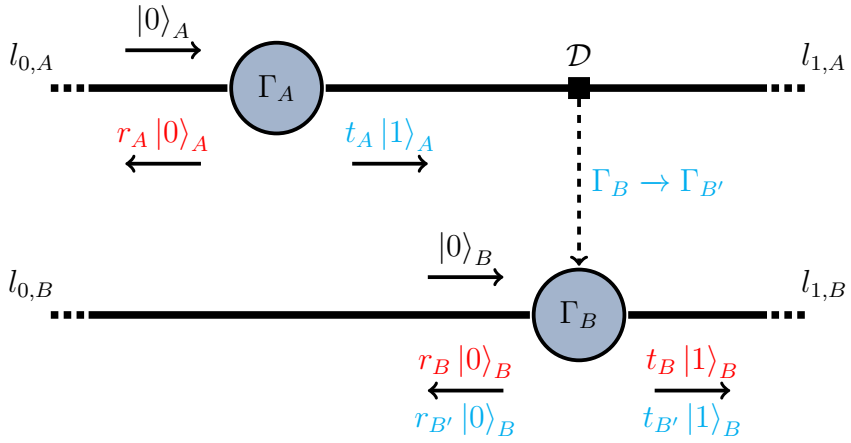

Source: the author.

Whose density matrix is given by $\rho = |\Psi\rangle\langle\Psi|$ and has the matrix form

$$\rho = \begin{pmatrix} |r_A|^2|r_B|^2 & |r_A|^2 r_B t_B^* & r_A r_B t_A^* r_{B'}^* & r_A r_B t_A^* t_{B'}^* \\ |r_A|^2 t_B r_B^* & |r_A|^2|t_B|^2 & r_A t_B t_A^* r_{B'}^* & r_A t_B t_A^* t_{B'}^* \\ t_A r_{B'} r_A^* r_B^* & t_A r_{B'} r_A^* t_B^* & |t_A|^2|r_{B'}|^2 & |t_A|^2 r_{B'} t_{B'}^* \\ t_A t_{B'} r_A^* r_B^* & t_A t_{B'} r_A^* t_B^* & |t_A|^2 t_{B'} r_{B'}^* & |t_A|^2|t_{B'}|^2 \end{pmatrix}, \tag{6.9}$$

which allows to verify the properties of this quantum system defined. Now, let us verify the possible measurements from Alice and Bob in the interacting system by analysing its density matrix.

6.1.1 Partial trace and measurements on states

The system proposed here is composed of Alice's system and Bob's system, both being denominated as subsystems of the QGs interaction system. These subsystems are on the Hilbert space $\mathcal{H}_A$ and $\mathcal{H}_B$. Defining the eigenstates $|u_i\rangle$ a basis of $\mathcal{H}_A$ and $|v_j\rangle$ a basis of $\mathcal{H}_B$, a total trace of the system would be defined as

$$\mathrm{Tr}\,\rho = \sum_i \sum_j \langle u_i, v_j|\,\rho\,|u_i, v_j\rangle\,. \tag{6.10}$$

Now, suppose that an observable on Alice's system is defined as M_A. The measurement M_A by Alice and no measurement by Bob implies in the average value of the outcomes given by

$$\langle M_A \otimes I_B\rangle_\rho = \mathrm{Tr}\left[(M_A \otimes I_B)\,\rho\right], \tag{6.11}$$

where I_B is an identity operator in Bob's system. Alice will have only access to her own system; thus it is interesting to describe the density matrix of the subsystem A. This is achieved by the partial trace that can be used to describe the observables outputs in quantum subsystems that compose a larger system. For instance, a partial trace of Bob's system, returns a the reduced density matrix related to Alice's system, written as

$$\mathrm{Tr}_B\,\rho = \rho^A. \tag{6.12}$$

The elements of the reduced density matrix ρ^A are

$$\langle u_i| \rho^A |u_{i'}\rangle = \sum_j \langle u_i v_j| \rho |u_{i'}, v_j\rangle . \tag{6.13}$$

Similarly, the elements of ρ^B are

$$\langle v_j| \rho^B |v_{j'}\rangle = \sum_i \langle u_i, v_j| \rho |u_i, v_{j'}\rangle . \tag{6.14}$$

From these definitions, it is possible to verify the measurements in the system of controlled changes on QGs.[104–106]

Applying the partial trace on the density matrix defined in Eq. (6.9), the reduced density matrix for Alice's subsystem is

$$\rho^A = \begin{pmatrix} |r_A|^2 |r_B|^2 + |r_A|^2 |t_B|^2 & r_A r_B t_A^* r_{B'}^* + r_A t_B t_A^* t_{B'}^* \\ t_A r_{B'} r_A^* r_B^* + t_A t_{B'} r_A^* t_B^* & |t_A|^2 |r_{B'}|^2 + |t_A|^2 |t_{B'}|^2 \end{pmatrix} \tag{6.15}$$

and simplifying with $|r_j|^2 + |t_j|^2 = 1$,

$$\rho^A = \begin{pmatrix} |r_A|^2 & r_A t_A^* (r_B r_{B'}^* + t_B t_{B'}^*) \\ t_A r_A^* (r_{B'} r_B^* + t_{B'} t_B^*) & |t_A|^2 \end{pmatrix} \tag{6.16}$$

As Alice have the controller system, the measurements in each channel will return $|r_A|^2$ and $|t_A|^2$. By doing the partial trace over the first subsystem, we obtain the reduced density matrix for Bob's subsystem

$$\rho^B = \begin{pmatrix} |r_A|^2|r_B|^2 + |t_A|^2|r_{B'}|^2 & |r_A|^2 r_B t_B^* + |t_A|^2 r_{B'} t_{B'}^* \\ |r_A|^2 t_B r_B^* + |t_A|^2 t_{B'} r_{B'}^* & |r_A|^2|t_B|^2 + |t_A|^2|t_{B'}|^2 \end{pmatrix} . \tag{6.17}$$

From that we obtain the expected transmission value in Bob's QG as

$$\langle 1| \rho^B |1\rangle = |r_A|^2|t_B|^2 + |t_A|^2|t_{B'}|^2, \tag{6.18}$$

that can be rewritten by defining a parameter $p = |t_A|^2$ and then we have

$$T_B(k, p) = (1 - p) |t_B|^2 + p|t_{B'}|^2, \tag{6.19}$$

similar to the case presented in Definition 5.2.1. Hence, the measurements in Bob's QG scattering channels can be studied as a linear combination of the two possible transmission probabilities of the system. A similar situation to the case studied in the last chapter for RQGs, but in this case with only two possible situations, with the parameter p related to the probability of the output in the controller.[107]

The partial trace, in addition to being used in the prediction of outcomes within individual subsystems, also enables the examination of information and entanglement characteristics of the system. Thus, the following subsection focusses on analysing the von Neumann entropy and the entanglement entropy.

6.1.2 Entanglement entropy

In classical information theory, there are some measurements, such as Shannon entropy, which gives a measurement of the information obtained from a set of events or a conditional entropy which measures the correlation between these events. Going to the theory of quantum information, some measurements of the information obtained in its respective systems are defined, which allows us to verify the differences between the information obtained between both cases. In this direction, there is a quantum information measurement that can be said to be an analogous approach to the Shannon entropy on quantum systems, the von Neumann entropy. The von Neumann entropy is defined from the density matrix ρ of the system as

$$H\left(\rho\right) = -\operatorname{Tr}\left(\rho \log_2 \rho\right), \tag{6.20}$$

which can be rewritten from the eigenvalues λ_j of ρ,

$$H(\rho) = -\sum_j \lambda_j \log_2 \lambda_j. \tag{6.21}$$

When taking the von Neumann entropy of the reduced matrix of a system defined by a pure state of two subsystems A and B, it receives

the name of *entropy of entanglement*, and for values different of zero, indicates that these subsystems are entangled. By taking the reduced density matrix for the two levels subsystem A, with eigenvalues λ_+ and λ_-, its entanglement entropy is

$$H\left(\rho^A\right) = -\lambda_+ \log_2 \lambda_+ - \lambda_- \log_2 \lambda_-. \tag{6.22}$$

This entropy is maximised in the case that both eigenvalues are equal, and is minimised when one of them is equal to 0. Also, this defines a measurement of entanglement for bipartite systems,

Returning to the proposed system of QGs, from the reduced density matrix obtained in Eq. (6.16), which have eigenvalues

$$\lambda_\pm = \frac{1}{2}\left(1 \pm \sqrt{\left(|r_A|^2 - |t_A|^2\right)^2 + 4\,|r_A|^2\,|t_A|^2\,|r_B r^*_{B'} + t_B t^*_{B'}|^2}\right). \tag{6.23}$$

The entanglement entropy of this system is maximized when these eigenvalues are equals, which is achieved when $\lambda_+ = \lambda_-$, which is satisfied for

$$\sqrt{\left(|r_A|^2 - |t_A|^2\right)^2 + 4\,|r_A|^2\,|t_A|^2\,|r_B r^*_{B'} + t_B t^*_{B'}|^2} = 0. \tag{6.24}$$

After some manipulation and using $|r_A|^2 = 1 - |t_A|^2$, we have

$$|r_A|^2\,|t_A|^2\left(1 - |r_B r^*_{B'} + t_B t^*_{B'}|^2\right) = \frac{1}{4}. \tag{6.25}$$

The only solution is obtained for $|r_A|^2 = |t_A|^2 = \frac{1}{2}$ with $|r_B r^*_{B'} + t_B t^*_{B'}|^2 = 0$.

The first condition, with $|r_A|^2 = |t_A|^2 = \frac{1}{2}$, retrieves the situation with maximal scattering entropy in this QG, which occurs under when there is an equal probability of scattering across all channels. This indicates that, in order to obtain maximal entanglement entropy within this system, the scattering entropy of the controller subsystem must also be maximal. This is only realised when the channel where the particle will be detected is completely indeterminate.

For the second condition, the scattering in Bob's QG must follows

$$r_B r^*_{B'} + t_B t^*_{B'} = 0 \tag{6.26}$$

that can be rewritten as

$$r_B r^*_{B'} = -t_B t^*_{B'}. \tag{6.27}$$

Taking the absolute squares of $r_B r^*_{B'}$ and $t_B t^*_{B'}$, and after some simplifications, we obtain

$$|r_B|^2 |r_{B'}|^2 = |t_B|^2 |t_{B'}|^2. \tag{6.28}$$

As $|r_j|^2 + |t_j|^2 = 1$, we thus have

$$(1 - |t_B|^2)(1 - |t_{B'}|^2) = |t_B|^2 |t_{B'}|^2, \tag{6.29}$$

$$1 - |t_B|^2 - |t_{B'}|^2 + |t_B|^2 |t_{B'}|^2 = |t_B|^2 |t_{B'}|^2, \tag{6.30}$$

$$|t_{B'}|^2 = 1 - |t_B|^2, \tag{6.31}$$

$$|t_{B'}|^2 = |r_B|^2. \tag{6.32}$$

This implies a flip between the scattering probabilities before and after the interaction.

Thus, we can simplify the restrictions to

$$\begin{cases} |r_A|^2 = |t_A|^2 = \frac{1}{2} \\ |r_{B'}|^2 = |t_B|^2 \\ |t_{B'}|^2 = |r_B|^2 \end{cases} \tag{6.33}$$

in which the maximal entanglement entropy is achieved.

However, if the entanglement entropy is 0, the system will be separable, in this case,

$$|r_A|^2 |t_A|^2 \left(1 - |r_B r^*_{B'} + t_B t^*_{B'}|^2\right) = 0, \tag{6.34}$$

This is obtained when the transmission probability in Alice's QG is either 0 or 1 in Alice's QG, or when $|r_B r^*_{B'} + t_B t^*_{B'}|^2 = 1$, which can be obtained

when there is no changes in the controlled quantum graph scattering probabilities. That is, the entanglement entropy of this system is zero if the scattering entropy in the first QG is zero, or if the operation performed in the second QG is equivalent to a global phase.

6.2 RESULTS

From the proposed system for interaction between two QG by controlled changes, it is possible to advance on the comprehension and verify the implications of this model by studying some cases. Therefore, in this section, we will exemplify some cases of possible controlled operations on QGs.

6.2.1 Two QGs with a controlled phase in the transmission channel

As a first example, let us define a system that does not actually change the structures of a QG, but affects its transmission amplitude. Consider Alice's QG Γ_A, with scattering amplitudes r_A and t_A and Bob's QG Γ_B, with scattering amplitudes r_B and t_B. Alice's subsystem contains a point $\mathcal{D}$ where its transmission channel $l_{1,A}$ interacts with the second system, applying a phase φ in the transmission channel $l_{1,B}$, as illustrated in

Figure 6.3 – The controlled scattering system of two quantum graphs Γ_A and Γ_B, where the controlled operation in the subsystem B is a phase φ applied on the scattering channel $l_{1,B}$

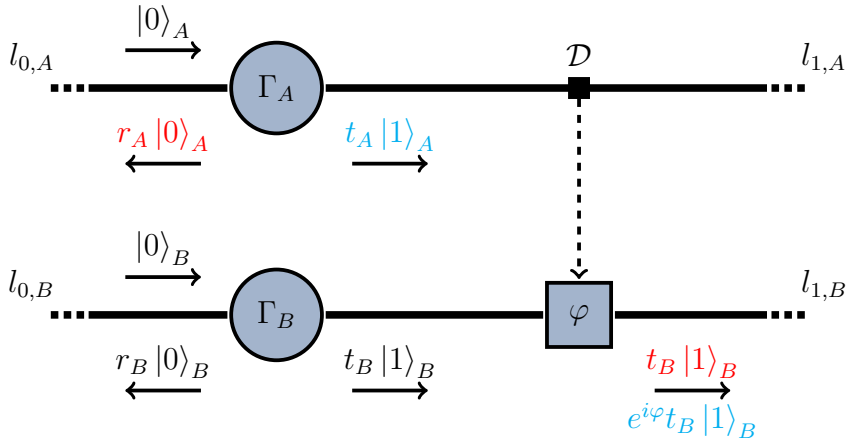

Source: the author.

Figure 6.3.

By applying a phase on the transmission channel of the second subsystem, its reflection is not affected, only its transmission will receive the increase in phase. Thus, after if the controlled phase is applied on Bob's subsystem, its scattering amplitudes become r_B and $e^{i\varphi}t_B$. In this way, the state of this system is obtained from Eq. (6.8) becomes

$$|\Psi\rangle = r_A r_B |0,0\rangle + r_A t_B |0,1\rangle + t_A r_B |1,0\rangle + e^{i\varphi} t_A t_B |1,1\rangle . \tag{6.35}$$

The conditions for obtaining maximum entanglement in this system are shown in Eq. (6.25). From that, we have

$$|r_A|^2 |t_A|^2 \left(1 - \left||r_B|^2 + e^{-i\varphi} |t_B|^2\right|^2\right) = \frac{1}{4}, \tag{6.36}$$

Figure 6.4 – The entanglement entropy as function of the transmission probability $|t_A|^2$ and $|t_B|^2$, from Alice and Bob quantum graphs, for controlled phase π is applied in Bob's QG changing its transmission to $t_{B'} = -t_B$).

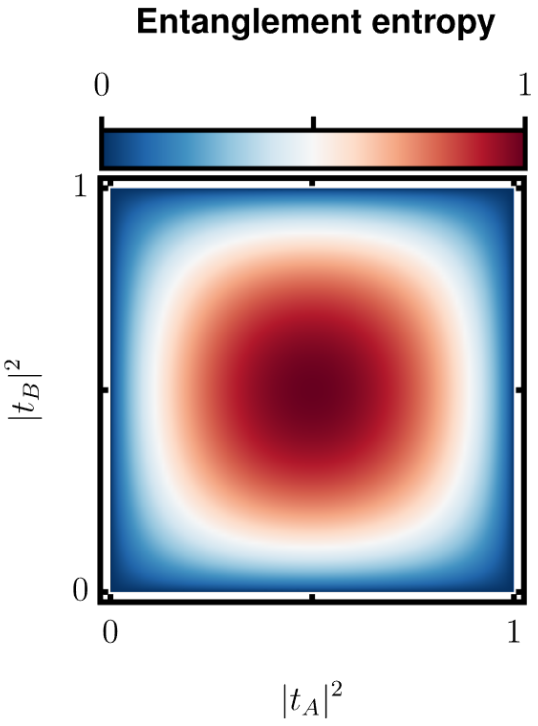

Source: the author.

expanding it with $|r_j|^2 = 1 - |t_j|^2$,

$$|t_A|^2 \left(1 - |t_A|^2\right) \left(1 - \left|1 - \left(1 - e^{-i\varphi}\right) |t_B|^2\right|^2\right) = \frac{1}{4}. \tag{6.37}$$

As $0 \leq |t_A|^2 \leq 1$, the only solution is found for

$$|t_A|^2 = \frac{1}{2}, \quad 1 - \left(1 - e^{-i\varphi}\right) |t_B|^2 = 0, \tag{6.38}$$

with $0 \leq |t_B|^2 \leq 1$ and for a real φ, we found that the only solution is given by

$$|t_A|^2 = |r_A|^2 = \frac{1}{2}, \quad |t_B|^2 = |r_B|^2 = \frac{1}{2}, \quad \varphi = (2n+1)\,\pi. \tag{6.39}$$

This implies that to achieve maximum entanglement in this system, the scattering probabilities on both QGs must be the same in each of its channels, together with the controlled phase on the second subsystem being $\varphi = \{\pi, 3\pi, 5\pi, ...\}$. Returning to the scattering entropy of QGs, both QGs must have maximal scattering entropy, having the same probability to both scattering channels. This reminds a case of the so called graph states, in which all the possible states have the same probability and it is prepared with a controlled-Z gate, which acts by applying a phase $\varphi = \pi$ in the controlled qubit.[14–17]

On the other hand, from the separability condition obtained on Eq. (6.34) this will be separable for

$$|r_A|^2 |t_A|^2 \left(1 - \left||r_B|^2 + e^{-i\varphi} |t_B|^2\right|^2\right) = 0. \tag{6.40}$$

This condition will be satisfied whenever $|r_A|^2 = 0$, $|t_A|^2 = 0$, or $\varphi = 2n\pi$ are satisfied. Thus, for separability of the systems, the scattering entropy of Alice's QG is 0, or the applied phase on Bob's QG does not affect its transmission amplitude.

The entanglement entropy of this system is illustrated in Figure 6.4, where the phase in which maximum entanglement is achieved, $\varphi = \pi$, was

applied. There, it is possible to visualise these limiting cases, where the maximal and minimal entanglement entropy are achieved as functions of the transmission probability in both QGs.

6.2.2 Quantum state from the scattering in a star QG.

As another example, consider the star QG as illustrated in Figure 6.5 (a), using the approach discussed in Section 3.2, we can obtain the scattering matrix

$$S_{\Gamma_{S_4}} = \frac{1}{2i + \tan(k\ell_{2,3})} \begin{pmatrix} -\tan(k\ell_{2,3})\, e^{2ik\ell_{1,2}} & 2ie^{ik(\ell_{1,2}+\ell_{2,4})} \\ 2ie^{ik(\ell_{1,2}+\ell_{2,4})} & -\tan(k\ell_{2,3})\, e^{2ik\ell_{2,4}} \end{pmatrix}. \tag{6.41}$$

As the edges length $\ell_{1,2}$ and $\ell_{2,4}$ only contribute in exponential terms, it is possible to redefine them as to the phase $\alpha = k\ell_{1,2}$, $\beta = k\ell_{2,4}$, as well as simplify $\ell_{2,3} = \ell$, which can also contain a phase change $k\ell \to k\ell + \phi$. This situation is illustrated in Figure 6.5 (b) in which the edges that contribute only with a phase shift on the scattering were replaced by an equivalent phase shift. From that, we thus have

$$S_{\Gamma_{S_4}} = \frac{1}{2i + \tan(k\ell + \phi)} \begin{pmatrix} -\tan(k\ell + \phi)\, e^{2ik\alpha} & 2ie^{ik(\alpha+\beta)} \\ 2ie^{ik(\alpha+\beta)} & -\tan(k\ell + \phi)\, e^{2ik\beta} \end{pmatrix}. \tag{6.42}$$

In order to reproduce the operation of some quantum logical gates, a possible case is the operator defined by the Hadamard matrix. In this

Figure 6.5 – (a) Star quantum graph with four vertices (Γ_{S_4}) and two leads l_0 and l_1 connected to v_1 and v_4 respectively. (b) A quantum graph with equivalent scattering amplitudes to the QG Γ_{S_4}, where the squares symbols represents phase shift operations.

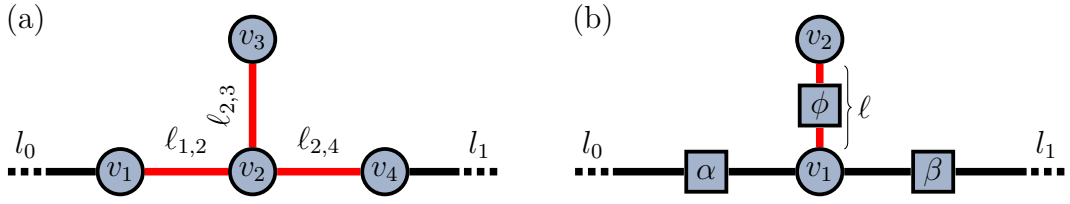

Source: the author.

case, it will obtained by solving

$$\frac{1}{2i+\tan(k\ell)}\begin{pmatrix} -e^{2i\alpha}\tan(k\ell) & 2ie^{i(\alpha+\beta)} \\ 2ie^{i(\alpha+\beta)} & -e^{2i\beta}\tan(k\ell) \end{pmatrix} = \frac{1}{\sqrt{2}}\begin{pmatrix} 1 & 1 \\ 1 & -1 \end{pmatrix}, \quad (6.43)$$

which solution is given by

$$\begin{cases} k\ell = n_{k\ell}\pi \pm \arctan(2) \\ \alpha = \left(2n_\alpha + \frac{1\pm 4}{16}\tan(k\ell)\right) \\ \beta = -3\alpha + (2n_\beta + 3)\,\pi \end{cases} \quad (6.44)$$

with $n_{k\ell}$, n_α and n_β integers. The first positive solutions are obtained with $n_1 = n_\alpha = n_\beta = 0$, in which we obtain $k\ell = \arctan(2)$, $\alpha = 5\pi/8$ and $\beta = 9\pi/8$.

Another possible case is by taking the values that remove these phases, $\alpha = n_\alpha\pi$ and $\beta = n_\beta\pi$. This leads to the scattering matrix

$$S_{\Gamma_{S_4}} = \frac{1}{2i+\tan(k\ell)}\begin{pmatrix} -\tan(k\ell) & 2i \\ 2i & -\tan(k\ell) \end{pmatrix}. \quad (6.45)$$

These results will be used in the following subsection.

Figure 6.6 – Illustration of the system composed by two quantum graphs Γ_A and Γ_B, where a controlled phase shift ϕ, activated by a coherent interaction $\mathcal{D}$, is applied on an edge of Γ_B.

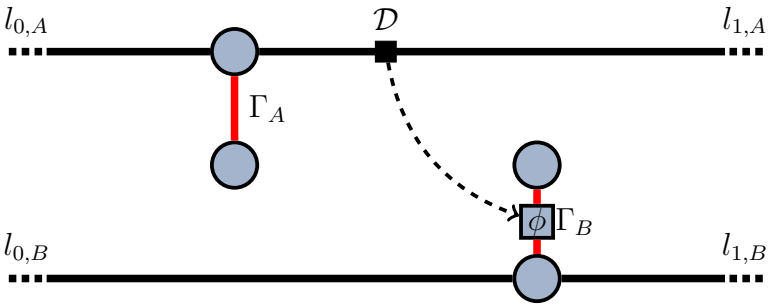

Source: the author.

6.2.3 Controlled operation between two QGs by a controlled phase gate on the internal edge.

In the interaction approach for QGs using a controlled change, let us assume that Alice and Bob QG are star quantum graphs, as illustrated in Figure 6.5, with the scattering matrix from equation (6.45), with defined wavenumber k_A and k_B for each subsystem A and B. Moreover, the controlled operation between them will be defined as a phase shift ϕ on Bob's QG when the particle scattering on Alice's QG is at the scattering channel $l_{1,A}$, as illustrated in Figure 6.6. Thus the scattering state in this system is given by

$$\begin{aligned}|\Psi\rangle = &\left(\frac{-\tan(k_A\ell)}{2i+\tan(k_A\ell)}\right)\left(\frac{-\tan(k_B\ell)}{2i+\tan(k_B\ell)}\right)|0,0\rangle \\ &+\left(\frac{-\tan(k_A\ell)}{2i+\tan(k_A\ell)}\right)\left(\frac{2i}{2i+\tan(k_B\ell)}\right)|0,1\rangle \\ &+\left(\frac{2i}{2i+\tan(k_A\ell)}\right)\left(\frac{-\tan(k_B\ell+\phi)}{2i+\tan(k_B\ell+\phi)}\right)|1,0\rangle \\ &+\left(\frac{2i}{2i+\tan(k_A\ell)}\right)\left(\frac{2i}{2i+\tan(k_B\ell+\phi)}\right)|1,1\rangle\,.\end{aligned} \tag{6.46}$$

From evaluating its density matrix, $\rho = |\Psi\rangle\langle\Psi|$, and its reduced density matrix, $\rho^A = \mathrm{Tr}_B(\rho)$, it is possible to obtain the entanglement entropy from the eigenvalues of ρ^A. Thus, the result obtained is illustrated in Fig. 6.7 (a) as a function of k_A, k_B and ϕ. From the condition for maximal entropy, Eq. (6.25), we got that

$$|r_A|^2\,|t_A|^2\left(1-|r_B r^*_{B'}+t_B t^*_{B'}|^2\right)=\frac{1}{4}, \tag{6.47}$$

which the solution are found with

$$\begin{cases}|r_A|^2=\dfrac{1}{2},\\ r_B r^*_{B'}+t_B t^*_{B'}=0.\end{cases} \tag{6.48}$$

Thus,

$$\begin{cases} \dfrac{4}{4+\tan^2(k_A\ell)} = \dfrac{1}{2}, \\ \tan(k_B\ell)\tan(k_B\ell+\phi) = -4, \end{cases} \tag{6.49}$$

which leads to the solutions as function of k_A and ϕ as

$$\begin{cases} k_A\ell = n_A\pi \pm \arctan(2), \\ \phi = -\arctan\left(\dfrac{3\sin(2k_B\ell)}{5+3\cos(2k_B\ell)}\right) + (2n+1)\dfrac{\pi}{2}. \end{cases} \tag{6.50}$$

Further details on obtaining ϕ is presented in Appendix D. These values were used in Figure 6.7 (b), where the cross section was taken from Figure 6.7 (a) at $k_A\ell = \arctan(2)$, and the dashed line in it shows the maximal entanglement entropy.

Finally, from the quantum states defined by Eq. (6.46) and the conditions for maximal entanglement entropy, we can obtain some maximal entangled quantum state. The first example is given by assuming $k_A\ell = \arctan(2)$ and $k_B\ell = \arctan(2)$, for which the phase can be defined as $\phi = \frac{\pi}{2} - \arctan\frac{3}{4}$ and results in the state

$$|\Psi_1\rangle = -\frac{i}{2}|0,0\rangle - \frac{1}{2}|0,1\rangle - \frac{i}{2}|1,0\rangle + \frac{1}{2}|1,1\rangle. \tag{6.51}$$

And, for a second example, when assuming $k_A\ell = \arctan(2)$ and $k_B\ell = \pi/2$, the entanglement entropy is maximal for $\phi = \pi/2$ and the obtained state is

$$|\Psi_2\rangle = \frac{e^{-i\pi/4}}{\sqrt{2}}(|0,0\rangle + i|1,1\rangle). \tag{6.52}$$

From which, the Bell state

$$\left|\Phi^+\right\rangle = \frac{1}{2}(|0,0\rangle + |1,1\rangle) \tag{6.53}$$

can be obtained by choosing one of the subsystems and applying a global phase $\pi/4$ and a phase shift $3\pi/2$ on its transmission channel.

Figure 6.7 – Entanglement entropy of a system with two quantum graphs Γ_A and Γ_B, as illustrated in Figure 6.6, with respective wavenumber k_A and k_B and a controlled phase shift ϕ applied in a edge of Γ_B. (a) Entanglement entropy as function of all the three variables $k_A\ell$, $k_B\ell$ and ϕ. (b) A cross section of the entanglement entropy of this system, taken in $k_A\ell = \epsilon = \arctan 2$, where the function of ϕ where the maximal entropy is achieved, is highlighted by a black dotted line.

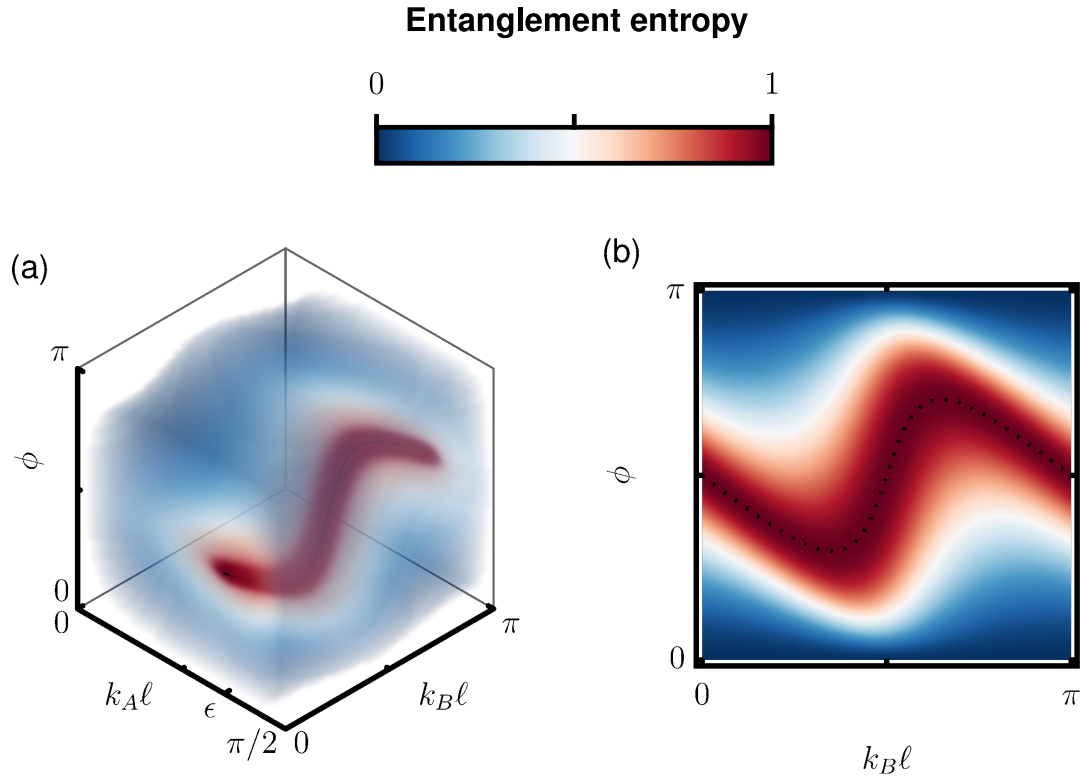

Source: the author.

7 FINAL REMARKS

In this thesis, the concepts of graphs and their application in the quantum graph model have been explored. Starting with matrix definition of graph, and the definition of quantum graphs, in which the Green's function approach can be defined from the adjacency matrix of the graph. With this method, we showed how to obtain the scattering amplitudes and the scattering matrix of these systems to understand the quantum transport on these structures.

We applied an informational entropy to the scattering probabilities of quantum graphs. This entropy aimed to show the distribution of the scattering over the different channels and was shown to be an interesting tool to investigate cases with a large number of probabilities involved, such as for quantum graphs with n channels. We also investigated the behaviour of the transmission amplitudes and the scattering entropy in some families of graphs, looking for the properties of their transport as a function of the wavenumber k. Furthermore, we obtained equations for series and parallel arrangements, which together with the methods used here can be applied to investigate larger networks recursively.

An application proposed here was to investigate filament formation and memristive devices. A computational routine was elaborated to evaluate filament formation by ions in the presence of a difference of potential between the electrodes and the respective graphs from these filaments. From these graphs, we evaluated the electrical current on them and the results showed a hysteresis, as expected for memristive devices. Finally, we applied a Monte Carlo method to evaluate many cycles of filament formation and compared their results, verifying the behaviour of the hysteresis as a function of some parameters of the system.

Next, motivated by the evaluation of transmission in random structures, we elaborate a method for studying randomisation on quantum graphs. Two approaches were considered, one of the exact transmission

coefficient, taking all the spanning subgraphs, and the approximated, taking random samples of possible subgraphs. This last method is suitable for randomisation of graphs with many edges, especially when treating graphs like the complete ones, as their number exponentially grows with the number of vertices. We also noticed the behaviour of the transport at some values of $k\ell$, and verified that some values of transmission can remain the same or close to it even with the removal of some edges. This can be used in optimising these networks, aiming at the transmission or suppression of the signal in some values of the wavenumber without needing a large number of connections.

Finally, we discuss an approach that uses a quantum state of scattering, obtained by the scattering matrix of the system. This allowed us to propose a case of interaction between two particles in different quantum graphs by a controlled operation in a graph induced by the other. From that we were able to discuss the state composed of both systems, whose amplitudes are controlled by the scattering amplitudes of the respective quantum graphs, and found a link to the randomised quantum graph, where the controller is acting as a randomisation parameter of the controlled system. We discussed the von Neumann entropy on them and found the conditions under which there will not be entanglement or the ones that led to an ideal controlled operation to find maximal entanglement; for this last situation we found a relationship with the scattering entropy of the graph used as a controller. Finally, examples of controlled operation between them were discussed, in the first one finding conditions similar to the graph states; and in the second one, where the operation is inside the second network, we discussed the necessary operations to achieve entanglement in such systems and exemplified the possible maximal entangled states that can be obtained for it.

For future works, we can list

- Studies on the inverse problem of quantum graphs, obtaining the possible quantum graphs in which a given scattering matrix is obtained.

- Analysis of the poles of the Green's function in quantum graphs and the change on its spectra with some parameter changes. This can also be studied together with the randomized quantum graph models, and even propose further randomization models.
- Extension of the model of filamentary switching in quantum graphs, by applying different potential along the edges according to its position.
- Apply the weight sum of transmission probabilities on quantum graphs to models of structure changes or even in dynamical graphs.
- Studies on the quantum graph interactions model to apply more controlled operations on it. This can lead to some directions, the first for interactions between more than two quantum graphs and the other for applying on quantum algorithms and modelling some of the already existing ones.

REFERENCES

1 A few holes to fill. **Nature Physics**, n. 4, p. 257, 2008.

2 SHARP, K.; MATSCHINSKY, F. Translation of ludwig boltzmann's paper "on the relationship between the second fundamental theorem of the mechanical theory of heat and probability calculations regarding the conditions for thermal equilibrium" sitzungberichte der kaiserlichen akademie der wissenschaften. mathematisch-naturwissen classe. abt. ii, lxxvi 1877, pp 373-435 (wien. ber. 1877, 76: 373-435). reprinted in wiss. abhandlungen, vol. ii, reprint 42, p. 164-223, barth, leipzig, 1909. **Entropy**, v. 17, n. 4, p. 1971–2009, 2015.

3 KELVIN, L. I. nineteenth century clouds over the dynamical theory of heat and light. **The London, Edinburgh, and Dublin Philosophical Magazine and Journal of Science**, v. 2, n. 7, p. 1–40, 1901.

4 PLANCK, M. On the law of distribution of energy in the normal spectrum. **Annalen der physik**, v. 4, n. 553, p. 1, 1901.

5 PAULING, L. The diamagnetic anisotropy of aromatic molecules. **The Journal of chemical physics**, v. 4, n. 10, p. 673–677, 1936.

6 FAROOQ, O. et al. Experimental investigation of the generalized euler characteristic of the networks split at edges. **Mathematics**, v. 10, n. 20, p. 3785, 2022.

7 GRIFFITH, J. S. A free-electron theory of conjugated molecules. part 1.—polycyclic hydrocarbons. **Transactions of the Faraday Society**, v. 49, p. 345–351, 1953.

8 GRIFFITH, J. S. A free-electron theory of conjugated molecules: *ii*. a derived algebraic scheme. **Mathematical Proceedings of the Cambridge Philosophical Society**, v. 49, n. 4, p. 650–658, 1953.

9 AHARONOV, D. et al. Quantum walks on graphs. In: **Proceedings of the thirty-third annual ACM symposium on Theory of computing**. [S.l.: s.n.], 2001. p. 50–59.

10 TANNER, G. K. From quantum graphs to quantum random walks. In: **Non-Linear Dynamics and Fundamental Interactions**. [S.l.: s.n.], 2006. v. 213, cap. From quantum graphs to quantum random walks, p. 69–87.

11 ATTAL, S.; PETRUCCIONE, F.; SINAYSKIY, I. Open quantum walks on graphs. **Physics Letters A**, v. 376, n. 18, p. 1545–1548, 2012.

12 HARTMANN, L. et al. Weighted graph states and applications to spin chains, lattices and gases. **Journal of Physics B: Atomic, Molecular and Optical Physics**, v. 40, n. 9, p. S1, 2007.

13 ESTARELLAS, M. P.; D'AMICO, I.; SPILLER, T. P. Robust quantum entanglement generation and generation-plus-storage protocols with spin chains. **Physical Review A**, v. 95, n. 4, p. 042335, 2017.

14 HEIN, M. et al. Entanglement in graph states and its applications. **arXiv preprint quant-ph/0602096**, 2006. Disponível em: `https://arxiv.org/abs/quant-ph/0602096`. Acesso em: 15 abr. 2025.

15 BRIEGEL, H. J. Cluster states. In: **Compendium of Quantum Physics**. [S.l.: s.n.], 2009. p. 96–105.

16 WU, J.-Y. et al. Randomized graph states and their entanglement properties. **Physical Review A**, v. 89, n. 5, p. 052335, 2014.

17 SALEM, V.; SILVA, A. A.; ANDRADE, F. M. Multipartite entanglement sudden death and birth in randomized hypergraph states. **Physical Review A**, v. 109, n. 1, p. 012416, 2024.

18 RAUSSENDORF, R.; BROWNE, D. E.; BRIEGEL, H. J. Measurement-based quantum computation on cluster states. **Physical Review A**, v. 68, n. 2, p. 022312, 2003.

19 BRIEGEL, H. J. et al. Measurement-based quantum computation. **Nature Physics**, v. 5, n. 1, p. 19–26, 2009.

20 KOTTOS, T.; SMILANSKY, U. Quantum chaos on graphs. **Physical Review Letters**, v. 79, p. 4794, 1997.

21 KOTTOS, T.; SMILANSKY, U. Periodic orbit theory and spectral statistics for quantum graphs. **Ann. Phys. (NY)**, v. 274, n. 1, p. 76–124, 1999.

22 KOTTOS, T.; SMILANSKY, U. Chaotic scattering on graphs. **Physical Review Letters**, v. 85, n. 5, p. 968, Jul 2000.

23 KOTTOS, T.; SMILANSKY, U. Quantum graphs: a simple model for chaotic scattering. **Journal of Physics A: Mathematical and General**, v. 36, n. 12, p. 3501, 2003.

24 ANDRADE, F. M.; LUZ, M. G. E. da. Green-function approach for scattering quantum walks. **Physical Review A**, v. 84, n. 4, p. 042343, 2011.

25 ANDRADE, F. et al. A generalized semiclassical expression for the eigenvalues of multiple well potentials. **Journal of Physics A: Mathematical and General**, v. 36, n. 1, p. 227, 2002.

26 ANDRADE, F. M. Exact green's function for rectangular potentials and its application to quasi-bound states. **Physics Letters A**, v. 378, n. 21, p. 1461–1468, 2014.

27 ANDRADE, F. M. **Métodos de funçao de green na análise de grafos quânticos e caminhadas quânticas**. Tese (Doutorado) — UFPR, Universidade Federal do Paraná, Curitiba, 2009.

28 ANDRADE, F. M. et al. Green's function approach for quantum graphs: an overview. **Physics Reports**, v. 647, p. 1–46, 2016.

29 ANDRADE, F. M.; SEVERINI, S. Unitary equivalence between the green's function and schrödinger approaches for quantum graphs. **Physical Review A**, v. 98, n. 6, p. 062107, 2018.

30 EULER, L. Solutio problematis ad geometriam situs pertinentis. **Commentarii academiae scientiarum Petropolitanae**, p. 128–140, 1741.

31 BIGGS, N.; LLOYD, E. K.; WILSON, R. J. **Graph Theory, 1736-1936**. [S.l.: s.n.], 1986.

32 WEST, D. B. **Introduction to graph theory**. [S.l.: s.n.], 2001.

33 SACHS, H.; STIEBITZ, M.; WILSON, R. An historical note: Euler's königsberg letters. **Journal of Graph Theory**, v. 12, p. 133 – 139, 10 2006.

34 FOULDS, L. R. **Graph theory applications**. Nova Iorque: [s.n.], 1992.

35 LEVINE, I. N. **Quantum chemistry**. 5. ed. New Jersey: [s.n.], 1999.

36 BERKOLAIKO, G.; KUCHMENT, P. **Introduction to Quantum Graphs**. Providence, RI: [s.n.], 2013. (Mathematical Surveys and Monographs, v. 186). ISBN 0-8218-9211-8.

37 BROUWER, A. E.; HAEMERS, W. H. **Spectra of graphs**. [S.l.: s.n.], 2012.

38 NEWMAN, M. **Networks: An Introduction**. [S.l.: s.n.], 2010.

39 SHAPIRO, B. Renormalization-group transformation for the anderson transition. **Physical Review Letters**, v. 48, n. 12, p. 823, 1982.

40 SHAPIRO, B. Quantum conduction on a Cayley tree. **Physical Review Letters**, v. 50, n. 10, p. 747, 1983.

41 BÜTTIKER, M.; IMRY, Y.; AZBEL, M. Y. Quantum oscillations in one-dimensional normal-metal rings. **Physical Review A**, v. 30, n. 4, p. 1982, 1984.

42 KOWAL, D. et al. Transmission through multiply-connected wire systems. **Physical Review B**, v. 42, n. 14, p. 9009, nov. 1990.

43 AVRON, J.; SADUN, L. Adiabatic quantum transport in networks with macroscopic components. **Annals of Physics**, v. 206, n. 2, p. 440–493, 1991.

44 KLESSE, R.; METZLER, M. Spectral compressibility at the metal-insulator transition of the quantum hall effect. **Physical Review Letters**, v. 79, n. 4, p. 721, Jul 1997.

45 EXNER, P.; ŠEBA, P. Free quantum motion on a branching graph. **Reports on mathematical physics**, v. 28, n. 1, p. 7–26, 1989.

46 BLÜMEL, R.; DABAGHIAN, Y.; JENSEN, R. V. Explicitly solvable cases of one-dimensional quantum chaos. **Physical Review Letters**, v. 88, n. 4, p. 044101, 2002.

47 BLÜMEL, R.; DABAGHIAN, Y.; JENSEN, R. V. Exact, convergent periodic-orbit expansions of individual energy eigenvalues of regular quantum graphs. **Physical Review E**, v. 65, n. 4, p. 046222, 2002.

48 KOTTOS, T.; SCHANZ, H. Quantum graphs: a model for quantum chaos. **Physica E: Low-dimensional Systems and Nanostructures**, v. 9, n. 3, p. 523, 2001. ISSN 1386-9477.

49 KAPLAN, L. Eigenstate structure in graphs and disordered lattices. **Physical Review E**, v. 64, n. 3, p. 036225, 2001.

50 BERKOLAIKO, G. An elementary introduction to quantum graphs. **Geometric and computational spectral theory**, Providence, Rhode Island, v. 700, p. 41–72, 2017.

51 EXNER, P. Lattice kronig-penney models. **Physical Review Letters**, v. 74, n. 18, p. 3503, 1995.

52 BOLTE, J.; ENDRES, S. The trace formula for quantum graphs with general self adjoint boundary conditions. In: SPRINGER. **Annales Henri Poincaré**. [S.l.], 2009. v. 10, n. 1, p. 189–223.

53 ECONOMOU, E. N. **Green's functions in quantum physics**. [S.l.: s.n.], 2006.

54 FEYNMAN, R. Space-time approach to non-relativistic quantum mechanics. **Reviews of Modern Physics**, v. 20, n. 2, p. 367–387, 1948.

55 LUZ, M. D.; HELLER, E.; CHENG, B. K. Exact form of green functions for segmented potentials. **Journal of Physics A: Mathematical and General**, v. 31, n. 13, p. 2975, 1998.

56 REDHEFFER, R. On the relation of transmission-line theory to scattering and transfer. **Journal of Mathematics and Physics**, v. 41, n. 1-4, p. 1–41, 1962.

57 MISTIRI, F.; WANG, A. P. The star-product and its algebraic properties. **Journal of the Franklin Institute**, v. 321, n. 1, p. 21–38, 1986.

58 KOSTRYKIN, V.; SCHRADER, R. The generalized star product and the factorization of scattering matrices on graphs. **Journal of Mathematical Physics**, v. 42, n. 4, p. 1563–1598, 2001.

59 SHANNON, C. E. A mathematical theory of communication. **The Bell system technical journal**, v. 27, n. 3, p. 379–423, 1948.

60 MANDAL, D.; QUAN, H.; JARZYNSKI, C. Maxwell's refrigerator: an exactly solvable model. **Physical Review Letters**, v. 111, n. 3, p. 030602, 2013.

61 PARRONDO, J. M.; HOROWITZ, J. M.; SAGAWA, T. Thermodynamics of information. **Nature physics**, v. 11, n. 2, p. 131–139, 2015.

62 GLEISER, M.; STAMATOPOULOS, N. Entropic measure for localized energy configurations: Kinks, bounces, and bubbles. **Physics Letters B**, v. 713, n. 3, p. 304–307, 2012.

63 CORREA, R.; DUTRA, A. de S.; GLEISER, M. Information-entropic measure of energy-degenerate kinks in two-field models. **Physics Letters B**, v. 737, p. 388–394, 2014.

64 SILVA, A. A.; ANDRADE, F. M.; BAZEIA, D. Average scattering entropy of quantum graphs. **Physical Review A**, v. 103, n. 6, p. 062208, 2021.

65 SILVA, A. A.; ANDRADE, F. M.; BAZEIA, D. Average scattering entropy for periodic, aperiodic and random distribution of vertices in simple quantum graphs. **Physica E: Low-dimensional Systems and Nanostructures**, v. 141, p. 115217, 2022.

66 SILVA, A. A.; ANDRADE, F. M.; BAZEIA, D. Scattering entropies of quantum graphs with several channels. **The European Physical Journal Plus**, v. 139, n. 7, p. 659, 2024.

67 TANNER, G. Spectral statistics for unitary transfer matrices of binary graphs. **Journal of Physics A: Mathematical and General**, v. 33, n. 18, p. 3567, 2000.

68 DRINKO, A.; ANDRADE, F. M.; BAZEIA, D. Simple quantum graphs proposal for quantum devices. **The European Physical Journal Plus**, v. 135, n. 6, p. 451, jun 2020.

69 AHMED, M. et al. Meta-networks: Reconfigurable cable network topologies for interference control. In: **2021 IEEE International Joint EMC/SI/PI and EMC Europe Symposium**. [S.l.: s.n.], 2021. p. 520–523.

70 MELNIKOV, D. Knots and signal transmission in topological quantum devices. **Journal of Physics A: Mathematical and Theoretical**, v. 54, n. 44, p. 445202, 2021.

71 LAWRIE, T.; TANNER, G.; CHRONOPOULOS, D. A quantum graph approach to metamaterial design. **Scientific Reports**, v. 12, n. 1, p. 18006, 2022.

72 LAWRIE, T.; TANNER, G.; CHAPLAIN, G. Engineering metamaterial interface scattering coefficients via quantum graph theory. **Acta Physica Polonica A ISSN 1898-794X**, v. 144, n. 6, p. 486–486, 2023.

73 CHUA, L. Memristor-the missing circuit element. **IEEE Trans. Circuit Theory**, v. 18, n. 5, p. 507–519, 1971.

74 PERSHIN, Y. V.; VENTRA, M. D. Memory effects in complex materials and nanoscale systems. **Advances in Physics**, v. 60, n. 2, p. 145–227, 2011.

75 VENTRA, M. D. **Electrical transport in nanoscale system**. [S.l.: s.n.], 2008.

76 BÜTTIKER, M. et al. Generalized many-channel conductance formula with application to small rings. **Physical Review B**, v. 31, n. 10, p. 6207, 1985.

77 LANDAUER, R. Johnson-nyquist noise derived from quantum mechanical transmission. **Physica D: Nonlinear Phenomena**, v. 38, n. 1-3, p. 226–229, 1989.

78 KAWABATA, A. Theory of ballistic transport through a constriction-quantization of conductance. **Journal of the Physical Society of Japan**, v. 58, n. 2, p. 372–375, 1989.

79 BÜTTIKER, M. Scattering theory of thermal and excess noise in open conductors. **Physical Review Letters**, v. 65, n. 23, p. 2901, 1990.

80 BÜTTIKER, M. Quantized transmission of a saddle-point constriction. **Physical Review B**, v. 41, n. 11, p. 7906, 1990.

81 LANDAUER, R.; MARTIN, T. Equilibrium and shot noise in mesoscopic systems. **Physica B: Condensed Matter**, v. 175, n. 1-3, p. 167–177, 1991.

82 LANDAUER, R.; MARTIN, T. Erratum equilibrium and shot noise in mesoscopic systems. **Physica B: Condensed Matter**, v. 182, p. 288, 1992.

83 BÜTTIKER, M. Scattering theory of current and intensity noise correlations in conductors and wave guides. **Physical Review B**, v. 46, n. 19, p. 12485, 1992.

84 AONO, M.; HASEGAWA, T. The atomic switch. **Proceedings of the IEEE**, v. 98, n. 12, p. 2228–2236, 2010.

85 CHENG, B. et al. Ultra compact electrochemical metallization cells offering reproducible atomic scale memristive switching. **Communications Physics**, v. 2, n. 1, p. 28, 2019.

86 AGRAIT, N.; YEYATI, A. L.; RUITENBEEK, J. M. V. Quantum properties of atomic-sized conductors. **Physics Reports**, v. 377, n. 2-3, p. 81–279, 2003.

87 MAKK, P.; CSONKA, S.; HALBRITTER, A. Effect of hydrogen molecules on the electronic transport through atomic-sized metallic junctions in the superconducting state. **Physical Review B**, v. 78, n. 4, p. 045414, 2008.

88 SCHEER, E. et al. The signature of chemical valence in the electrical conduction through a single-atom contact. **Nature**, v. 394, n. 6689, p. 154–157, 1998.

89 FRENKEL, J. On pre-breakdown phenomena in insulators and electronic semi-conductors. **Physical Review**, v. 54, n. 8, p. 647, 1938.

90 SIMMONS, J. G. Generalized formula for the electric tunnel effect between similar electrodes separated by a thin insulating film. **Journal of Applied Physics**, v. 34, n. 6, p. 1793–1803, 1963.

91 SILVA, A. A. **filamentary switching - quantum graph**. 2025. Disponível em: `https://youtu.be/-HUG8_25aas`. Acesso em: 03 fev. 2025.

92 TÖRÖK, T. N. et al. Breaking the quantum pin code of atomic synapses. **Nano Lett.**, v. 20, n. 2, p. 1192–1200, 2020.

93 SILVA, A. A.; ANDRADE, F.; CARAVELLI, F. **Quantum graph models for transport in filamentary switching**. 2024. Wolfram Community, STAFF PICKS. Disponível em: `https://community.wolfram.com/groups/-/m/t/3332704`. Acesso em: 15 abr. 2025.

94 SILVA, A. A.; ANDRADE, F. M.; CARAVELLI, F. Quantum graph models for transport in filamentary switching. **Physical Review B**, v. 111, n. 4, p. 045145, 2025.

95 RAPOPORT, A. Cycle distributions in random nets. **The bulletin of mathematical biophysics**, v. 10, p. 145–157, 1948.

96 BARABASI, A.-L. **Network Science**. [S.l.: s.n.], 2016. Disponível em: `https://www.ebook.de/de/product/24312547/albert_laszlo_barabasi_network_science.html`. Acesso em: 15 abr. 2025. ISBN 1107076269.

97 SOLOMONOFF, R.; RAPOPORT, A. Connectivity of random nets. **The bulletin of mathematical biophysics**, v. 13, p. 107–117, 1951.

98 ERDŐS, P.; RÉNYI, A. On random graphs |. **Publicationes Mathematicae**, v. 6, p. 290–297, 1959.

99 GILBERT, E. N. Random graphs. **The Annals of Mathematical Statistics**, v. 30, n. 4, p. 1141–1144, 1959.

100 PERSEGUERS, S. et al. Quantum random networks. **Nature Physics**, v. 6, n. 7, p. 539–543, 2010. ISSN 1745-2481.

101 BIAMONTE, J.; FACCIN, M.; DOMENICO, M. D. Complex networks from classical to quantum. **Communications Physics**, v. 2, n. 1, p. 53, 2019.

102 ARUTE, F. et al. Quantum supremacy using a programmable superconducting processor. **Nature**, v. 574, n. 7779, p. 505–510, 2019.

103 SCHUMACHER, B. Quantum coding. **Physical Review A**, v. 51, n. 4, p. 2738, 1995.

104 NIELSEN, M. A.; CHUANG, I. **Quantum computation and quantum information**. Cambridge: [s.n.], 2010.

105 COHEN-TANNOUDJI, C.; DIU, B.; LALOË, F. **Quantum Mechanics**. [S.l.: s.n.], 1977.

106 WILLIAMS, C. P. **Explorations in quantum computing**. [S.l.: s.n.], 2010.

107 SILVA, A. A.; BAZEIA, D.; ANDRADE, F. M. Quantum transport in randomized quantum graphs. **APL Quantum**, v. 1, n. 4, p. 046126, 12 2024. ISSN 2835-0103.

108 SILVA, A. A.; ANDRADE, F. M.; BAZEIA, D. Average scattering entropy of quantum graphs. **Physical Review A**, v. 103, n. 6, p. 062208, 2021.

109 SILVA, A. A.; BAZEIA, D.; ANDRADE, F. M. Entangled states from simple quantum graphs. **arXiv preprint quant-ph/2503.04066**, 2025. Disponível em: `https://arxiv.org/abs/2503.04066`. Acesso em: 6 mar. 2025.

APPENDIX A LIST OF PUBLICATIONS

Parts of this thesis is based on material published in the following papers:

- **Average scattering entropy of quantum graphs**[108]
  A. A. Silva, F. M. Andrade, D. Bazeia
  Physical Review A **103** (6), 062208 (2021)

- **Average scattering entropy for periodic, aperiodic and random distribution of vertices in simple quantum graphs**[65]
  A. A. Silva, F. M. Andrade, D. Bazeia
  Physica E: Low-dimensional Systems and Nanostructures **141**, 115217 (2022)

- **Scattering entropies of quantum graphs with several channels**[66]
  A. A. Silva, F. M. Andrade, D. Bazeia
  The European Physical Journal Plus **139** (7), 1-16 (2024)

- **Quantum transport in randomized quantum graphs**[107]
  A. A. Silva, D. Bazeia, F. M. Andrade
  APL Quantum **1** (4) (2024)

- **Quantum graph models for transport in filamentary switching**[94]
  A. A. Silva, F. M. Andrade, F. Caravelli
  Physical Review B **111** (4), 045145 (2025)

- **Entangled states from simple quantum graphs**[109]
  A. A. Silva, D. Bazeia, F. M. Andrade
  Submitted, arXiv:2503.04066 (2025)

The author has contributed to this paper that is not covered in this thesis:

- **Multipartite entanglement sudden death and birth in randomized hypergraph states**[17]
  V. Salem, A. A. Silva, F. M. Andrade
  Physical Review A **109** (1), 012416 (2024)

APPENDIX B TRANSMISSION COEFFICIENT IN QGS

This appendix is dedicated to show the obtaining of transmission coefficients in some quantum graphs from the Green's function approach. From Eq. 3.15 for the scattering in a quantum graph between two different leads, we have

$$\mathcal{G}_{\Gamma_G}(x_f, x_i; k) = \frac{m}{i\hbar^2 k} T^{(f,i)}_{\Gamma_G}(k)\, e^{ik(x_f+x_i)}, \tag{B.1}$$

and

$$T^{(f,i)}_{\Gamma_G}(k) = t_i \sum_{j=1}^{|V|} A_{i,j} P_{i,j} \tag{B.2}$$

we can go directly to the obtaining of the equation systems that gives $P_{i,j}$ and for then obtain this transmission amplitudes.

B.1 Path graph P_2 The transmission is obtained from the equation system

$$\begin{cases} P_{1,2} = r_2 e^{ik\ell} P_{2,1} + t_2 e^{ik\ell}, \\ P_{2,1} = r_1 e^{ik\ell} P_{1,2}. \end{cases} \tag{B.3}$$

Solving for $P_{1,2}$

$$P_{1,2} = r_1 r_2 e^{2ik\ell} P_{1,2} + t_2 e^{ik\ell}. \tag{B.4}$$

Simplifying,

$$P_{1,2}(1 - r_1 r_2 e^{2ik\ell}) = t_2 e^{ik\ell}, \tag{B.5}$$

$$P_{1,2} = \frac{t_2 e^{ik\ell}}{(1 - r_1 r_2 e^{2ik\ell})}. \tag{B.6}$$

Multiplying by the transmission amplitude in the entrance vertex, we obtain it transmission amplitude

$$T_{\Gamma_{P_2}} = \frac{t_1 t_2 e^{ik\ell}}{(1 - r_1 r_2 e^{2ik\ell})}. \tag{B.7}$$

Similarly, the reflection amplitude is obtained from

$$\begin{cases} P_{1,2} = r_2 e^{ik\ell} P_{2,1}, \\ P_{2,1} = r_1 e^{ik\ell} P_{1,2} + t_1 e^{ik\ell}. \end{cases} \tag{B.8}$$

Solving for $P_{1,2}$,

$$P_{1,2} = r_2 e^{ik\ell} \left(r_1 e^{ik\ell} P_{1,2} + t_1 e^{ik\ell} \right), \tag{B.9}$$

$$P_{1,2} \left(1 - r_1 r_2 e^{2ik\ell} \right) = t_1 r_2 e^{2ik\ell}. \tag{B.10}$$

Then, the reflection amplitude is obtained by

$$R_{\Gamma_{P_2}} = r_1 + t_1 P_{1,2} \tag{B.11}$$

$$R_{\Gamma_{P_2}} = r_1 + \frac{t_1^2 r_2 e^{2ik\ell}}{1 - r_1 r_2 e^{2ik\ell}}. \tag{B.12}$$

B.2 Cycle graph C_4 The transmission amplitude on a quantum graph C_4 entering in the vertex 1 and exiting in the vertex 4 is obtained by the equation system

$$\begin{cases} P_{1,2} = z_1 \left(r_2 P_{2,1} + t_2 P_{2,4} \right) \\ P_{2,1} = z_1 \left(r_1 P_{1,2} + t_1 P_{1,3} \right) \\ P_{1,3} = z_2 \left(r_3 P_{3,1} + t_3 P_{3,4} \right) \\ P_{3,1} = z_2 \left(r_1 P_{1,3} + t_1 P_{1,2} \right) \\ P_{2,4} = z_1 \left(r_4 P_{4,2} + t_4 P_{4,3} + t_4 \right) \\ P_{4,2} = z_1 \left(r_2 P_{2,4} + t_2 P_{2,1} \right) \\ P_{3,4} = z_2 \left(r_4 P_{4,3} + t_4 P_{4,2} + t_4 \right) \\ P_{4,3} = z_2 \left(r_3 P_{3,4} + t_3 P_{3,1} \right) \end{cases} \tag{B.13}$$

Here, to illustrate, we will do some simplifications to obtain the transmission in two edges in parallel between two vertices. To do that, we will assume from the Neumann-Kirchhoff boundary conditions that $r_1 = r_4 = -1/3$, $t_1 = t_4 = 2/3$, $r_2 = r_3 = 0$ and $t_2 = t_3 = 1$. In addition, we will redefine the metric at these edges by $z_1 = z_{\ell_1}^{1/2}$ and $z_2 = z_{\ell_2}^{1/2}$. Thus, we

have

$$\begin{cases} P_{1,2} = z_{\ell_1}^{1/2}\,(P_{2,4}) \\ P_{2,1} = z_{\ell_1}^{1/2}\left(-\frac{1}{3}P_{1,2} + \frac{2}{3}P_{1,3}\right) \\ P_{1,3} = z_{\ell_2}^{1/2}\,(P_{3,4}) \\ P_{3,1} = z_{\ell_2}^{1/2}\left(-\frac{1}{3}P_{1,3} + \frac{2}{3}P_{1,2}\right) \\ P_{2,4} = z_{\ell_1}^{1/2}\left(-\frac{1}{3}P_{4,2} + \frac{2}{3}P_{4,3} + \frac{2}{3}\right) \\ P_{4,2} = z_{\ell_1}^{1/2}\,(P_{2,1}) \\ P_{3,4} = z_{\ell_2}^{1/2}\left(-\frac{1}{3}P_{4,3} + \frac{2}{3}P_{4,2} + \frac{2}{3}\right) \\ P_{4,3} = z_{\ell_2}^{1/2}\,(P_{3,1}) \end{cases} \tag{B.14}$$

Solving that for $P_{1,2}$ and $P_{1,3}$, as they are the path families that starts in the entrance vertex,

$$\begin{cases} P_{1,2} = \frac{2z_{\ell_1}\left(3-2z_{\ell_1}z_{\ell_2}-z_{\ell_2}^2\right)}{9-8z_{\ell_1}z_{\ell_2}-z_{\ell_2}^2-z_{\ell_1}^2+z_{\ell_1}^2z_{\ell_2}^2}, \\ P_{1,3} = \frac{2z_{\ell_2}\left(3-2z_{\ell_1}z_{\ell_2}-z_{\ell_1}^2\right)}{9-8z_{\ell_1}z_{\ell_2}-z_{\ell_2}^2-z_{\ell_1}^2+z_{\ell_1}^2z_{\ell_2}^2}. \end{cases} \tag{B.15}$$

In this system, the transmission is obtained by

$$T_{\Gamma_{\varrho(\ell_1,\ell_2)}} = t_1(P_{1,2} + P_{1,3}). \tag{B.16}$$

Then, we have

$$T_{\Gamma_{\varrho(\ell_1,\ell_2)}} = \frac{2}{3}\frac{2z_{\ell_1}\left(3-2z_{\ell_1}z_{\ell_2}-z_{\ell_2}^2\right)+2z_{\ell_2}\left(3-2z_{\ell_1}z_{\ell_2}-z_{\ell_1}^2\right)}{9-8z_{\ell_1}z_{\ell_2}-z_{\ell_2}^2-z_{\ell_1}^2+z_{\ell_1}^2z_{\ell_2}^2}, \tag{B.17}$$

$$T_{\Gamma_{\varrho(\ell_1,\ell_2)}} = \frac{\frac{4}{3}\left(3z_{\ell_1}-2z_{\ell_1}^2z_{\ell_2}-z_{\ell_1}z_{\ell_2}^2+3z_{\ell_2}-2z_{\ell_1}z_{\ell_2}^2-z_{\ell_1}^2z_{\ell_2}\right)}{9-8z_{\ell_1}z_{\ell_2}-z_{\ell_2}^2-z_{\ell_1}^2+z_{\ell_1}^2z_{\ell_2}^2}. \tag{B.18}$$

Which can be simplified to

$$T_{\Gamma_{\varrho(\ell_1,\ell_2)}} = \frac{4\left(z_{\ell_1}-z_{\ell_1}^2z_{\ell_2}+z_{\ell_2}-z_{\ell_1}z_{\ell_2}^2\right)}{9-8z_{\ell_1}z_{\ell_2}-z_{\ell_2}^2-z_{\ell_1}^2+z_{\ell_1}^2z_{\ell_2}^2}, \tag{B.19}$$

arriving in the final equation

$$T_{\Gamma_{\varrho(\ell_1,\ell_2)}} = \frac{4\left[\left(1-z_{\ell_2}^2\right)z_{\ell_1}+\left(1-z_{\ell_1}^2\right)z_{\ell_2}\right]}{\left(3-z_{\ell_1}z_{\ell_2}\right)^2-\left(z_{\ell_1}+z_{\ell_2}\right)^2}. \tag{B.20}$$

APPENDIX C TRANSMISSION AMPLITUDES OF SOME QUANTUM GRAPH FAMILIES

Table C.1 – Transmission amplitudes of path, star, cycle and complete quantum graphs with n vertices.

n	P_n	S_n	C_n	K_n
3	z^2	$\frac{2\left(z+z^3\right)}{3+z^2}$	$\frac{4z\left(1+2z+2z^2+z^3\right)}{9+9z+8z^2-z^4-z^5}$	$\frac{4z\left(1+2z+2z^2+z^3\right)}{9+9z+8z^2-z^4-z^5}$
4	z^3	$\frac{2\left(z+z^3\right)}{4}$	$\frac{4z\left(1+z^2\right)^2}{9+8z^2-z^6}$	$\frac{z\left(3+5z+5z^2+3z^3\right)}{12+4z+9z^2-5z^3-z^4-3z^5}$
5	z^4	$\frac{2\left(z+z^3\right)}{5-z^2}$	$\frac{4z\left(z^3(1+z)+\sum_{j=0}^{7} z^j\right)}{(1+z)(1-z^8)+8\sum_{j=0}^{4} z^j}$	$\frac{2z\left(2+3z+3z^2+2z^3\right)}{25+21z-17z^3-9z^5}$
6	z^5	$\frac{2\left(z+z^3\right)}{6-2z^2}$	$\frac{4z\left(1+z^2+2z^4+z^6+z^8\right)}{9+8z^2+8z^4-z^{10}}$	$\frac{z\left(5+7z+7z^2+5z^3\right)}{45-9z+43z^2-39z^3+4z^4-20z^5}$
7	z^6	$\frac{2\left(z+z^3\right)}{7-3z^2}$	$\frac{4z\left(z^5(1+z)+\sum_{j=0}^{11} z^j\right)}{(1+z)(1-z^{12})+8\sum_{j=0}^{6} z^j}$	$\frac{4z\left(3+4z+4z^2+3z^3\right)}{147-49z+156z^2-148z^3+25z^4-75z^5}$
8	z^7	$\frac{2\left(z+z^3\right)}{8-4z^2}$	$\frac{4z\left(1+z^2+z^4+2z^6+z^8+z^{10}+z^{12}\right)}{9+8z^2+8z^4+8z^6-z^{14}}$	$\frac{z\left(7+9z+9z^2+7z^3\right)}{112-48z+129z^2-125z^3+27z^4-63z^5}$
9	z^8	$\frac{2\left(z+z^3\right)}{9-5z^2}$	$\frac{4z\left(z^7(1+z)+\sum_{j=0}^{15} z^j\right)}{(1+z)(1-z^{16})+8\sum_{j=0}^{8} z^j}$	$\frac{2z\left(4+5z+5z^2+4z^3\right)}{162-81z+199z^2-195z^3+49z^4-98z^5}$
10	z^9	$\frac{2\left(z+z^3\right)}{10-6z^2}$	$\frac{4z\left(1+z^2+z^4+z^6+2z^8+z^{10}+z^{12}+z^{14}+z^{16}\right)}{9+8z^2+8z^4+8z^6+8z^8-z^{18}}$	$\frac{z\left(9+11z+11z^2+9z^3\right)}{225-125z+291z^2-287z^3+80z^4-144z^5}$

Source: the author.

APPENDIX D PHASE ϕ FOR MAXIMAL ENTANGLEMENT ENTROPY

From equations (6.49) we got the the maximal entanglement in that case is obtained for

$$\tan\left(k_B\ell\right)\tan\left(k_B\ell+\phi\right)=-4. \tag{D.1}$$

A solution for obtaining ϕ is straightforward from

$$\tan\left(k_B\ell+\phi\right)=-4\cot\left(k_B\ell\right) \tag{D.2}$$

and

$$\phi=\arctan\left(-4\cot\left(k_B\ell\right)\right)-k_B\ell+n_\phi\pi. \tag{D.3}$$

However, for each integer n_ϕ this function is discontinuous at $2j\pi$ with j integer. When considering all functions for the integer n_ϕ, they constitute a set of continuous solutions on $k_B\ell$, and they are the ones that we will find in this appendix.

Let us step back and return to the equation

$$\tan\left(k_B\ell+\phi\right)=-4\cot\left(k_B\ell\right), \tag{D.4}$$

rewriting the tangent of a sum, we have

$$\frac{\tan\left(k_B\ell\right)+\tan\left(\phi\right)}{1-\tan\left(k_B\ell\right)\tan\left(\phi\right)}=-4\cot\left(k_B\ell\right), \tag{D.5}$$

which becomes

$$\tan\left(k_B\ell\right)+\tan\left(\phi\right)=-4\cot\left(k_B\ell\right)\left(1-\tan\left(k_B\ell\right)\tan\left(\phi\right)\right), \tag{D.6}$$

and can be expanded to

$$\tan\left(k_B\ell\right)+\tan\left(\phi\right)=-4\cot\left(k_B\ell\right)+4\cot\left(k_B\ell\right)\tan\left(k_B\ell\right)\tan\left(\phi\right) \tag{D.7}$$

Simplifying now the product between cotangent and tangent of $k_B\ell$, be-

comes

$$\tan\left(k_B\ell\right)+\tan\left(\phi\right)=-4\cot\left(k_B\ell\right)+4\tan\left(\phi\right) \tag{D.8}$$

which can be simplified to

$$-3\tan\left(\phi\right)=-4\cot\left(k_B\ell\right)-\tan\left(k_B\ell\right) \tag{D.9}$$

obtaining

$$\tan\left(\phi\right)=\frac{4\cot\left(k_B\ell\right)+\tan\left(k_B\ell\right)}{3}. \tag{D.10}$$

Finally, we have that

$$\phi=\arctan\left(\frac{4\cot\left(k_B\ell\right)+\tan\left(k_B\ell\right)}{3}\right)+n\pi. \tag{D.11}$$

Now, let us consider the following property of the arctan(x),

$$\arctan\left(x\right)-\frac{\pi}{2}=-\arctan\left(x^{-1}\right) \tag{D.12}$$

which can be rewritten as

$$\arctan\left(x\right)=-\arctan\left(x^{-1}\right)+\frac{\pi}{2} \tag{D.13}$$

Applying this property on the equation obtained on eq. (D.11), it becomes

$$\phi=-\arctan\left(\frac{3}{4\cot\left(k_B\ell\right)+\tan\left(k_B\ell\right)}\right)+n\pi+\frac{\pi}{2}. \tag{D.14}$$

By rewritting the tangent and cotangent in the sine and cosine forms,

$$\phi=-\arctan\left(\frac{3}{4\frac{\cos(k_B\ell)}{\sin(k_B\ell)}+\frac{\sin(k_B\ell)}{\cos(k_B\ell)}}\right)+n\pi+\frac{\pi}{2}, \tag{D.15}$$

that can be rewritten as

$$\phi=-\arctan\left(\frac{3\sin\left(k_B\ell\right)\cos\left(k_B\ell\right)}{4\cos^2\left(k_B\ell\right)+\sin^2\left(k_B\ell\right)}\right)+n\pi+\frac{\pi}{2} \tag{D.16}$$

and since $\sin^2(x) + \cos^2(x) = 1$, we got

$$\phi = -\arctan\left(\frac{3\sin\left(k_B\ell\right)\cos\left(k_B\ell\right)}{1+3\cos^2\left(k_B\ell\right)}\right) + n\pi + \frac{\pi}{2}. \tag{D.17}$$

With $\sin(2x) = 2\sin(x)\cos(x)$ and $\cos(2x) = 2\cos^2(x) - 1$,

$$\phi = -\arctan\left(\frac{\frac{3}{2}\sin\left(2k_B\ell\right)}{1+\frac{3}{2}\cos\left(2k_B\ell\right)+\frac{3}{2}}\right) + n\pi + \frac{\pi}{2}. \tag{D.18}$$

Finally we obtain,

$$\phi = -\arctan\left(\frac{3\sin\left(2k_B\ell\right)}{5+3\cos\left(2k_B\ell\right)}\right) + (2n+1)\frac{\pi}{2} \tag{D.19}$$

which is a continuous function along $k_B\ell$ for each integer n.